HIGHWAY RESEARCH RECORD

Number 185

Tunneling, Geophysical Studies, and Soil-Culvert Interactions

6 Reports

Subject Area

22 Highway Design
33 Construction
34 General Materials
61 Exploration-Classification (Soils)
63 Mechanics (Earth Mass)

HIGHWAY RESEARCH BOARD
DIVISION OF ENGINEERING NATIONAL RESEARCH COUNCIL
NATIONAL ACADEMY OF SCIENCES—NATIONAL ACADEMY OF ENGINEERING

Washington, D.C., 1967 Publication 1516

Department of Soils, Geology and Foundations

Eldon J. Yoder, Chairman
Joint Highway Research Project
Purdue University, Lafayette, Indiana

Chester McDowell, Vice Chairman
Materials and Tests Soils Engineer
Texas Highway Department, Austin

HIGHWAY RESEARCH BOARD STAFF

J. W. Guinnee, Engineer of Soils, Geology and Foundations

DIVISION B

H. Bolton Seed, Chairman
Department of Civil Engineering
University of California, Berkeley

Carl L. Monismith, Vice Chairman
University of California, Berkeley

COMMITTEE ON BURIED STRUCTURES
(As of December 31, 1966)

Reynold K. Watkins, Chairman
Professor and Head, Mechanical Engineering Department,
Utah State University, Logan

Jay Allgood, Senior Project Engineer, Structures Division, U. S. Naval Civil Engineering Laboratory, Port Hueneme, California
Bernard E. Butler, New York State Department of Public Works, Albany
T. Y. Chu, Civil Engineering Department, University of South Carolina, Columbia
T. F. deCapiteau, Drainage Products Engineer, Manufacturing Division, Republic Steel Corporation, Youngstown, Ohio
Ronald Drawsky, Kaiser Center, Oakland, California
Kenneth S. Eff, Chief, Hydraulic Section, Civil Engineering Branch, Office, Chief of Engineers, Department of the Army, Washington, D.C.
L. H. Gabriel, Department of Civil Engineering, Sacramento State College, Sacramento, California
Delon Hampton, Research Engineer, Soil Mechanics Section, IIT Research Institute, Chicago, Illinois
D. A. Linger, Manager, Structural Mechanics Division, Eric H. Wang Civil Engineering Research Facility, Albuquerque, New Mexico
Alex E. Mansour, Jr., Chief Structural Engineer, Utah State Department of Highways, Salt Lake City
Ernest T. Selig, Manager, Soil Mechanics, IIT Research Institute, Chicago, Illinois
Harry H. Ulery, Soils Division, U. S. Army Engineer Waterways Experiment Station, Vicksburg, Mississippi
Howard L. White, Chief Engineer, Metal Products Division, Armco Steel Corporation, Middletown, Ohio

DIVISION C

O. L. Lund, Chairman
Assistant Engineer of Materials and Tests
Nebraska Department of Roads, Lincoln

L. F. Erickson, Vice Chairman
Materials and Research Engineer
Idaho Department of Highways, Boise

COMMITTEE ON ENGINEERING GEOLOGY
(As of December 31, 1966)

Ernest Dobrovolny, Chairman
U. S. Geological Survey, Engineering Geology Branch,
Denver, Colorado

A. C. Dodson, Chief Geologist, North Carolina State Highway Commission, Raleigh
Spenst M. Hansen, Geological Engineer, Plowshare Division, Lawrence Radiation Laboratory, Livermore, California
Duncan J. McGregor, State Geologist, University of South Dakota, Vermillion
John D. McNeal, Engineer of Planning and Research, State Highway Commission of Kansas, Topeka
Shailer S. Philbrick, Ithaca, N.Y.
Charles S. Robinson, Denver, Colorado
David L. Royster, Chief, Soils and Geological Section, Tennessee Department of Highways, Nashville
Rockwell Smith, Research Engineer—Roadway, Association of American Railroads, Chicago, Illinois
Travis W. Smith, Assistant Materials and Research Engineer—Foundation, California Division of Highways, Sacramento

Department of Materials and Construction

R. L. Peyton, Chairman
Assistant State Highway Engineer
State Highway Commission of Kansas, Topeka

HIGHWAY RESEARCH BOARD STAFF

R. E. Bollen, Engineer of Materials and Construction
W. G. Gunderman, Assistant Engineer of Materials and Construction

GENERAL MATERIALS DIVISION

John L. Beaton, Chairman
Materials and Research Engineer
Materials and Research Department
California Division of Highways, Sacramento

COMMITTEE ON CULVERTS AND CULVERT PIPE
(As of December 31, 1966)

Kenneth S. Eff, Chairman
Chief, Hydraulic Section, Civil Engineering Branch
Office, Chief of Engineers
Department of the Army, Washington, D. C.

T. F. deCapiteau, Drainage Products Engineer, Manufacturing Division, Republic Steel Corporation, Youngstown, Ohio
W. B. Drake, Assistant State Highway Engineer for Planning, Research & Materials, Kentucky Department of Highways, Lexington
C. J. Francis, Director, Engineering Division, Soil Conservation Service, U. S. Department of Agriculture, Washington, D. C.
R. T. Healy, Executive Secretary, Connecticut Concrete Pipe Association, Inc., South Windham, Connecticut
John G. Hendrickson, Jr., Water Resources Bureau, Portland Cement Association, Chicago, Illinois
A. H. Koepf, Consulting Engineer, Orinda, California
L. R. Lawrence, Director of Engineering, Highway Market, Reynolds Metals Company, Richmond, Virginia
J. Alan Myers, Manager, Architectural Products, United States Steel Corporation, Pittsburgh, Pennsylvania
F. Dwayne Nielson, New Mexico State University, University Park
Eric Nordlin, Supervising Highway Engineer, Materials and Research Department, California Division of Highways, Sacramento
C. E. Proudley, Materials Consultant, Raleigh, North Carolina
E. P. Sellner, Lahore, West Pakistan
Rockwell Smith, Research Engineer—Roadway, Association of American Railroads, Chicago, Illinois
M. G. Spangler, Civil Engineering Department, Iowa State University, Ames
Harold V. Swanson, Manager, Civil Engineering, International Pipe and Ceramics Corporation, Parsippany, New Jersey
Adrianus Van Kampen, Director of Engineering, American Concrete Pipe Association, Arlington, Virginia
Reynold K. Watkins, Professor and Head, Mechanical Engineering Department, Utah State University, Logan
H. L. White, Chief Engineer, Metal Products Division, Armco Steel Corporation, Middletown, Ohio

Foreword

This RECORD presents three papers dealing with tunnel driving, two papers with underground structures in soils and one with physical properties.

The development of rapid, safe and economical methods of driving tunnels is becoming increasingly more important and necessary in long-range planning of transportation facilities. Several aspects of tunnel construction relating to methods and prediction of ground conditions at tunnel level are considered in the first three papers. Bennett compares tunnel driving by conventional methods with a mechanical boring machine. The comparison is made under controlled conditions in the same rock media, a situation rarely encountered in practice. Although the author generally favors the boring machine technique, he lists ten advantages and disadvantages of each method. Final determination of which method would best serve on a given project depends in large part on local ground conditions and length and diameter of tunnel needed.

Robinson and Lee compare the actual geologic measurements and ground conditions encountered in driving the Straight Creek tunnel pilot bore, Colorado, with their preconstruction prediction that was published in 1964 in Highway Research Record 57. Based on a statistical study of surface and drill hole data and observations, predictions as to kind and extent of conditions were accurate, but not as to their exact locations. Predictions were accurate on percentage of rock types, linear feet of faulted and sheared rock, and attitudes of foliation. Rock loads and final swell pressures in gouge and altered rocks agreed well with actual measurements. Estimates made of the amount of temporary support, footage of feeler holes and quantity of grouting provided a reliable basis for estimating tunnel costs.

Scott and Carroll used geophysical techniques and instrumentation that were developed mainly in petroleum exploration to measure rock properties in the Straight Creek tunnel pilot bore, Colorado. Preconstruction geophysical measurements on the surface and in drill holes from the surface are useful in site selection where several alternative tunnel routes are under consideration. Correlations indicate that certain basic relationships exist between the measurable properties of rock and the economic and engineering aspects of tunneling. After the site has been selected, geophysical measurements made during the early stages of construction in long feeler holes drilled ahead of the working face can be used to predict engineering and economic parameters ahead of blasting operations.

F. D. Nielson applies the concept of the soil arch to make an analysis of pressure distribution over underground structures (conduits). This analysis is compared with a similar analysis taken from

elasticity theory and with an experiment in which lead shot and X-ray are used to define deformation zones. Agreements exist in all the methods. Further experimental-analytical correlations are urged.

Gabriel and Dabaghian present an analytical-experimental method that works backward from displacement on the internal boundary of a buried culvert to determine unique loading on the external (outer) boundary of the culvert. Fourier series is used in the procedure and the mathematical steps are extensively detailed including computer example calculation of constants.

In the last paper Mr. Nielson evaluates the modulus of soil reaction as determined from the triaxial shear test to conclude that it can be used satisfactorily for design work. The modulus is sensitive to the value of Poisson's ratio and a value of 0.25 is recommended for use.

— Ernest Dobrovolny

Contents

Mole Versus Conventional: A Comparison of Two Tunnel Driving Techniques

NEWCOMB B. BENNETT, III, U. S Bureau of Reclamation

In northwest New Mexico the U. S. Bureau of Reclamation is building the Navajo Indian Irrigation Project. As a part of the water conveyance system, two tunnels were built. Tunnel 1, 2 mi long, was driven with a Hughes tunneling machine. One-quarter mile away is Tunnel 2, which will eventually be 5 mi long (only 2 mi had been excavated at the time of this writing). The second tunnel is being driven by conventional methods. Both tunnels are in the San Jose formation consisting of sandstone, siltstone, and shale.

The author presents observations made while working in both tunnels. Comparisons are made of rock behavior, supports, techniques, personnel, and advantages and disadvantages of using a "mole."

A tunneling machine offers the following advantages: near-continuous operation; high daily footage; minimum overbreak resulting in a nearly 50 percent reduction in concrete; fewer personnel; safer operation; fewer supports required; minimum cleanup operations; and dynamite not required resulting in increased savings. Disadvantages include: long section needed to pay for itself; circular section only; specialized operator required; supports difficult to install; long wait for delivery; large initial investment; machine has to be designed for tunnel because of different diameters and geologic conditions; limited to softer materials; large ventilation system needed.

•IN THE San Juan Basin of New Mexico, the U.S. Bureau of Reclamation is building the Navajo Indian Irrigation Project, a 135-million dollar project to furnish water to the desert lands of the Navajo Reservation. Water from the Navajo Dam will be diverted through a system of tunnels, siphons, and canals. Because the surrounding country is so rugged, it was necessary to begin the diversion through a 2-mi tunnel, referred to as Tunnel 1. A second tunnel, which will be 5 mi long when completed, is located ¼ mi from Tunnel 1. At the time of this writing, 2 mi had been excavated. Both tunnels will be 20 ft in diameter.

Two entirely different techniques were used to excavate these tunnels: a boring machine in Tunnel 1 and conventional methods in Tunnel 2.

GENERAL OBSERVATIONS

In a comparison such as this, it is not accurate to state that a mole-driven tunnel is capable of progress x times as fast as a conventionally driven one, because of certain factors involved which may occasionally balance out or eliminate one another. For instance, a mole could not be used in tunnels of too short a length because the time to build one could conceivably consume 100 percent of the contract period.

It took practically a full year to build the mole for Tunnel 1. Therefore, the tunnel must be sufficiently long to allow the mole, once on the job, to catch up with where conventional methods would ordinarily be in the same amount of time. It was thought that the 2-mi Tunnel 1 was the minimum that the mole could handle and still pay for itself.

Paper sponsored by Committee on Engineering Geology and presented at the 46th Annual Meeting.

Diameter is also an important factor, because it determines the size of the mole, influences the length of the construction period, and bears a direct relation to the capital cost. Therefore, the tunnel length would have to be proportionately longer in relation to the diameter for a mole to pay its way.

Too long a tunnel can also cause problems. The engineer on the mole stated that his machine could probably bore for 5 mi before an overhaul would be necessary. Overhauls of any sort are not done easily within the confines of a tunnel, nor is a mole moved to the outside easily or in a short time. Tunneling machines are presently designed for circular section tunnels only. A highway tunnel would require a horseshoe section. To design a mole for a horseshoe tunnel would require new concepts and would probably increase costs.

AREA GEOLOGY

The geology of the area is quite simple. Both tunnels are in the San Jose formation of Eocene Age. This is a typical continental deposit laid down in a deltaic environment. The rock types consist of sandstone alternating with lenticular layers of shale and siltstone. None of the shales or siltstones can be traced over long distances. The shales are commonly 3 to 4 ft thick, although they may reach 15 ft locally. Very few of the siltstones exceed 5 ft.

The sandstones range from fine to coarse and are sometimes conglomeritic although the majority are medium grained. A few are cemented by calcite, a few by iron cement, and some are clay cemented. Most are friable to moderately cemented. The sandstone is composed of about 70 percent siliceous materials. No compressive tests were run by the Bureau of Reclamation, but the designer of the mole did conduct a few and came up with a strength of 5,000 to 6,000 psi. Tests were not run on the shales or siltstones.

The shales are predominately the compaction type and are both silty and clayey, thinly bedded to laminated. They air slake rapidly to flaky particles. On steep slopes there is an almost constant rain of fine shale. Under natural conditions the shales assume stability on a slope of about $1\frac{1}{2}$:1.

The rocks dip 3 to 5 deg to the southeast. Folding or faulting was never observed any place within the San Jose formation. In several places the shales may dip as much as 45 deg; however, this is the result of initial deposition rather than any local or regional structure.

Geologically one could not ask for better conditions with which to make comparisons of such radically different tunnel driving techniques.

GEOLOGIC COMPARISONS

No attempt is made to make comparisons on a station-to-station basis. Rather, comparisons are made of the behavior of similar rock types during and after excavation.

In a tunnel driven in shaley conditions, the question is how did the shale react. The shales in both tunnels were of the compaction type and air slaked rapidly after exposure to air. Whether the shale is above or below the surface, the process of air slaking is an attempt on the part of the shale to assume stability. When a shale in a tunnel starts lying on a 1:$1\frac{1}{2}$-slope, the overlying rock will no longer be stable. When a sandstone is undercut by a rapidly retreating shale, it will fall. It is the large sandstone blocks which cause damage when they fall, but their falling is generally the fault of the shale.

The shales reacted the same in both tunnels in that they tried to reach stability. The difference appears in the amount of time it takes the shale to begin air slaking. In either tunnel it would generally take 1 to 2 days to begin falling, even after its initial exposure. However, once exposed, differences occurred. In Tunnel 1 the shale would begin dropping immediately after a new reach was exposed. It was believed that this was due to the compressive effects of the cutterhead. After the mole passed, the shale would almost spring into the tunnel and, unless immediately supported, would continue falling.

In Tunnel 2 the shale always took 1 to 2 days to begin falling, even after its initial occurrence. The difference in time was probably due to the arch and sides being scaled right away and the dangerous rock removed. Also, the effect of the blasting undoubtedly removed much of the loose material.

The shape the arch took as the shale fell was an interesting observation. In Tunnel 1 the arch took the shape of an inverted V.

In Tunnel 2, because of the flat-lying attitude of the rock, the arch was flat. Here the shale would simply fall away from a poorly bonded bedding plane and leave a flat sandstone. Had the arch in Tunnel 1 been left unsupported, this flat-type back would surely have developed also.

In Tunnel 1, because of the arching effect of an almost perfectly circular section, the sandstones could stand quite a bit of undercutting. The sandstone was strong enough to cantilever itself. Often only a thin wedge of sandstone would remain, and it remained stable.

Even relatively thin shales would undercut the sandstone in Tunnel 2, but few attempts were made to stabilize any of them. Because perched water seeped from the top of practically every shale, any protective material such as asphalt or gunnite would soon come off.

Water caused minor problems in both tunnels. In Tunnel 2 the main problem was one of constant seeps which would weaken the bond in the bedding planes and cause the shale to fall in large pieces.

In Tunnel 1 the same problem occurred with one addition. Because the water was associated with the shales and leaked from the top of them, they became lubricated and quite slick. For one stretch, shale formed the entire side of the tunnel. With the shale slick, it was impossible for the mole to maintain a bearing while pressure was exerted at the cutterhead. The whole machine would slide backward. It became necessary to drill shallow holes behind the bearing pads and insert 3-in. steel pins so that the mole would slide against them and come to rest. Needless to say, progress was quite slow through this reach. If this condition had been expected to extend for a long distance, then permanent teeth would have been welded to the pads.

Bedding and jointing played an important role in the stability of Tunnel 2. It was, of course, the flat-lying bedding plane of a sandstone which formed the flat back so commonly found. As the shale or sandstone broke off, it fell in the shape of cubical pieces, the result of intersecting bedding and jointing.

These geologic features went practically unnoticed in Tunnel 1 for two reasons. First, as the mole performed its excavation, it very neatly plastered a thin layer of silt, clay, sand, and dust over the entire section. In most cases it was difficult just to pick out rock types. To distinguish the degree of bedding or jointing was practically impossible. Second, a true circular section tunnel theoretically offers the strongest available geometric figure. Rock fall under the given geologic conditions depends on the relationship between bedding and jointing. By creating a self-supporting circular section, the chances for rock fall are reduced and the beds and joints are rarely seen.

SUPPORTS

Supports in Tunnel 2 were of the usual type, either I-beams or rock bolts. Four-inch I-beams were used almost exclusively where thick shales formed the arch. The use of bolts was limited more to pinning rather than support. Bolts ranging in length from 6 to 12 ft were used. These were torqued to about 180 ft-lb.

In Tunnel 1, because of space limitations, 4-in. I-beam half-rings were the main means of support. When bad rock was first encountered, an attempt was made to use rock bolts. As the working room on top of the mole was less than standing room, bolts of adequate length could not be installed. Only short bolts could be used, and this usually resulted in the anchor being in shale. These bolts would rapidly fail.

The contractor had some success with 4-in. channel irons, which were for the most part 12 ft long and anchored in sandstone at each end with rock bolts. The bolts were installed after the mole had passed and working room became available. As the shale spread across the tunnel, the channel irons were useless because they would then be entirely in shale. At this stage, the contractor began installing 4-in. I-beam half-ring supports (Fig. 1). Because the top was a near perfect circle, these rolled supports could be used. They were placed by pinning each end at springline with two 18 by 1-in. rebars. This was adequate until the shale began another downward plunge. Five-foot dutchmen were added at the crown so the springline pins would drop below the shale.

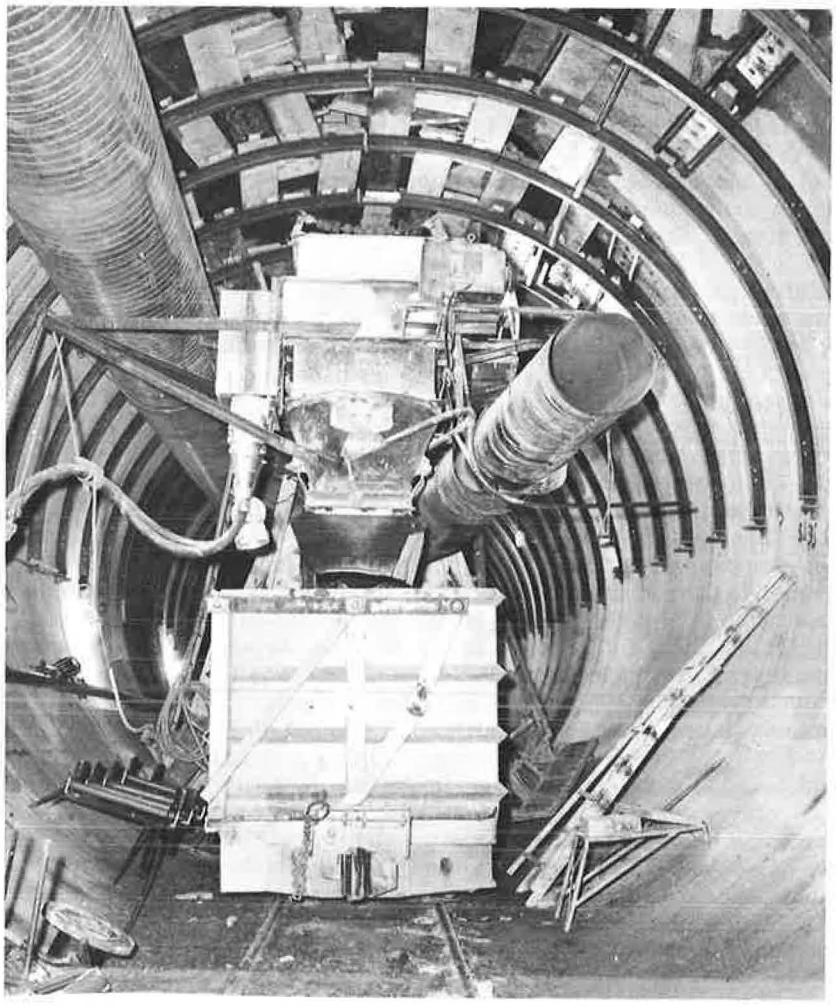

Figure 1. Half-ring supports used in Tunnel 1; conveyor belt in center dumps muck in car at lower center.

By this time the shale was out of the crown, but the slaking and overbreak actually became more severe on the sides than it ever was on the arch.

In Tunnel 1 the supported reaches totaled 44 percent of the entire length of mechanically driven tunnel. These supports were used exclusively in sections where shale was a problem.

Possibly one of the greatest advantages in using a mole is the savings on concrete due to less overbreak. Practically 50 percent less concrete is used for lining a nearly perfect circular tunnel when compared with a conventionally driven tunnel. The specification quantity for concrete in Tunnel 1 was 36,350 cu yd. If conventional methods had been used, it is estimated that 54,000 yd would have been required. Overbreak concrete is at the contractor's expense, although its costs will be hidden in his specification amounts.

Tunnel 2 required 72 percent support for an almost similar length. Seven percent was supported by 4-in. wide-flange steel supports whereas the remaining 65 percent used rock bolts. This does not include sections where bolts were used as pins or where it was felt that the bolts were improperly installed. In addition, supports were required in both sandstone and shale sections.

COMPARISON OF TECHNIQUES

Tunnel 1

The mole, properly called a tunneling machine, was developed for the prime contractor on Tunnel 1 (Fig. 2). Approximately 1 yr was spent building this tunneling titan. Exact costs were never revealed, but they have been estimated to be in excess of $750,000. When completely assembled, the machine was 64 ft long and weighed 280 tons. Three major components made up the machine: the head assembly, the outer frame, and the inner frame. Connected to each frame were hydraulic jacks which served a dual purpose: (a) bearing against the tunnel sides while drilling, and (b) locomotion. The cutterhead was actually connected to the outer frame so that jacks from the inner frame maintained the bearing while drilling. When moving forward, the outer jacks were extended, the inner ones withdrawn and the inner frame moved ahead 5 ft. The inner jacks were then extended, the outer withdrawn, and drilling began again and the cycle repeated.

The machine was capable of drilling 5 ft at a time before moving became necessary. Under ideal conditions, the mole could advance up to 10 ft per hr. Geologic conditions, of course, made the difference between poor or good advances. Using actual maximum advance figures, the machine could excavate up to 100 ft per day in supported ground, although this was considerably higher than the average. Excavating in unsupported sections, the maximum advance was 166 ft in 1 day. Generally, the average footage per day was 60.45 or 6.07 ft/hr.

The main cause of delay when going through supported ground was the placing of supports. It was necessary to hand carry the half-ring supports, in two pieces, to the mole and install them by manpower.

Other reasons for delay or complete shutdown included changing the diameter of the cuttinghead, repairs on the mole (mostly minor), muck cars jumping the tracks, and power changes or troubles.

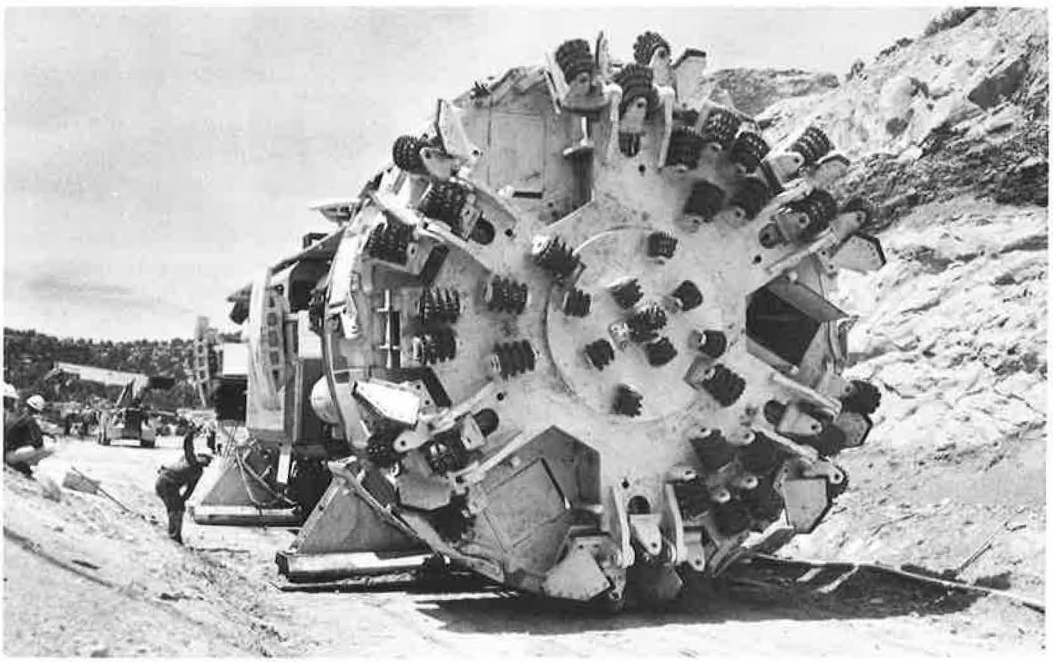

Figure 2. Tunneling machine used in Tunnel 1; lower bearing pads are part of outer frame; shoes are attached for walking to tunnel.

The tunneling machine was equipped with a cuttinghead capable of cutting three different diameters: 19 ft 10 in., 20 ft 10 in., and 21 ft 2 in. For an unsupported section, the 19-ft 10-in. diameter was used, but for supported reaches, to accommodate the steel, the bore was increased to 20 ft 10 in. Either decreasing or increasing the diameter could be done in about 2 hr.

Control for line and grade was accomplished by a laser beam. The source of the beam was set on a platform about 12 ft off the invert and offset 5 ft from centerline. The beam was then projected to a grid screen on the mole which showed the operator his position with regard to line and grade. Any deflection of the mole would immediately be detected and corrected by use of the hydraulic jacks. Highly accurate survey control by the engineers was necessary to locate the laser beam source box properly and keep it located. The source box was moved ahead approximately every 200 ft. Correction for grade was also made at 200-ft intervals.

To achieve an almost constantly running operation, which is not divided into separate cycles, a different method of removing muck was used in Tunnel 1. Fastened directly to the rear of the mole was a 150-ft conveyor belt mounted on a frame. The front of the frame was supported by legs and wheels which rode on the tracks. The rear of the frame rode on legs and wheels which angled out and rode against the tunnel sides. The conveyor was high enough to allow a string of muck cars to drive under the entire length of the belt. The car next to the motor was filled, the train backed one car length and the next car filled. When the train was full, it backed several hundred feet to a passing track. An empty train then pulled ahead to the belt and the cycle repeated.

Tunnel 2

The major equipment used in Tunnel 2 consisted of a railroad, three passing tracks, one flying carpet (sliding floor), drill jumbo, six rotary drills, and two Goodman-Conway mucking machines.

All tunneling equipment traveled on a single 36-in. gage railroad track. Three movable passing tracks were installed at various intervals in the tunnel and were used for storage of muck cars, both full and empty.

The sliding floor was located at the heading. Sliding a section of track to within a few feet of the heading allowed the mucker to move in quickly and begin work without the need of men installing track.

The six rotary drills worked off three levels of the drill jumbo. The jumbo itself was 64 ft long and weighed over 110,000 lb.

The mucking machine could load about 1½ cu yd at a time. It took about 2 min 40 sec to fill a 15-cu yd muck car. About 45 sec was required to switch cars.

A complete cycle of drilling, blasting, and mucking could be accomplished under ideal conditions in 3 hr 20 min. This would advance the tunnel about 11 ft. Breaking the cycle down into its component parts, the following average times were required: drilling (63±, 12-ft deep holes), 45 min; loading (18 lb of dynamite and 50 lb of ammonium nitrate), 40 min; ventilation time, 10 to 30 min; and mucking, 1 hr 15 min.

In the same amount of time the mole could excavate slightly more than 20 ft. The average daily footage in Tunnel 2 was 51 ft, using 4.6 cycles.

Causes of delay or shutdown in Tunnel 2 were of the types ordinarily found in conventional tunneling techniques (i.e., mechanical breakdowns, derailments, installation of supports, scaling of loose rock, and removal of misfires). Control for line and grade in Tunnel 2 was accomplished by standard survey methods.

Personnel

The number of personnel on any job depends on the management and can vary considerably. In making a comparison between the two tunnels, similar jobs have been eliminated (such as superintendents, warehousemen, and cat operators). Use of a mole automatically eliminates positions commonly found in conventional methods, such as miners, drillers, and nippers. Under typical operating conditions the personnel working in Tunnel 1 in a 24-hr period was 30. When supports were installed, the number increased to 42. Tunnel 2, under different contract, required an average of 32 people

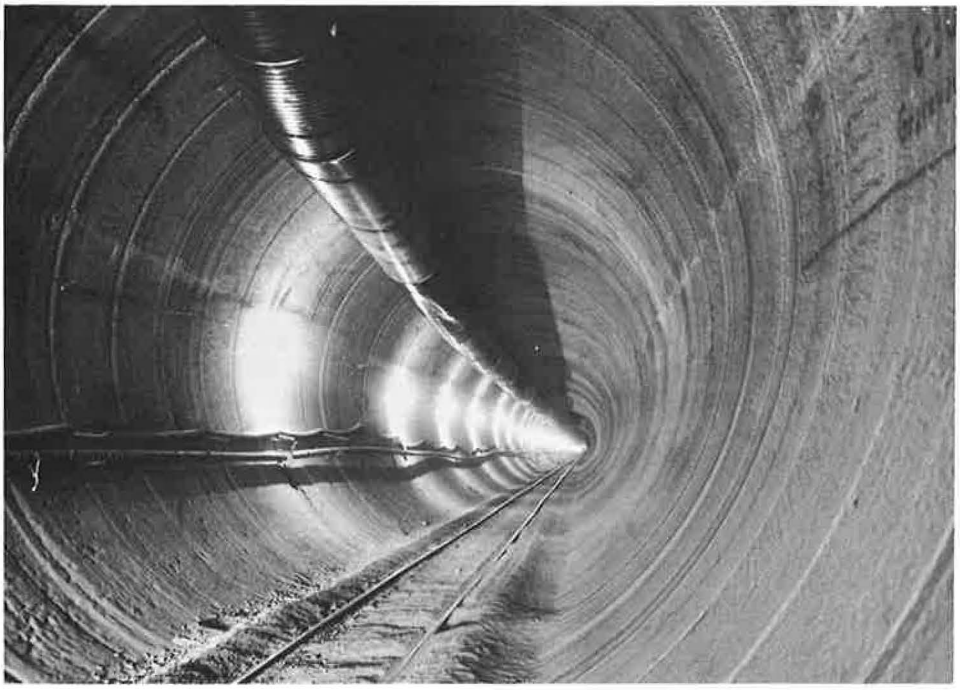

Figure 3. Tunnel 1 showing typical unsupported section.

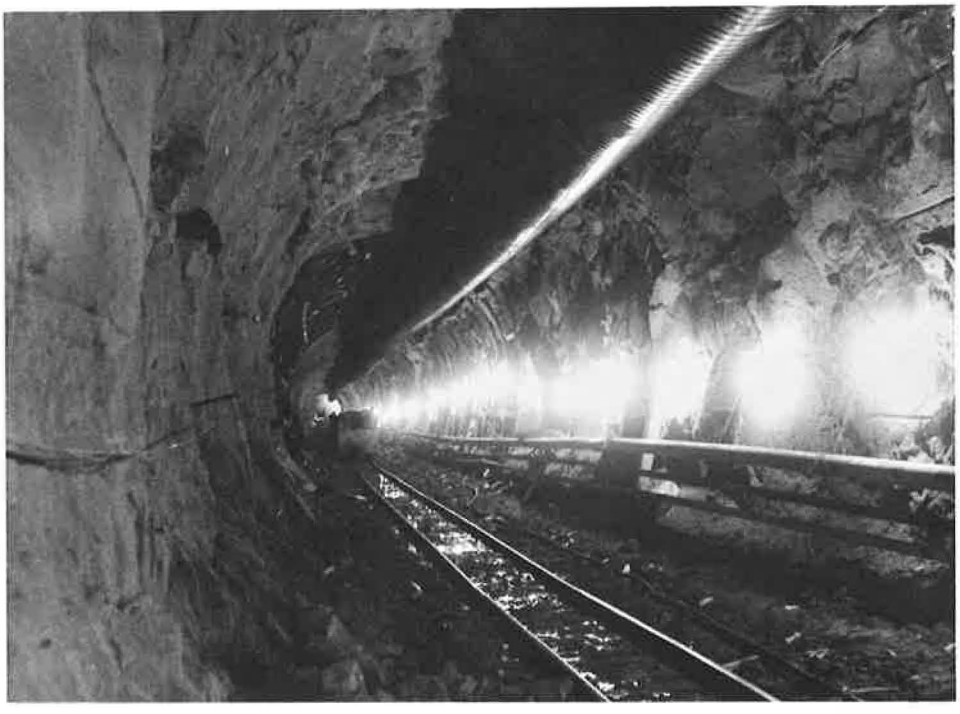

Figure 4. Tunnel 2 showing typical supported and unsupported sections.

per 24 hours. Under different management personnel requirements might have varied considerably.

SUMMARY

In summarizing, it might be advantageous at this time to compare the pros and cons of using a mechanical boring machine.

Advantages

1. Near continuous operation.
2. Greater daily footage.
3. Minimum overbreak resulting in about a 50% reduction in concrete when compared with a conventionally driven tunnel.
4. Fewer personnel required under proper management.
5. No drilling or blasting required resulting in a safer operation.
6. Surrounding rock remains undistrubed and minimum of new stresses are introduced.
7. Excavates a near self-supporting section.
8. Very good bit footage.
9. Practically no cleanup time required.
10. A substantial savings realized since dynamite is not required.

Disadvantages

1. Long section needed to pay for itself.
2. Circular section only.
3. Specialized operator required.
4. Supports difficult to install.
5. Long wait for delivery.
6. Large initial investment.
7. Still in developmental stage.
8. Machine has to be designed for each tunnel because of different diameters and geologic conditions.
9. Presently limited to softer materials.
10. Ventilation system must be larger to provide for dust control.

In the comparison, it appears that the advantages far outweigh the disadvantages, and Figures 3 and 4 offer the final proof.

Results of Geologic Research at the Straight Creek Tunnel Pilot Bore, Colorado

CHARLES S. ROBINSON, Consulting Geologist, and
FITZHUGH T. LEE, Geologist, U.S. Geological Survey, Denver, Colorado

Projection of details of surface geology to depth before construction has met with only limited success in many tunneling operations. However, in the research project on the Straight Creek Tunnel pilot bore, good results were obtained by the prediction, based on a statistical study of surface and drill hole features, of the kinds of conditions and their extent, but not their exact locations, that could be expected at tunnel level.

Successful predictions were made regarding percentages of rock types, linear feet of faulted and sheared rock, and attitudes of foliation and fractures, including faults and joints. Predicted rock loads and final swell pressures in gouge and altered rocks agreed well with actual measurements. Groundwater flows occurred in expected amounts, but criteria for estimations proved unsound.

Estimates of the amount of temporary support, footage of feeler holes, and the amount of grouting required provided engineers with a sound basis for estimates of tunnel costs.

•THE U.S. Geological Survey, in cooperation with the Colorado Department of Highways, conducted a research project in engineering geology at the Straight Creek Tunnel site, Colorado, from 1962 to 1966. The purpose of this project was to apply recently developed geologic and geophysical methods and to develop new methods for predicting geologic conditions at the tunnel depth, to present the geologic information in such a manner that it could be used by design and construction engineers, and to evaluate the accuracy of the predictions on construction of a pilot bore.

The preliminary results of the pre-construction investigations, together with the engineering predictions based on that work, were published by the authors (5, 6). Extensive investigations conducted during construction of the pilot bore are summarized here, and geologic conditions and engineering practices predicted are compared with those actually found and used during construction.

The Straight Creek Tunnel site (Fig. 1) is approximately 55 mi west of Denver. The final tunnel will consist of twin bores, each about 8,300 ft long and 42 ft in diameter. The tunnel, which will be part of I-70, is designed to provide an all-weather route through the Continental Divide and so eliminate the use of Loveland Pass on the present US 6.

SUMMARY OF PRE-CONSTRUCTION INVESTIGATIONS

The pre-construction investigations consisted of detailed geologic mapping of approximately 6 sq mi at the site of the tunnel, geologic and geophysical logging of core holes, geophysical investigations at the surface, and laboratory studies in support of the field investigations (6).

These investigations showed that the bedrock in the area consists predominantly of granite with inclusions of metamorphic rocks—chiefly varieties of biotite gneiss, of

Paper sponsored by Committee on Engineering Geology and presented at the 46th Annual Meeting.

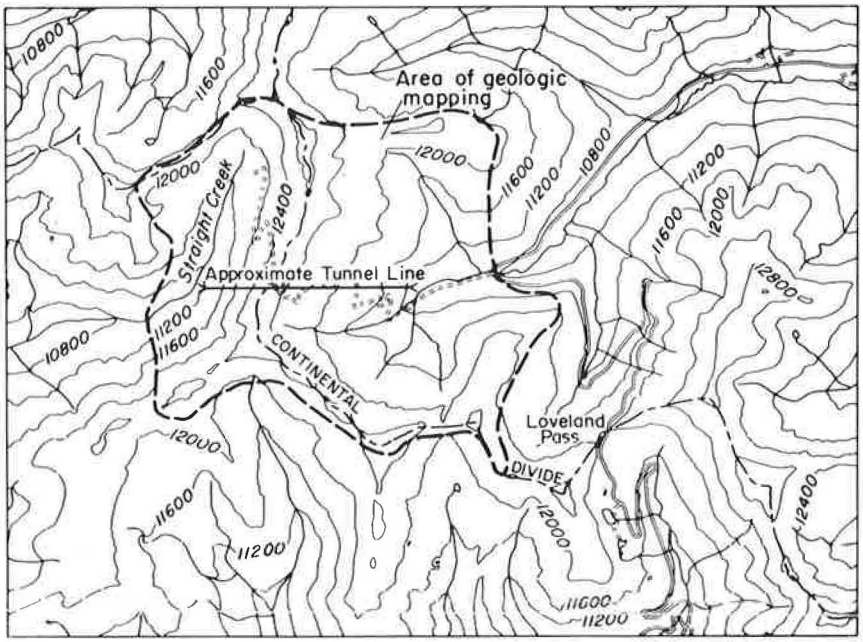

Base map from Loveland Pass quadrangle, 1958

0 2 MILES

CONTOUR INTERVAL 400 FEET
DATUM IS MEAN SEA LEVEL

Map of Straight Creek area

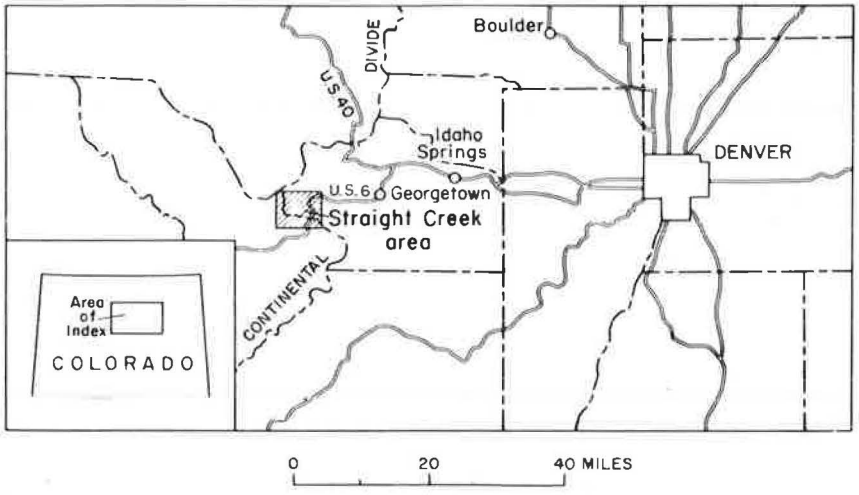

Location of Straight Creek area

Figure 1. Index maps of Straight Creek Tunnel area, Colorado.

TABLE 1

PREDICTIONS VS FINDINGS IN STRAIGHT CREEK TUNNEL PILOT BORE, COLORADO

Item	Predictions	Findings
(a) Geologic Measurements[a]		
Rock type (% pilot-bore length)		
Granite	75	75.4
Metamorphic rock	25	23.8
Diorite dikes	[minor]	0.8
Fracture density (% pilot-bore length)		
<0.1 to 0.5 ft	40.1	38.7
0.5 to 1 ft	49.3	42.6
>1 ft	10.6	18.7
Faults and shear zones (% pilot-bore length)	51	49
Faults, principal ranges in trend or attitude (surface, >5 ft wide; pilot bore, >1 ft wide)		
Strike	N. 20°-80° E.	N. 20°-45° E.
Dip	75° NW. or SE.	40°-75° SE.
Joints (principal range and avg. attitude)		
Strike	Any direction	Any direction
Dip	45°-90°	8°-90°
Avg. dip	60°	45°
Foliation (principal range)		
Strike	N.-N. 30° E.	N. 10°-60° E.
Dip	60°-90° SE. or NW.	10°-50° SE.
Statistical maxima		
Strike	N. 15° E.	N. 45° E.
Dip	65° SE. or 70° NW.	30° SE.
Strike	N. 30° E.	
Dip	75° NW.	
Avg. dip	60°	30°
(b) Engineering Measurements		
Rock loads (psf)		
Predicted maximum rock load calculated from Terzaghi (10) on 10.5 × 11.5-ft pilot bore	5900	—
Predicted maximum rock load recalculated from Terzaghi (10) on 13 × 13-ft pilot bore	6970	—
Calculated geometric midpoint for maximum stable geologic rock load from measurements in pilot bore, 13 × 13 ft	—	6600
Avg. final swell pressure (psf) of altered rock and gouge	2233[b]	1727[c]
Groundwater (gal/min)		
Maximum initial flow from any section	1000	750
Maximum flow from portal	500	800
Flow at portal 2 wk after completion of pilot bore	300	130
(c) Construction Practices[d]		
Set spacing (% pilot-bore length)		
1-ft centers	1.6	2
2-ft centers	23	22
3-ft centers	40	30
5-ft centers	35	20.9
Invert struts	1.4	8
Total no. of sets	2691	2172
Total no. of invert struts	113	210
Lagging and blocking (footage in pilot bore)		
100 to 67 percent lagged and blocked	1731	1456
66 to 34 percent lagged and blocked	3659	2447
33 to 0 percent lagged and blocked	2660	4447
Feeler holes (lin ft)	2905	9816
Grout (lin ft of pilot bore)	403	0

[a]Predictions based on 4.0 percent outcrop.
[b]Six samples.
[c]Twenty-nine samples.
[d]Predictions based on pilot-bore length of 8,050 ft; findings based on length of 8,350 ft.

Precambrian age, and a few small dikes of diorite, of probable Tertiary age. Faults, shear zones, and joints are numerous in the tunnel area, which is within a wide zone of regional faulting and shearing that is probably related to the Loveland Pass fault (4, pl. 2).

The pre-construction geologic, geophysical, and laboratory data were compiled and statistically analyzed. These data were the basis for the prediction of geologic conditions

at the depth of the pilot bore and for the calculation of engineering data for estimating the cost of construction (Table 1).

INVESTIGATIONS DURING CONSTRUCTION

During construction of the pilot bore, which began in November 1963 and was completed in December 1964, geological, geophysical, and laboratory investigations were conducted. In addition, rock mechanics investigations were made. The final results of this work are not yet available, but sufficient data were compiled to evaluate the preconstruction geologic projections and predictions. A preliminary report of the results of the investigations is available (7).

Geology

The geology of the pilot bore was mapped at various scales and sampled for various purposes throughout its length. The walls of the bore were mapped at 1:600. On these maps were recorded rock type; attitude of the foliation, faults and shear zones, and joints; percentage of altered minerals in the wall rock; and occurrence of groundwater. Geologic sections of the tunnel face at about 800 stations were made, at a scale of 1:24, by engineers of the Colorado Department of Highways and by the authors. In support of the geophysical investigations and the instrumentation, the geology of one wall or the other was mapped in plan view at 1:60 for 50 ft or more to either side of a geophysical or instrument station.

The wall rock of the tunnel was sampled during the geologic mapping for various laboratory determinations. Systematic samples were collected for petrographic analysis. Samples of altered wall rock and fault gouge were collected for determination of swelling pressures and mineralogy. Linear chip samples from 5 ft on either side of instrument stations were collected for grain size and mineral analyses. Blocks of wall rock about 1 ft in largest dimension were collected and cored in the laboratory for the determination, by dynamic and static tests, of elastic properties.

As the construction of the pilot bore progressed, and as the results of the instrumentation and geophysical investigations became available, a particular effort was made to determine the geologic and engineering conditions influencing these results. It soon became apparent that the categories of fracture density, or the average spacing between fractures (6), as determined from surface mapping, were not definitive enough. At the surface, the fracture density categories mapped were less than 0.1 to 0.5 ft, 0.5 to 1 ft, and 1 to 3 ft. Underground, the fracture density categories mapped were changed to less than 0.1 ft, 0.1 to 0.5 ft, 0.5 to 1 ft, and greater than 1 ft. The instrumentation and geophysical work also dictated the need for mapping the percentage of wall-rock alteration and for sampling for grain size and mineral analyses.

Geophysics

Geophysical investigations were undertaken in the pilot bore to determine whether geophysical instruments and techniques could be used effectively to define the physical conditions around the pilot bore, and whether these conditions could be correlated with the results of the instrumentation and the construction practices used in the pilot bore.

Both resistivity and seismic velocity measurements were made at selected points along the walls of the pilot bore. The apparent resistivity was measured along the wall at 30 stations which corresponded to 30 of the instrument stations. Seismic velocity measurements were made at 5 localities selected to give the best representation of the geologic conditions in the pilot bore. The instruments and procedures used and the results of the geophysical investigations in the pilot bore are described elsewhere (9).

Groundwater

Groundwater investigations were conducted during the construction of the pilot bore and have been continued on a limited scale since its completion. The results of these groundwater investigations were reported by Hurr and Richards (3).

The groundwater investigations included the recording of water flows near the portal and at different intervals within the pilot bore. Where possible, engineers of the Department of Highways recorded initial water flows at the face and from feeler holes, and also the decrease in rates of flow from the face, from the fractures in the walls, and from feeler holes. The water level in a drill hole at the surface above the tunnel was periodically recorded. One water-pressure measurement was made on water flowing from a feeler hole. The specific conductance of the water in the tunnel was measured at many points, and samples for chemical analysis were taken from different points within the tunnel.

Hurr and Richards concluded, from a preliminary analysis of the groundwater data, that the pilot bore could be divided into active and passive groundwater zones. In the active zones, which were near either portal, the groundwater flows were in direct response to the precipitation and runoff at the surface. In the passive zone, which was the central portion of the tunnel, the groundwater flows were initially large, but they decreased rapidly and were not appreciably affected by the annual precipitation and runoff.

Instrumentation

The Colorado Department of Highways retained a contractor to instrument the pilot bore for the purpose of measuring the loads on the sets and for the determination of strain rates and total strain around the pilot bore.

Two types of instruments were installed, in a total of 41 instrument stations, to make the measurements: electronic load cells and bore-hole extensometers. The load cells were placed between the legs of the sets and the foot blocks, and at a few stations they were also placed in horizontal positions in the crown of the sets and between the legs and invert struts to measure horizontal loads. The bore-hole extensometers, which were of single-anchor and multiple-anchor types, were placed in bore holes, generally 25 ft in depth, drilled into the roof and walls of the tunnel. A detailed description of the instrumentation was presented by Abel (1) and Grosvenor and Abel (2).

In support of the instrumentation, the position of the wooden blocking placed between the instrumented sets and the walls and arch of the pilot bore was mapped at 1:24.

From the data furnished it was possible to calculate the total maximum and stable loads on the sets in pounds, the maximum and stable geologic rock loads in pounds per square foot as defined by Terzaghi (10), the wall and arch deflections in inches, and the height of the ground arch (10, p. 60) in feet and to relate these to the geologic conditions and the engineering practices in the pilot bore (7).

Comparison of Predictions and Findings

One of the main purposes of the Straight Creek project was to evaluate a statistical method of compiling geological information and predicting geologic conditions at depth in the pilot bore. Table 1 gives a compilation of the predictions and the findings of this project. In general, there is a relatively close agreement between most of the predictions and the findings, indicating the validity of the method. The table, however, does not tell the complete story, neither where the prediction and findings are in close agreement nor where they are not in agreement; both cases are important and both need some explanation.

The predictions were based on a pilot bore 8,050 ft long, 10.5 ft wide, and 11.5 ft high, supported by square-set timbers. As a result of a landslide at the east portal (8), the east portal was moved about 150 ft south and the portal grade lowered about 16 ft. This lengthened the pilot bore to about 8,350 ft. Also, during construction, steel rather than timber sets were used for the most part, and the diameter of the pilot bore, outside the steel, averaged about 13 ft. Two types of steel sets were used: 4-in. I-beam weighing 7.7 lb/ft and 6-in. H-beam weighing 25 lb/ft.

Geologic Measurements

The geologic features predicted were the percentage of pilot bore length that would be within the different rock types; the percentage that would be within the different

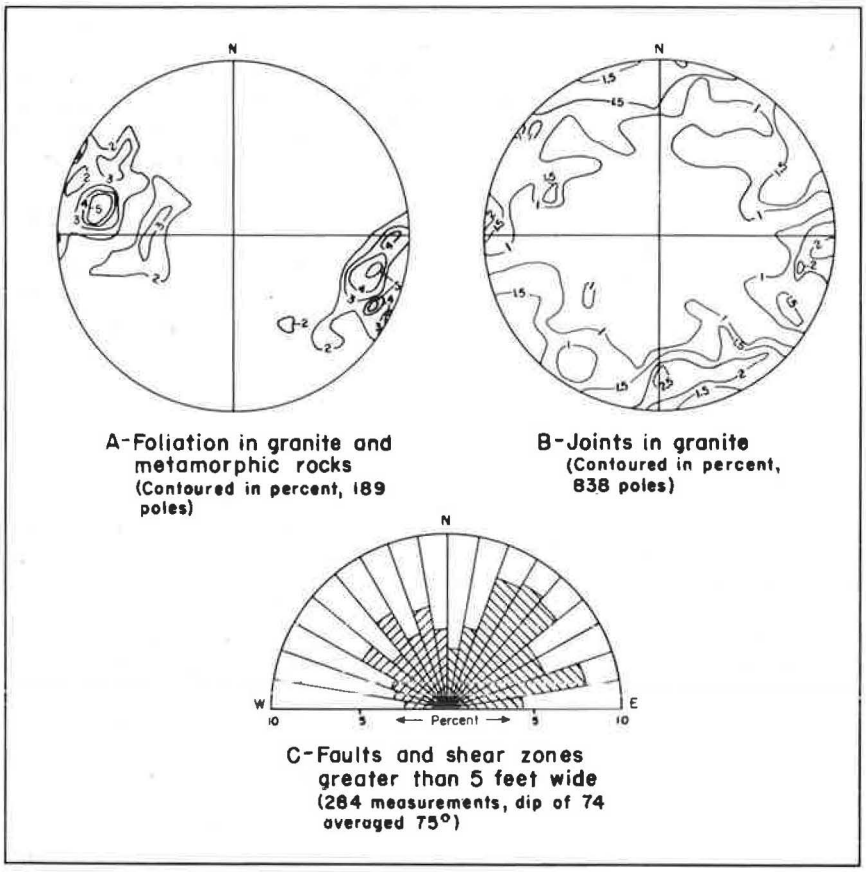

Figure 2. Contour diagrams (lower hemisphere) of the foliation and joints, and a strike-frequency diagram of the trends of faults and shear zones compiled from surface mapping.

categories of fracture density; the percentage that would be in faults or shear zones; and the attitudes of the foliation, joints, faults, and shear zones.

Rock Types—The findings in the pilot bore of 75.4 percent granite, 23.8 percent metasedimentary rocks, and 0.8 percent diorite dikes compare well with the predicted 75 percent granite and 25 percent metasedimentary rock. The results show that the surface and drill-hole data were adequate to define the rock-type percentages.

Fracture Density—The fracture density categories as defined on the surface were modified in the underground mapping. The fracture density categories given in Table 1 are a combination of the surface and the underground systems. This combining was done to make the predictions and findings comparable.

A preliminary analysis of the results of the instrumentation and of the geology of the pilot bore indicates that the fracture density categories used are probably not the most significant ones from an engineering standpoint (7). Apparently, when the average-size block of rock or the average distance between fractures exceeds 0.5 ft, the rock loads that develop are more dependent on the nature of the surface of the fracture than on the size of blocks or the spacing of fractures. Also, the loads increase greatly with an increase in rock alteration. The largest loads developed in the shear zones where the rock had been ground to fine sand or smaller size; most of the minerals were altered to clay minerals, and the zone was damp. A better definition of fracture density, taking into account the amount of alteration, is needed. The attitude and degree of foliation, even in schistose rocks, had only a minor influence on rock loads.

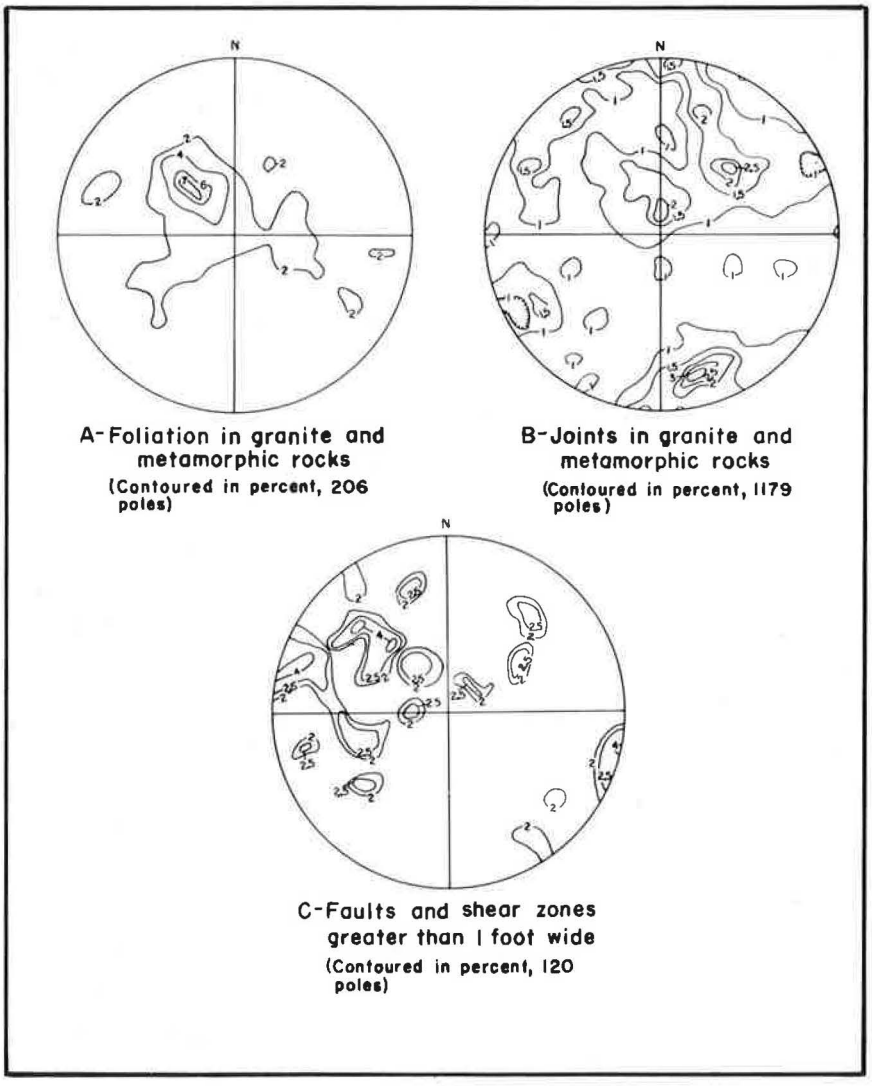

Figure 3. Contour diagrams (lower hemisphere) of the foliation, joints, and faults and shear zone compiled from pilot-bore mapping.

Faults and Shear Zones—Underground, faults or shear zones greater than 1 ft wide were used to calculate the sum of the widths of the faults and shear zones. The prediction, however, was based on surface faults and shear zones greater than 5 ft wide. The change in criterion was made because the pilot bore could be mapped with more precision than was possible on the surface. The prediction that 51 percent of the total length of the pilot bore would be in faults and shear zones is considered well within the limits of mapping accuracy for the measured 49 percent.

In the 6-sq mi area, the strike or trend of 284 faults greater than 5 ft wide was measured, but the dip could be measured on only 74 (Fig. 2c). Of these, 24.7 percent had a strike or trend between N. 20° E. and N. 50° E., and 44.8 percent between N. 20° E. and N. 80° E. The average dip of the 74 faults was 75° either southeast or northwest. Underground, the attitude of 120 faults and shear zones greater than 1 ft wide was measured (Fig. 3c). Two maxima are defined—one representing faults that strike about N. 45° E. and dip 40°-60° SE. and one representing faults that strike about N. 20° E. and dip about 75° SE.

These figures would appear to compare favorably with the predictions when it is considered that there is only 4.0 percent outcrop at the surface in the 6-sq mi area and that the pilot bore is essentially a linear feature across the area but with 100 percent exposure. The prediction that no fault or shear zone greater than 5 ft in width would be expected to follow the tunnel for considerable distance was upheld.

The preliminary analysis of the geology and the results of the instrumentation in the pilot bore (7) indicated that in part the loads are probably related to the apparent angle of dip of the faults and shear zones in relation to the trend of the pilot bore. The maximum loads developed where the apparent dip of faults and shear zones was about 45°. The loads were less where the dips were greater or less than 45°. It was also indicated that the width of a fault or shear zone must be about one-half the diameter of the pilot bore before any effect on the loads could be noticed. Better methods, possibly the geophysical methods, for defining the widths and attitudes of faults and shear zones at the surface are needed.

Attitudes of Joints—The prediction that the joints in the pilot bore would strike in any direction was confirmed by the mapping of the pilot bore (Figs. 2b, 3b). The average dip of 60° determined at the surface was high when compared to the average dip of 45° determined in the pilot bore.

In the mapping of the pilot bore, the attitudes of the joints on the walls and on the heading faces were compiled separately, which resulted in considerably different contour diagrams. On the walls, relatively fewer joints having a N. 45° E. strike and northwest dip were recorded, whereas on the faces fewer joints having a N. 20° E.-N. 20° W. strike and northwest or southwest dip were recorded. This comparison indicates that what is considered a significant joint, and so recorded, depends on the trend of the surface in the tunnel being mapped in relation to the attitude of the joint and the direction of the tunnel heading. Figure 3b was compiled from all the recorded joints on the wall and from about an equal number randomly selected from the face mapping. About four times as many joints were measured on the faces as on the walls because of the scale of mapping and the number of faces mapped.

Attitudes of Foliation—The strike of the foliation at the surface (Fig. 2a) agrees closely with that in the pilot bore (Fig. 3a), but the dip at the surface is considerably higher than that in the pilot bore. A possible explanation of this difference may lie in the number of measurements made in the granite in relation to the number made in the metamorphic rocks; the measurements of both have been combined on the diagrams. Data from surface mapping (Fig. 2a) represent 161 measurements in granite and 28 in the metamorphic rocks; data from pilot-bore mapping (Fig. 3a) represent 93 measurements in granite and 113 in the metamorphic rocks. Also, in the pilot bore, the relation of the surface of measurement to the attitude of the foliation (as with the joints) probably influences the number of observations made.

Engineering Measurements

The items considered under the engineering measurements are rock load, final swell pressure of fault gouge, and groundwater flow.

Rock Load—The maximum rock load of 5,900 psf was based on the preliminary design of a 10.5 × 11.5-ft tunnel, utilizing the theories of Terzaghi (10). The final pilot bore, however, averaged about 13 ft in diameter. The predicted maximum rock load for this size tunnel would be 6,970 psf.

The results of the instrumentation of the pilot bore required a modification of the theories of Terzaghi (10) for stress around a tunnel. As the face advances away from a point, a maximum load develops on the support at that point, which after a period of time usually declines to a stable load. The time required for the development of the maximum load and the magnitude of the maximum load, and the time required for the load to stabilize and the magnitude of the stable load, are dependent on the geologic conditions, the construction practices, and the dimensions of the tunnel. It is possible within certain limits to determine the part of the load that is the result of the construction practices and the part that is the result of geologic conditions (7).

The part of the rock load that is the result of the geologic conditions is termed the geologic rock load, and the part that is the result of the construction practices is termed the engineering rock load. The geologic conditions were divided into three categories, representing the range in rock quality or competency, depending on a range in fracture density and a range in the percentage or alteration. The range in the geologic rock loads for each geologic category was calculated from the results of the instrumentation. From this range in geologic rock loads a geometric midpoint for each geologic category was calculated. The geometric midpoint is that geologic rock load that, when multiplied by or divided by a range factor, gives the range in geologic rock loads for the geologic category. The range factor is simply the number which, when multiplied by the geometric midpoint of the geologic rock load, yields the maximum geologic rock load. The minimum geologic rock load is obtained by dividing the geometric midpoint of the geologic load by the same range factor. For the pilot bore, the geometric midpoint for the worst geologic category, where the maximum geologic rock loads developed, was 6,600 psf with a range factor of 1.5. Thus, the range in geologic rock loads for the worst geologic category was 4,400 to 9,900 psf. As a result of the worst geologic conditions and the construction practices, the maximum rock load that developed in the pilot bore was about 20,000 psf.

The predicted rock load and the measured geologic rock load cannot be directly compared because the existing theories for predicting loads are not entirely adequate. Probably, the calculated geometric midpoint for the worst geologic conditions most closely fits the theory as developed by Terzaghi (10).

Final Swell Pressure of Fault Gouge—Swell pressure predictions were based on the assumption that the clay mineralogy of fault gouge and altered rock would be essentially the same in the pilot bore as at the surface. The average final swell pressure of 29 samples collected from the pilot bore was 1,727 psf, which compares favorably with an average final swell pressure of 2,233 psf from 6 surface samples. Thus, the assumption that the final swell pressures of samples from the surface would be about the same as for samples from the pilot bore appears valid.

Groundwater—The figures for the prediction of the average flow from the portal and the flow actually measured have little significance. The authors failed in their original calculations and predictions to consider the time of year and the influence of the spring runoff. The average groundwater flow from the portal was increased by a factor of 7.5 times as a result of the spring runoff.

The predicted flow of 300 gpm from the portal 2 wk after completion of the pilot bore was based on a constant rate of advance of the pilot bore of 1,000 ft per month. The average rate for the pilot bore, however, was only about 610 ft per month. At this rate of advance, the estimated flow would have been about 183 gpm. These figures, although comparable, are meaningless because the influence of the spring runoff was not considered. If the pilot bore had been completed in the spring, the measured flow would have been much greater than the predicted flow.

All the flow calculations were based on estimates of the porosity and permeability of the faults and shear zones. In the pilot bore, however, the faults and shear zones were essentially dry until they were opened up. The principal water flows came from open joints in relatively competent rock that were beyond the limits of the faults and shear zones. The approximate agreement of the predicted and measured groundwater flows, therefore, can be considered due more to luck than to skill.

Construction Practices

The predictions of the spacing of sets, lagging and blocking, feeler holes, and amount of grout were, of necessity, empirical, because actual requirements can be determined at the time of construction. It was felt that such predictions, however, would be of value in estimating the cost of construction. Geologic conditions alone do not determine requirements; other factors, some of which have been discussed in relation to the geologic rock load, also exert an influence.

Set Spacing—In the pilot bore, the sets were not uniformly spaced, particularly where jump sets were added. For the purpose of comparison with the prediction, spacings of

0.5 to 1.5 ft were combined and compared with predicted spacing of 1 ft, 1.5 to 2.5 with 2 ft, 2.5 to 4.5 with 4 ft, and 4.5 and greater with 5 ft.

The predicted and actual spacing of sets agree very well when all the factors that influence support are considered, plus the fact that the length of the pilot bore was increased by approximately 300 ft. The total number of sets calculated from the predicted spacing of sets was 2,691. The actual number used was 2,059, although the calculated number of sets based on our combining of the actual set spacings is 2,274.

It was predicted that 1.4 percent of the pilot-bore length would require invert struts on 1-ft centers, or a total of 113 struts. The contractor used struts for 8.0 percent of the pilot-bore length or 210 struts, but these were on 1 to 3-ft centers.

Lagging and Blocking—The predictions for lagging and blocking specified sections of the pilot bore that would require blocking only, blocking and lagging along the arch, and blocking and lagging along the arch and walls. In practice, it was more convenient to record the percentage of blocking and lagging around the walls and arch. The predicted figures in Table 1 are converted to percentages for comparative purposes.

Feeler Holes—The drilling of feeler holes was recommended in the pre-construction report (5), and the approximate areas in which they might be advisable were indicated. In practice, the Colorado Department of Highways and the contractor considered it advisable to keep at least one feeler hole about 40 ft in advance of the face for most of the length of the pilot bore, a decision in which the authors concurred. For that reason, there is a considerable difference—by a factor of almost 4 times—between the predicted number of linear feet of feeler holes and the footage actually drilled. The larger percentage of the feeler holes did not intersect broken, water-saturated ground, which was their purpose. From economic and safety points of view, however, feeler holes were advisable in that they gave the contractor a better idea of the ground in advance of the face and allowed him to plan more economically for such things as lengths of round and supplies (sets, timber, etc.) needed in the pilot bore.

Grout—It was predicted that it might be economically advantageous to grout, in advance of the face, certain types of ground as determined by feeler holes. The purpose of the grout is to consolidate bad ground and seal off water, and thus reduce the amount of support required and the difficulty of driving through that section. The alternative is closely spaced supports and forepoling. This decision is the prerogative of the contractor and the owner, and it was decided that grout was not needed in the pilot bore.

Cost—The pilot bore was holed through during the first week of December 1964 and cleanup work was completed in January 1965. The total cost of construction of the pilot bore was approximately $1,400,000, which compares favorably with the contractor's bid of $1,300,000.

CONCLUSIONS

The accuracy of a geologic projection depends on the understanding of the geometry of the geology, the amount of time available for surface examination, the amount of time and money for physical exploration involving drill holes and the application of geophysical techniques, and the knowledge and experience of the geologists. The Straight Creek Tunnel project has established that geology can be treated statistically to predict the kinds and percentages of different geologic conditions at depth, and that engineering requirements can be equated with predicted geologic conditions to provide a sound basis for estimating probable cost of construction. The failures of some of the predictions of the project have shown those fields in which there is not adequate geologic and engineering knowledge. Continued research in the prediction of geologic and engineering conditions at the depth of a tunnel should make possible more accurate predictions and so reduce the cost of construction by the amount required for contingencies.

The Straight Creek Tunnel project was conducted in an area with a limited number of geologic variables, which probably in part accounts for its success. It is believed, however, that a similar approach can be successfully applied to the projection of geology to depth in any geologic environment if the geometry of the geology is thoroughly understood and carefully analyzed.

REFERENCES

1. Abel, J. F., Jr. Tunnel Instrumentation. The Mines Magazine, Vol. 55, No. 1, pp. 20-23, 1965.
2. Grosvenor, N. E., and Abel, J. F., Jr. Measurements on the Pilot Bore for the Straight Creek Tunnel. Highway Research Record 135, pp. 27-34, 1966.
3. Hurr, R. T., and Richards, D. B. Ground-Water Engineering Geology of the Straight Creek Tunnel (pilot bore), Colorado. Eng. Geology (in press), 1966.
4. Lovering, T. S., and Goddard, E. N. Geology and Ore Deposits of the Front Range, Colorado. U.S. Geol. Survey Prof. Paper 223, 1950.
5. Robinson, C. S., and Lee, F. T. Geology of the Straight Creek Tunnel Site, Clear Creek and Summit Counties, Colorado, and Its Predicted Effect on Tunnel Construction. U.S. Geol. Survey Open-File Rept., 1962.
6. Robinson, C. S., and Lee, F. T. Geologic Research at the Straight Creek Tunnel Site, Colorado. Highway Research Record 57, pp. 18-34, 1964.
7. Robinson, C. S., and Lee, F. T. Preliminary Report on the Engineering Geology of the Straight Creek Tunnel Pilot Bore, Clear Creek and Summit Counties, Colorado. U.S. Geol. Survey Open-File Rept., 1965.
8. Robinson, C. S., Carroll, R. D., and Lee, F. T. Preliminary report on the Geologic and Geophysical Investigations of the Loveland Basin Landslide, Clear Creek County, Colorado. U.S. Geol. Survey Open-File Rept., 1964.
9. Scott, J. H., and Carroll, R. D. Surface and Underground Geophysical Studies at Straight Creek Tunnel Site, Colorado. Presented at the 46th Annual Meeting and published in this RECORD.
10. Terzaghi, Karl. Rock Defects and Loads on Tunnel Supports. In Rock Tunneling with Steel Supports (R. S. Proctor, and T. L. White), Commercial Shearing and Stamping Co., Youngstown, Ohio, pp. 17-99, 1946.

Surface and Underground Geophysical Studies At Straight Creek Tunnel Site, Colorado

JAMES H. SCOTT and RODERICK D. CARROLL, Geophysicists, U. S. Geological Survey, Denver, Colo.

Seismic and electrical resistivity measurements were made in the Straight Creek tunnel pilot bore during and immediately after the period of construction. These underground geophysical measurements were interpreted to obtain the seismic velocity and electrical resistivity of rock behind the disturbed layer surrounding the pilot bore. Velocity and resistivity values were correlated statistically with the following economic and engineering parameters: time rate of construction, cost of construction per foot, rock quality, set spacing, percentage lagging and blocking, type of steel support required, height of tension arch, and vertical load. The quality of these correlations was quite good, with correlation coefficients ranging from about 0.8 to nearly 1.0 in absolute value.

Results indicated that if correlations such as these were established during the early stages of construction of a tunnel, or if they were established from previous measurements in another tunnel of similar dimensions, constructed by similar techniques, and in rock of a similar type, predictions of economic and engineering parameters could be made to guide construction in the new tunnel. Predictions could be based on geophysical measurements made on the surface above the tunnel, or on measurements made underground in feeler holes drilled ahead of the working face.

The accuracy of predictions based on surface geophysical measurements was tested by making seismic and resistivity surveys on the surface and in holes drilled from the surface along the line of the pilot bore. Results indicated that reasonably accurate predictions are possible from surface measurements. Greater accuracy and more detailed information would be obtained if predictions were based on geophysical logging measurements made in feeler holes drilled ahead of the working face. Because the cost of geophysical surveys is small compared with the cost of tunnel construction, it is concluded that predictions of this type would reduce the total cost of tunnels by increasing construction efficiency.

•THE U. S. Geological Survey made surface and underground geophysical measurements in the area of the Straight Creek tunnel pilot bore as part of a general program of research conducted in cooperation with the Colorado Department of Highways. Geophysical measurements of seismic velocity and electrical resistivity were made underground along the walls of the pilot bore. Additional measurements of velocity and resistivity were made on the surface and in holes drilled from the surface over the line of the bore.

Paper sponsored by Committee on Engineering Geology and presented at the 46th Annual Meeting.

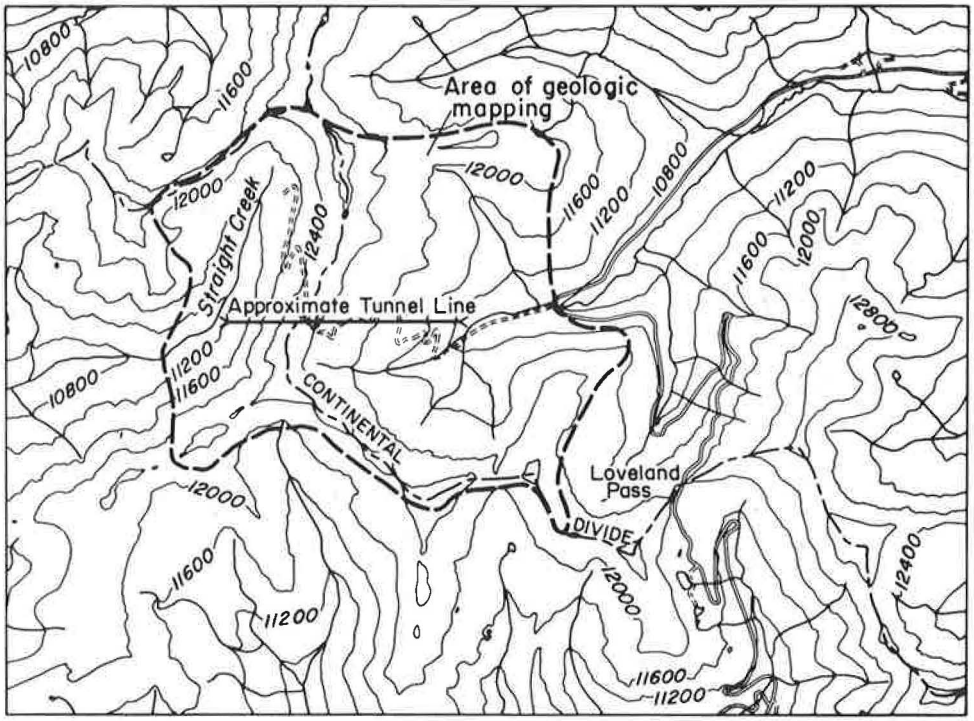

Base map from Loveland Pass quadrangle, 1958

0 2 MILES

CONTOUR INTERVAL 400 FEET
DATUM IS MEAN SEA LEVEL

Map of Straight Creek area

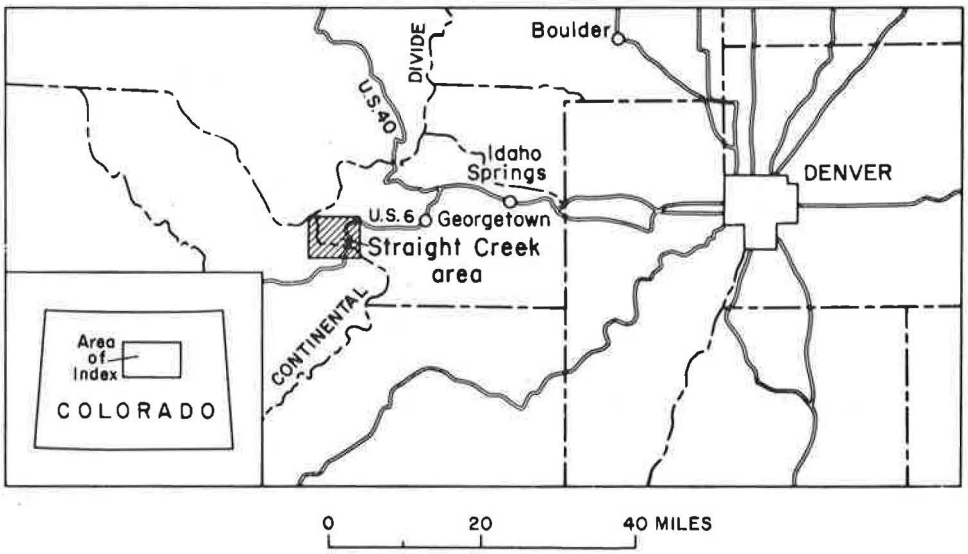

Location of Straight Creek area

Figure 1. Index maps of Straight Creek area, Colorado.

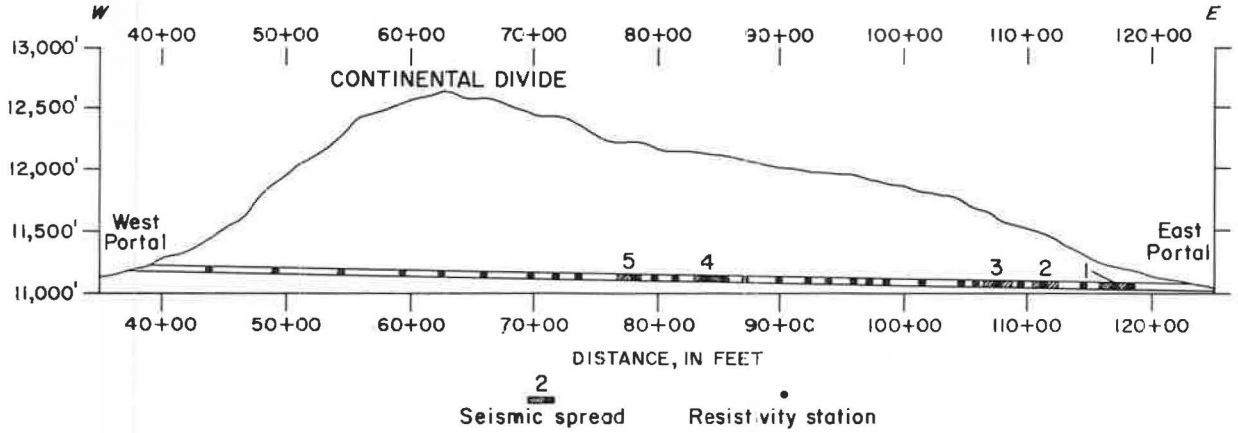

Figure 2. Cross section of Straight Creek tunnel pilot bore showing locations of underground geophysical measurements.

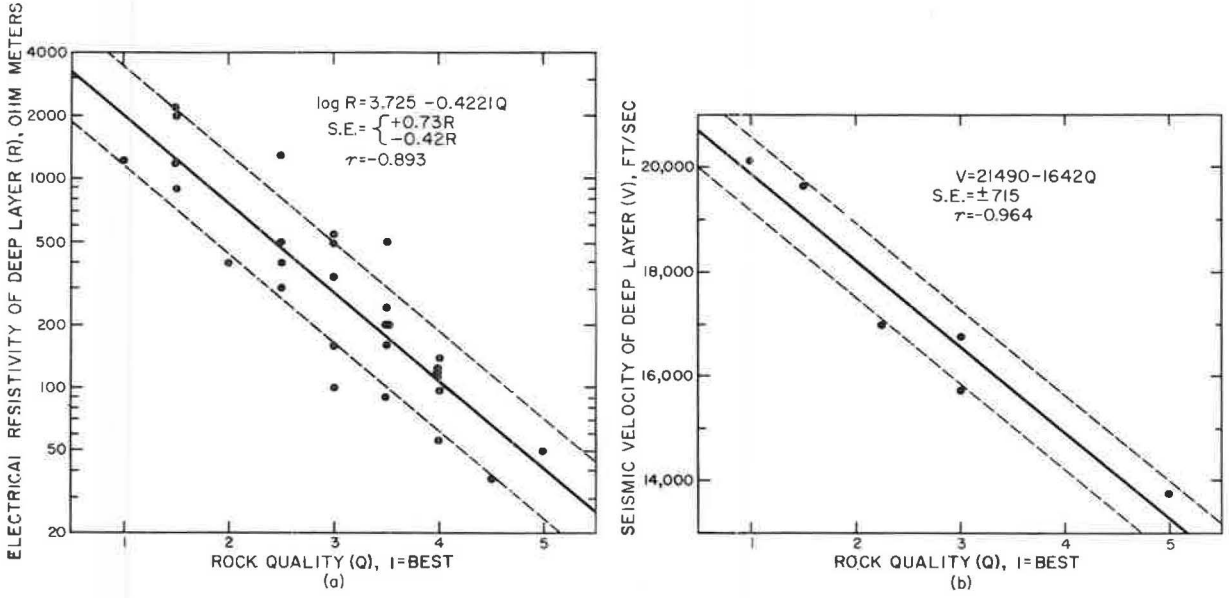

Figure 3. Rock quality (see Table 1) plotted against: (a) electrical resistivity of deep layer and (b) seismic velocity of deep layer.

This report discusses the results of the underground studies, the statistical relationships developed from them, and the results obtained from geophysical measurements made on the surface and in holes drilled from the surface.

The pilot bore in which the geophysical measurements were made is approximately 13 ft in diameter and 8, 300 ft long. The bore is located about 55 mi west of Denver, and passes beneath the Continental Divide between the Loveland ski area on the eastern slope and the headwaters of Straight Creek on the western slope of the Rocky Mountains (Fig. 1). The pilot bore was driven to obtain geologic and engineering information required for efficient construction of a twin-bore highway tunnel to be part of I-70.

GEOLOGY

A detailed surface geologic mapping program in the vicinity of the Straight Creek tunnel pilot bore was completed before construction of the bore (1). Results indicated that bedrock in this area consists chiefly of Precambrian granite (about 75 %) with inclusions of Precambrian metasedimentary rock (about 25 %—composed of biotite-rich gneiss, schist, and migmatite), and a few small dioritic dikes of probable Tertiary age. The bedrock is extensively faulted and sheared and is locally altered. Regional geology and major faulting in the area are described by Lovering and Goddard (2). Although outcrops are plentiful, most of the bedrock is overlain by thin deposits of colluvium, talus, landslide material, and swamps. Results of the pre-construction surface geologic mapping were used to predict general geologic conditions and engineering characteristics of the rocks at the depth of the pilot bore. These predictions, and the information on which they are based, are described by C. S. Robinson and F. T. Lee (3).

UNDERGROUND GEOPHYSICAL MEASUREMENTS

Electrical resistivity and seismic refraction measurements were made in the pilot bore at locations shown in Figure 2. Measurement locations were chosen so that the full range of rock quality existing in the pilot bore was sampled. Rock of lowest quality was characterized by intensive fracturing and severe mineral alteration. Rock of highest quality was nearly free of fractures and mineral alteration.

Underground seismic measurements were made with high-resolution 10-channel refraction seismic equipment capable of detecting energy in the frequency range 10 to 4, 000 cps. Accelerometers, used to detect the seismic energy from explosive energy sources, were emplaced along the tunnel walls about 4 ft above the floor in linear arrays about 200 ft long. Spacings between accelerometers ranged from 5 to 25 ft. Small explosive charges (0. 1-lb dynamite) were detonated in 1-ft deep shot holes drilled into the rock at both ends and at the midpoint of each array of 10 accelerometers. Seismic energy was recorded on photosensitive paper by means of an oscillograph having a paper speed of 250 in./sec. The time intervals between detonation of the explosive charge and arrival of seismic energy at each accelerometer were determined from the oscillograph records, and were plotted on graph paper against distance between the shot point and each detector. Average rock velocity along the detector arrays was obtained from these graphs. Interpretations of velocity layering indicated that a zone of anomalously low velocity rock (4, 200 to 10, 800 ft/sec) surrounds the opening and has a thickness ranging from less than 1 ft to about 17 ft. The existence of this layer is attributed to blast damage and to movement of rock toward the center of the opening along fracture and fault surfaces in response to stresses created by the bore. This movement, confirmed by extensometer measurements, evidently causes the velocity of rock in the disturbed layer to decrease because of enlargement of gaps along fractures and faults. The velocity of rock behind the anomalous layer is characteristic of the undisturbed rock (13, 750 to 20, 150 ft/sec). A more detailed discussion of seismic instrumentation, field procedure, and interpretation methods is given by Scott et al (4).

Underground electrical resistivity measurements were made with conventional Gish-Rooney equipment and special sponge-rubber electrodes impregnated with a mixture of brine and bentonite to provide good electrical contact with the rock exposed along the walls of the pilot bore. Measurements were made using the Wenner electrode configuration with electrode spacings expanded from 1 to 30 ft in a stepwise manner,

keeping the array symmetrical about a center point and parallel with the tunnel axis. This procedure provided a means of interpreting resistivity layering from the surface to a depth of 10 ft or more. Apparent resistivity values obtained from these measurements were corrected for tunnel geometry and plotted against electrode spacing on log-log graph paper. The plotted points were then interpreted by curve-matching methods, using theoretically derived curves representing two layers having a variety of resistivity contrasts (5). Interpretations indicated that a rock layer having a relatively high resistivity (60 to 5, 300 ohm-meters) surrounds the opening and has a thickness ranging from less than 1 ft to about 10 ft. The anomalously high resistivity of this layer is attributed to evaporation of moisture from rock exposed to air. The depth of exposure is probably affected by the depth of severe fracturing caused by blasting. The resistivity of rock occurring behind this layer is characteristic of undisturbed rock (36 to 2, 200 ohm-meters). A more detailed discussion of electrical resistivity instrumentation, field procedure, and interpretation techniques for the underground measurements is given by Scott et al (4).

Interpretations of the geophysical data indicated that the layer of high-resistivity rock surrounding the tunnel was generally thinner than the corresponding layer of low-velocity rock. The difference in thickness may be attributed to a difference in the mechanism causing the anomalous layers detected by the two types of measurements. In electrical resistivity, the anomalous layer is probably caused by evaporation and fracturing chiefly within the blast-damaged zone which in most places is restricted to a depth of only a few feet. In seismic velocity, however, the anomalous layer is believed to be caused by the adjustment of rock in response to stress and subsequent enlargement of gaps along fractures and faults that may occur at depths of 10 ft or more in poor-quality rock.

STATISTICAL CORRELATIONS BASED ON UNDERGROUND MEASUREMENTS

Statistical correlations of underground geophysical data with engineering and construction data were based on the resistivity and velocity of rock behind, rather than within, the anomalous layers surrounding the pilot bore. The reasons for using values for the deep layer were (a) the correlations appeared to be more consistent than those made with data from within the anomalous layers, and (b) appraisal of the predictability of engineering and economic data from geophysical data obtained ahead of construction would require that the correlations be based on geophysical data from relatively undisturbed rock.

Rock Quality

Cursory comparisons of geophysical data and rock quality at various locations in the pilot bore suggested that as rock quality improved, seismic velocity and electrical resistivity both tended to increase. To test the degree of apparent correlation statistically, it was necessary to establish a numerical scale for rating rock quality along the walls of the pilot bore. An arbitrary numerical scale of 1 through 5 was established (4) in which 1 represented the best, and 5 the poorest, rock (Table 1). Quantitative criteria used for rating rock quality included fracture spacing and mineral alteration (% rock); qualitative criteria were faulting, foliation and schistosity, and rock type. The criteria are given in the table in descending order of importance in determining the numerical rating. Figure 3 shows rock quality plotted against electrical resistivity and seismic velocity of rock behind the disturbed layer. In this figure, and in all other figures showing statistical correlations, the solid line represents the regression line determined by the method of least squares, and the dashed lines represent plus and minus one standard error. Numerical values of standard error are indicated in the figures by S. E. and the correlation coefficient by r. Because the values of r in Figure 3 are numerically close to ± 1, the quality of the correlations between geophysical values and rock quality is very good. For a perfect correlation $r = \pm 1$, and for a complete lack of correlation $r = 0$.

In Figure 3, and in the other figures showing correlations, electrical resistivity data generally show a greater degree of scatter than seismic velocity data. This difference in

TABLE 1

ROCK QUALITY BASED ON GEOLOGIC CHARACTERISTICS—STRAIGHT CREEK TUNNEL PILOT BORE

Quality[a]	Fracture Spacing (ft)	Mineral Alteration (% rock)	Faulting	Foliation and Schistosity	Rock Type
1	>3	< 5	None	None; prominent banding in migmatite.	Predominantly granite or diorite dikes; sparse migmatite.
2	1 to 3	5 to 10	Minor; a few slicks and minor gouge.	Poorly defined; prominent banding in migmatite.	Commonly granite; sparse gneiss and migmatite.
3	0.3 to 1	10 to 15	Moderate; slicks common, minor gouge.	Poorly to well defined; may be absent in granite.	Granite and metamorphics, occurrences about equal.
4	0.1 to 0.3	15 to 20	Moderate to severe; slicks and gouge on most surfaces.	Well defined in metamorphics; may be absent in granite.	Commonly schist, gneiss, or migmatite; sparse granite.
5	<0.1	>20	Intense; frequency of gouge seams may be greater than fracture spacing.	Very well defined; may be absent in granite.	Predominantly schist; sparse granite.

[a]In this scale, 1 represents the best, and 5 the poorest, rock.

scatter is attributed to a difference in the volume of rock sampled by the two geophysical measurements. Velocity values represent averages over sections of the pilot bore that are 3 to 6 times longer than those from which resistivity data were obtained.

Because it could be expected that nearly all engineering and economic aspects of construction would be affected to some degree by the quality of rock penetrated by the pilot bore, and because the geophysical data correlated quite well with rock quality, a series of correlations were made using the geophysical data and the following parameters: (a) height of tension arch, (b) stable vertical load, (c) set spacing, (d) lagging and blocking, and (e) rate of construction and cost per foot.

Height of Tension Arch

The height of the tension arch was determined from extensometer and load cell measurements. These measurements indicated that after the large initial stress associated with the advancing face had declined to a stable value, rock near the periphery along the back and walls of the pilot bore had moved inward toward the opening in response to tensional stress, and that rock at greater depths had moved outward away from the opening in response to compressional stress. The height of the tension arch was taken as the point of no movement that separated the two zones. At locations where extensometer measurements were not made, the height of the tension arch was estimated from load cell data, using the following formula:

$$H = L/D \qquad (1)$$

where

H = height of tension arch, ft,
L = stable vertical rock load, psf, and
D = rock density, pcf.

Estimates based on this formula are considered justified because the load on tunnel sets is largely determined by the height of the column of rock in the tension arch above the tunnel.

Figure 4 shows the statistical correlations between the height of the tension arch and electrical resistivity and seismic velocity of rock behind the disturbed layers.

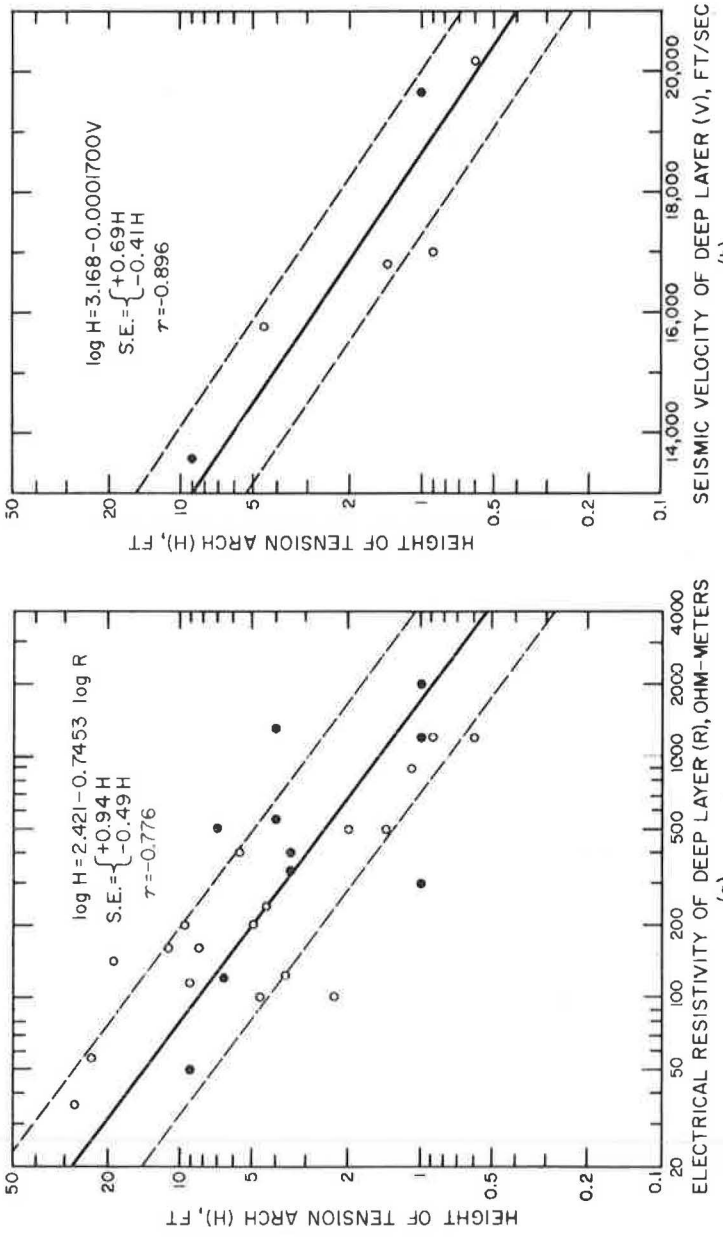

Figure 4. Height of tension arch plotted against: (a) electrical resistivity of deep layer and (b) seismic velocity of deep layer; solid circles represent values of H obtained from extensometer measurements and open circles represent values estimated from load cell data.

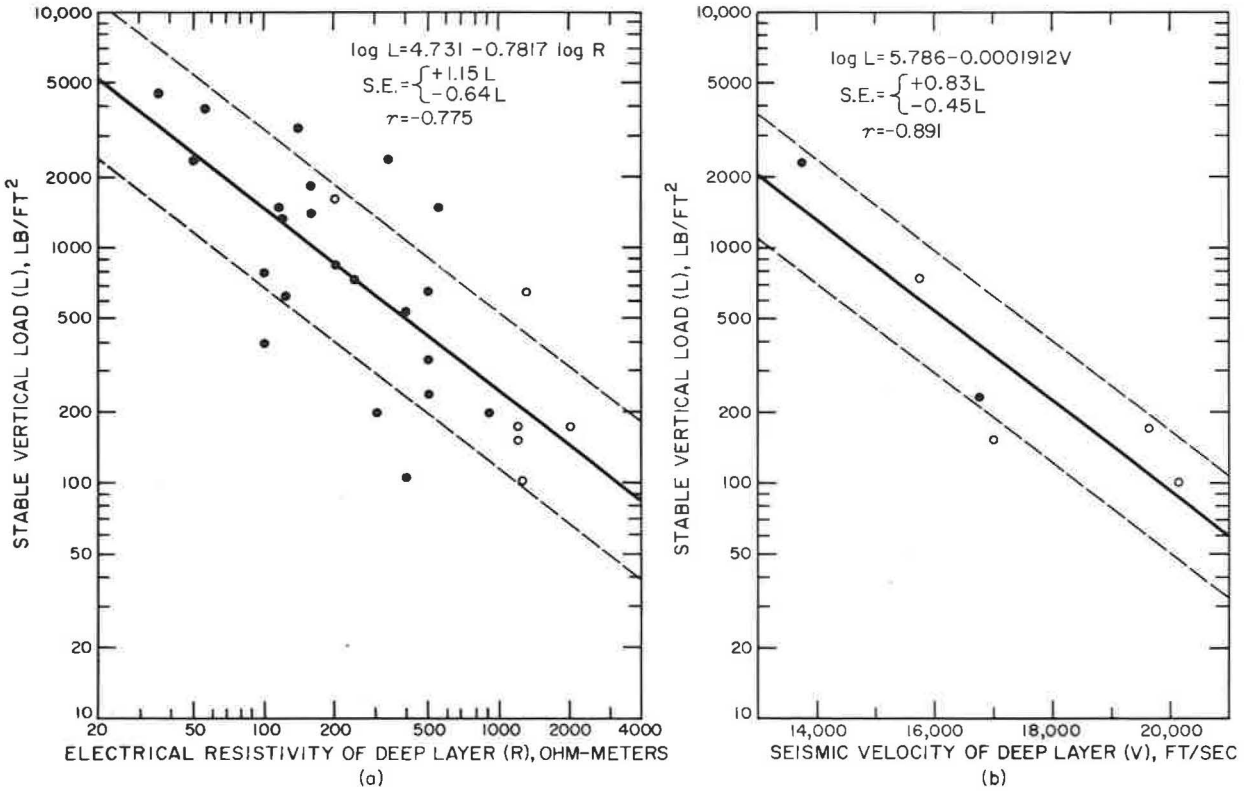

Figure 5. Stable vertical rock load plotted against: (a) electrical resistivity of deep layer and (b) seismic velocity of deep layer; solid circles represent values of L obtained from load cell measurements and open circles represent values estimated from extensometer data.

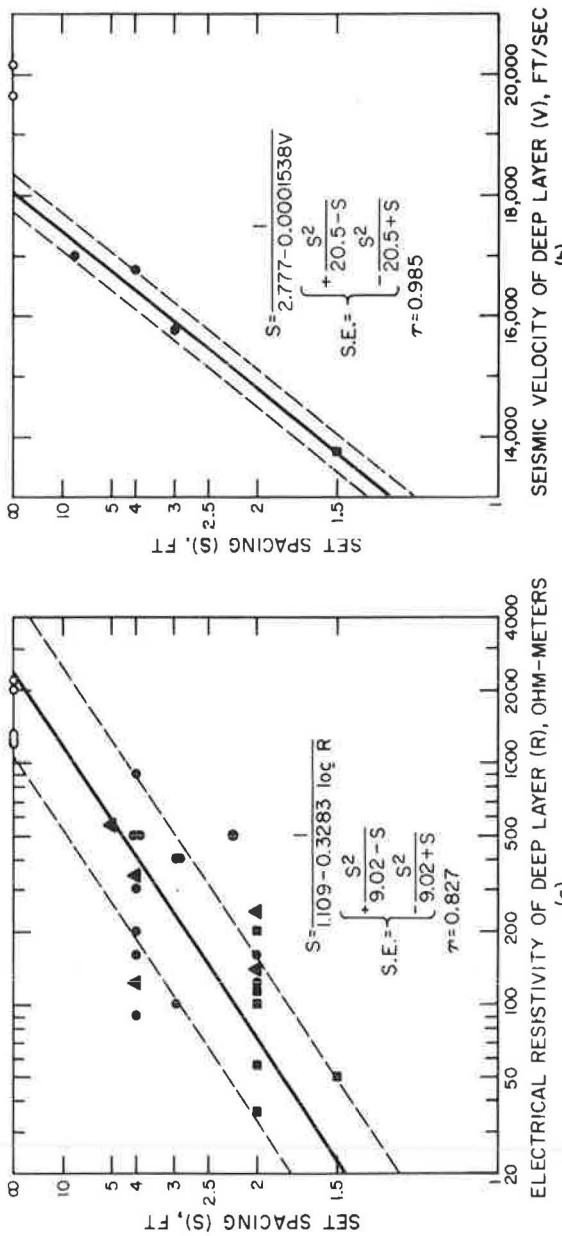

Figure 6. Set spacing plotted against: (a) electrical resistivity of deep layer and (b) seismic velocity of deep layer. (In graph b data points representing no support, open circles, were omitted in calculating the equation of the regression line because the data suggest an abrupt change of slope.)

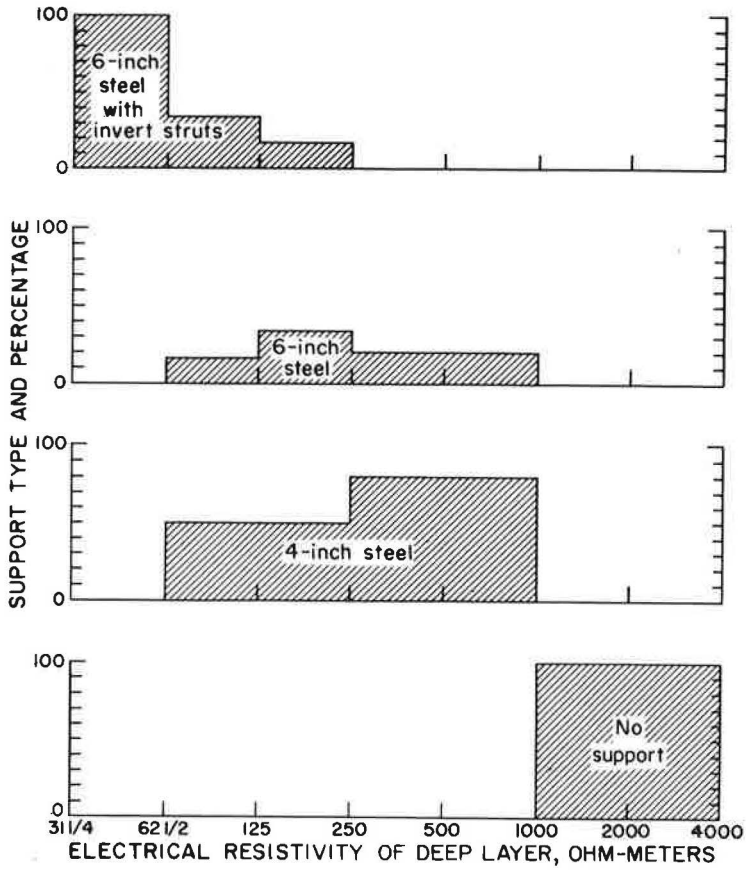

Figure 7. Support type and percentage used in rock classified on the basis of electrical resistivity of deep layer; resistivity class intervals are logarithmic.

Stable Vertical Rock Load

Load cell measurements were used as the basis for correlations between stable vertical rock load, electrical resistivity, and seismic velocity. Stable vertical rock loads were calculated from the load cell measurements by the following formula:

$$L = W/A \qquad (2)$$

where

L = stable vertical rock load, psf,
W = weight measured by load cell, lb, and
A = area of influence; sq ft = tunnel width × set spacing.

At locations where load cell measurements were not made, but estensometer measurements were available, loads were estimated from Eq. 1 solved for L.

Figure 5 shows statistical correlations between stable vertical rock load and electrical resistivity and seismic velocity.

Set Spacing and Type of Support

Average set spacing was determined over the intervals where underground geophysical measurements were made, and correlations were established between average set

spacing and corresponding values of velocity and resistivity. Figure 6 shows that reasonably good statistical correlations exist between set spacing and both electrical resistivity and seismic velocity.

Figure 7 shows that a relationship also exists between resistivity data and the type of support required in a section of tunnel. In the Straight Creek tunnel pilot bore, for example, 6-in. steel arches and invert struts were required in all sections where resistivity was less than about 62 ohm-meters, and no support of any kind was required in sections where resistivity exceeded 1,000 ohm-meters. A similar relationship could probably have been established between type of support and seismic velocity if sufficient velocity data had been available.

Predictions of set spacing and type of support required, based on geophysical measurements made in advance of construction, would improve the efficiency of tunneling by providing the contractor with estimates of required supplies.

Lagging and Blocking

Another statistical study was made using lagging and blocking data. Figure 8 shows that the percentage of lagging and blocking correlates rather well with both electrical resistivity and seismic velocity. For the purposes of this correlation, the percentage scale is based on the following extremes: 0 percent implies that no lagging or blocking was necessary, and 100 percent implies that all available space around the steel sets was lagged and blocked.

Rate of Construction and Cost Per Foot

The quality of the previously described correlations suggests that there might be a direct correlation between the geophysical values and the rate of construction and cost per foot. Cost and rate of construction information were obtained from Miles (8). Figure 9 shows that these correlations do exist. The cost per foot values were obtained by assuming a constant average cost per day and dividing this value by rate of construction. This is not completely valid, because cost per day fluctuated as the cost of labor and materials varied during the period of construction. However, the assumption of constant cost per day is considered sufficiently accurate for obtaining first approximation cost estimates from the correlations.

SURFACE GEOPHYSICAL MEASUREMENTS

Electrical resistivity and seismic refraction measurements were made on the ground surface and in holes drilled from the surface over the line of the pilot bore (Fig. 10).

Surface seismic measurements were made with five mobile seismic refraction units provided by the U. S. Geological Survey. These units are described in detail by Warrick et al (6). Geophones were placed on the ground surface over the line of the pilot bore at intervals of approximately 600 ft. In addition, probes containing geophones were lowered into and fastened to the walls of drill holes 2 and 3 at depths of 712 and 526 ft, respectively. Charges of 25 to 50 lb of dynamite (60% gel) were stemmed with water and detonated at depths ranging from 70 to 100 ft in shot holes drilled near the two portals of the pilot bore. Air shots of 15 to 20 lb of dynamite were detonated 4 ft above the ground surface at three locations between the portals to determine the thickness of shallow velocity layers not detectable from in-hole shots. Velocity layering interpretations were made by plotting the refraction travel times obtained from the seismic records against the distance between shot holes and surface geophones, and then computing the thickness of layers represented by the plotted points. Results of the interpretation indicated that three distinct layers of rock occur approximately parallel to the surface (Fig. 10). The upper layer has an average velocity of 5,070 ft/sec and extends to depths ranging from 35 to 90 ft. This layer probably represents rock that is badly weathered and heavily fractured. The middle layer has an average velocity of 12,400 ft/sec and extends to depths ranging from 180 to 465 ft. The third layer has an average velocity of 16,400 ft/sec and an unknown thickness. Underground seismic measurements indicate that the velocity of the third layer is somewhat higher than

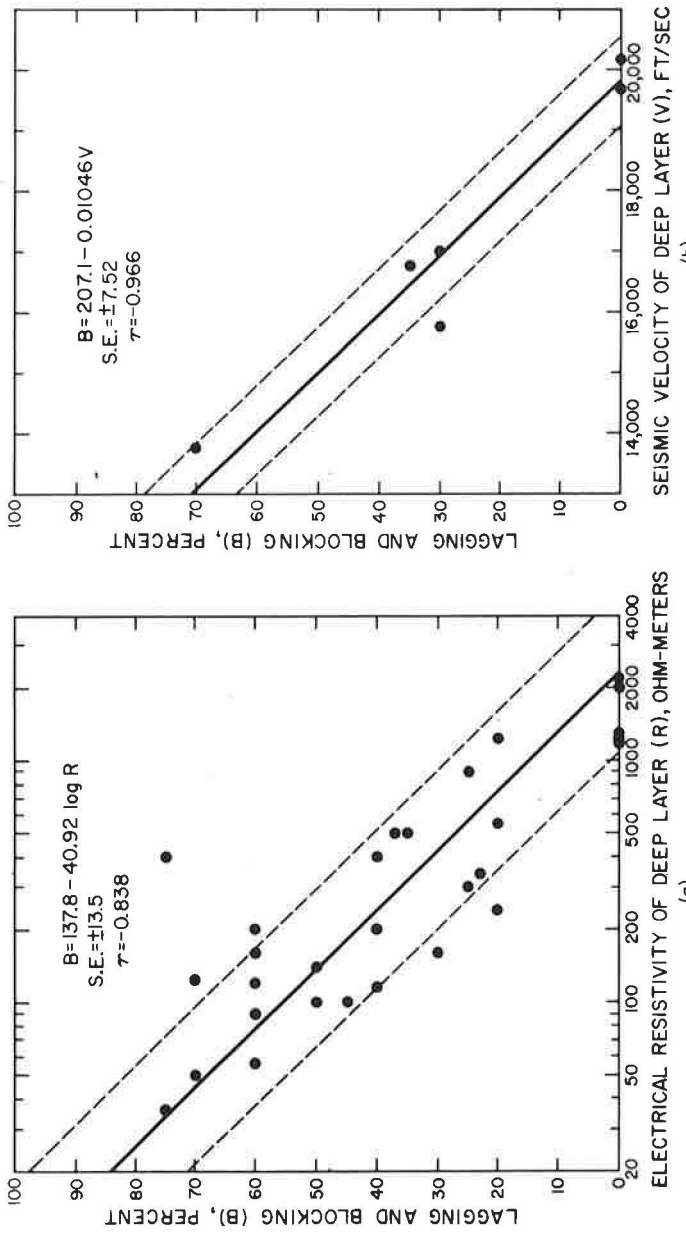

Figure 8. Lagging and blocking plotted against: (a) electrical resistivity of deep layer and (b) seismic velocity of deep layer.

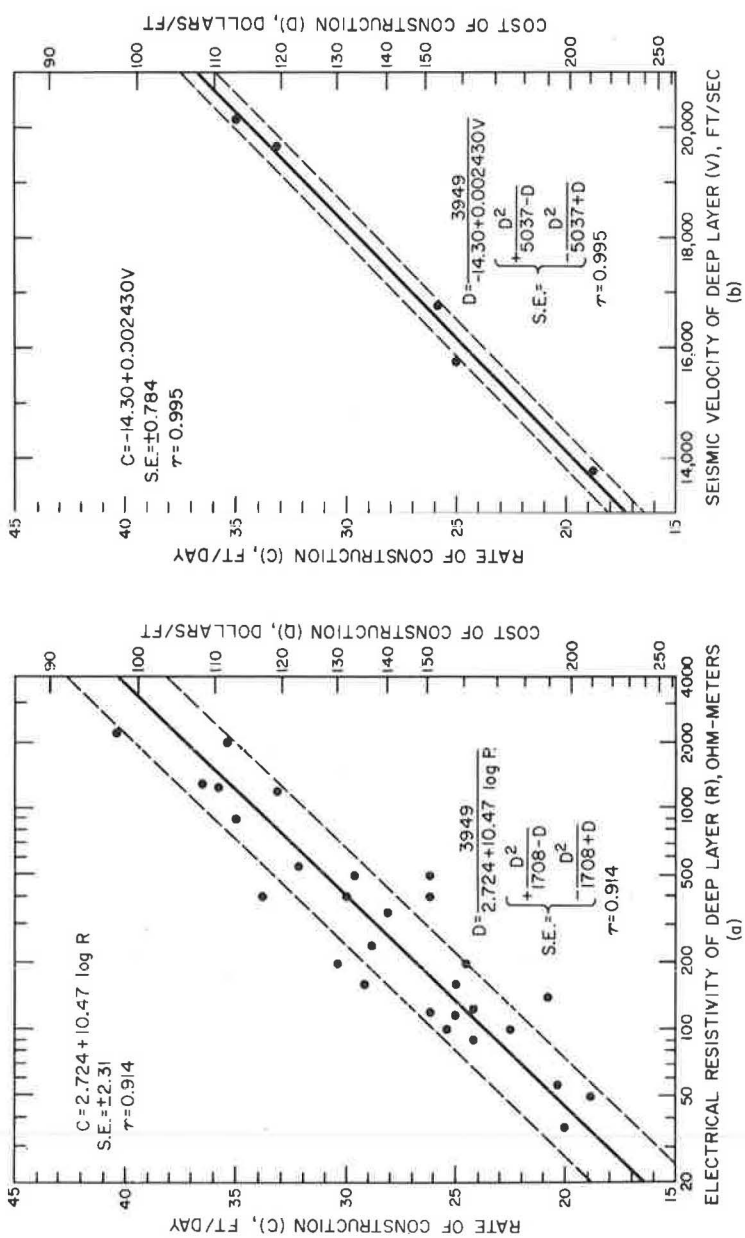

Figure 9. Rate of construction and cost per linear foot plotted against: (a) electrical resistivity of deep layer and (b) seismic velocity of deep layer.

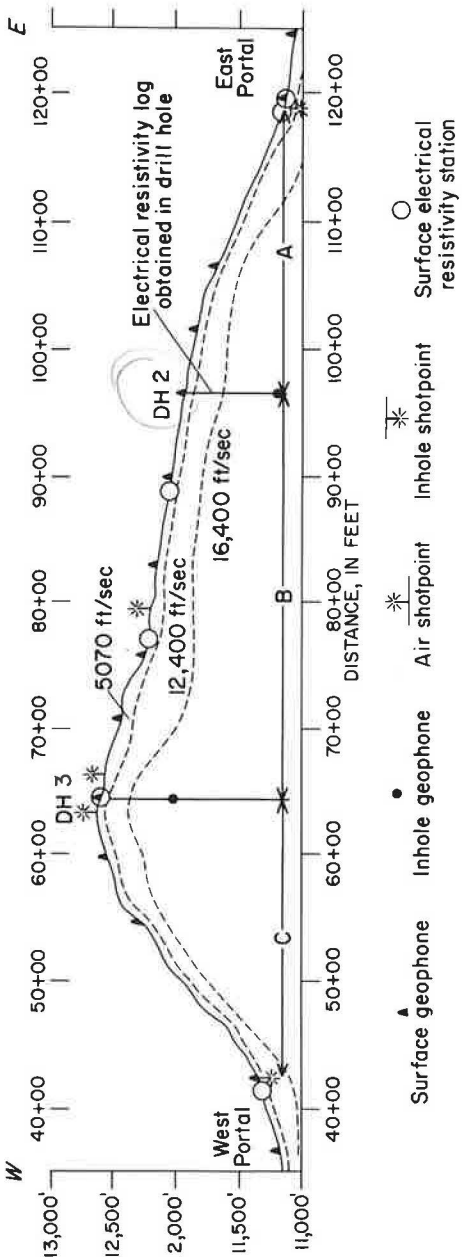

Figure 10. Cross section of Straight Creek tunnel pilot bore showing locations of surface and in-hole geophysical measurements and interpretation of seismic refraction survey. (A, B, C, indicate intervals discussed in text.)

the average velocity of rock occurring along the pilot bore. Because first arrival refraction energy followed this high-velocity layer, it was not possible to determine the velocity of rock at the depth of the pilot bore from the refraction seismic data. Fortunately, data for the direct seismic travel paths between the in-hole shot points and the in-hole geophones (intervals A, B, and C, Fig. 10) provided velocities that were more representative of rock at the level of the pilot bore. Estimates of engineering and economic parameters based on these direct travel-path velocities were made, using the correlations established underground. The results indicate that the estimates were reasonably accurate (Table 2).

Electrical resistivity measurements were made along the surface, at locations shown in Figure 10, with electrodes arranged in the Schlumberger configuration. A series of measurements was made at each location by expanding the electrode spacings in a stepwise manner, keeping the center of the array at a fixed location. This procedure caused current to flow over a range of depths from the near surface to below the level of the pilot bore. Interpretations were made by the curve-matching technique using two-layer Schlumberger curves and auxiliary curves (7). Resistivity values interpreted from the surface measurements were used, together with resistivity values obtained from an electric log in drill hole 2, to estimate the average resistivity of rock over intervals A, B, and C (Fig. 10) in the pilot bore. Results of estimates based on these average values are given in Table 3. These estimates are less accurate than those based on seismic velocity (Table 2). One possible cause for the difference in accuracy is that seismic velocity was determined along straight-line segments near the pilot bore, whereas surface resistivity measurements represented a large volume of rock surrounding the bore. The discrepancies between actual values and estimates based on resistivity indicate that the resistivity of rock in the immediate vicinity of the pilot bore was generally lower than the average resistivity of the large volumes of rock that influenced the surface resistivity measurements.

CONCLUSIONS

The statistical correlations relating underground geophysical measurements to

TABLE 2

ESTIMATED VS ACTUAL VALUES OF ENGINEERING AND ECONOMIC PARAMETERS, WITH ESTIMATES BASED ON DIRECT TRAVEL-PATH SEISMIC VELOCITIES[a] AND STATISTICAL CORRELATIONS[b]— STRAIGHT CREEK TUNNEL PILOT BORE

Section	Parameter								
	Seismic Velocity (ft/sec)	Avg. Set Spacing (ft)		Avg. Lagging and Blocking (%)		Avg. Rate of Construction (ft/day)		Cost of Construction ($)[c]	
		Est.	Act.	Est.	Act.	Est.	Act.	Est.	Act.
Interval A	15,360	2.4	3.7	46	51	23	17	420,000	420,000
Interval B	15,260	2.3	2.9	48	35	23	26	560,000	540,000
Interval C	17,360	9.4	7.3	26	13	28	29	370,000	440,000
East portal to west portal	15,740	4.5	4.6	40	33	24	23	1,350,000	1,400,000

[a]Velocities measured between in-hole shot points and in-hole geophones (intervals A, B, and C, Fig. 10).
[b]Established from underground geophysical measurements.
[c]Data derived from Ref. 8.

engineering and economic parameters in the Straight Creek tunnel pilot bore indicate that the efficiency of tunneling, in general, may be improved by the judicious application of a geophysical program before and during construction.

Pre-construction geophysical measurements on the surface or in holes drilled from the surface would be useful for selecting a site if several alternative tunnel routes were under consideration. Although the correlations described in this paper would not be directly applicable to a tunnel driven in a different geologic environment, or to a tunnel of a different size driven in the same environment, the correlations do indicate that certain basic relationships exist between the measurable properties of rock and the economic and engineering aspects of tunneling. More specifically, in any given geologic environment, rock having high seismic velocity and high electrical resistivity is generally stronger and easier to excavate than rock having a low velocity and low resistivity. Therefore, even if appropriate correlations are not available, geophysical measurements would be useful for estimating the relative cost and difficulty of construction along each of several possible routes. If correlations are available from measurements made in a similar tunnel in the same environment, then quantitative estimates may be made.

After a site is selected, geophysical measurements made during the early stages of construction in long feeler holes drilled ahead of the working face could be used to establish correlations, or to improve existing ones. Then, when statistical tests indicate that sufficient data have been obtained to make the correlations valid, they could be

TABLE 3

ESTIMATED VS ACTUAL VALUES OF ENGINEERING AND ECONOMIC PARAMETERS, WITH ESTIMATES BASED ON SURFACE ELECTRICAL RESISTIVITY MEASUREMENTS, ELECTRIC LAG MEASUREMENTS[a], AND STATISTICAL CORRELATIONS[b]—STRAIGHT CREEK TUNNEL PILOT BORE

Section	Parameter								
	Electrical Resistivity (ohm-meters)	Avg. Set Spacing (ft)		Avg. Lagging and Blocking (%)		Avg. Rate of Construction (ft/day)		Cost of Construction ($)[c]	
		Est.	Act.	Est.	Act.	Est.	Act.	Est.	Act.
Interval A	177	2.7	3.7	46	51	26	17	380,000	420,000
Interval B	234	3.0	2.9	41	35	28	26	460,000	540,000
Interval C	606	5.1	7.3	24	13	32	29	320,000	440,000
East portal to west portal	332	3.6	4.6	37	33	29	33	1,160,000	1,400,000

[a]Drill hole 2.
[b]Established from underground geophysical measurements.
[c]Data derived from Ref. 8.

used to predict engineering and economic parameters ahead of construction. New data points could be added to the correlations as construction progressed, so that the accuracy of predictions would continue to improve throughout the period of construction.

Geophysical techniques and instrumentation are presently available for making measurements on the surface and in vertical drill holes before construction. Instrumentation for making seismic velocity and electrical resistivity logging measurements in feeler holes is not yet sufficiently developed to make measurements in a routine manner. It is considered feasible, however, to adapt standard geophysical logging equipment and techniques, most of which have been developed by the petroleum industry, to application in horizontal holes in tunnels. The main obstacle to overcome is that most standard logging techniques require the presence of fluid (water or drilling mud) in drill holes, so that it would be necessary either to develop methods for providing fluid in the feeler holes or to develop instrumentation capable of obtaining measurements in air-filled holes.

RECOMMENDATIONS

It is recommended that research be continued along two lines: (a) develop instrumentation and methods for making geophysical logging measurements in feeler holes drilled ahead of the working face, and (b) further test the validity of the correlations by collecting additional geophysical data, both on the surface and underground, in or near other existing tunnels. Eventually, if suitable geophysical instrumentation is developed, and if correlations are established for tunnels of different sizes constructed by various techniques in wide variety of geologic environments, it may be possible to make valid economic and engineering predictions for any tunnel from geophysical measurements made on the surface or underground in advance of construction. A predictive capability such as this would increase the efficiency of tunneling, and would probably eliminate the need for costly and time consuming pilot-bore construction.

REFERENCES

1. Robinson, C. S., and Lee, F. T. Geologic Research at the Straight Creek Tunnel Site, Colorado. Highway Research Record 57, pp. 18-34, 1964.
2. Lovering, T. S., and Goddard, E. N. Geology and Ore Deposits of the Front Range, Colorado. U. S. Geological Survey Prof. Paper 223, 1950, 319 pp.
3. Robinson, C. S., and Lee, F. T. Results of Geologic Research, Straight Creek Tunnel Pilot Bore, Colorado. Presented at the 46th Annual Meeting and published in this RECORD.
4. Scott, J. H., Lee, F. T., Carroll, R. D., and Robinson, C. S. The Relationship of Geophysical Measurements to Engineering and Construction Parameters in the Straight Creek Tunnel Pilot Bore, Colorado. Int. Jour. Rock Mechanics and Mining Sciences, 1967.
5. Roman, Irwin. Apparent Resistivity of a Single Uniform Overburden. U. S. Geological Survey Prof. Paper 365, 1960, 99 pp.
6. Warrick, R. E., Hoover, D. B., Jackson, W. H., Pakiser, L. C., Jr., and Roller, J. C. The Specification and Testing of a Seismic-Refraction System for Crustal Studies. Geophysics, Vol. 26, No. 6, pp. 820-824, 1961.
7. Zohdy, Adel A. R. The Auxiliary Point Method of Electrical Sounding Interpretation, and Its Relationship to Dar Zurrouk Parameters. Geophysics, Vol. 30, No. 4, pp. 644-660, 1965.
8. Miles, G. N. Oral communication, Colorado Dept. of Highways, March 1965.

Soil Structure Arching Analysis of Buried Flexible Structures

F. DWAYNE NIELSON, Assistant Professor of Civil Engineering, Engineering Experiment Station, New Mexico State University

Recent observations on buried structures made in the laboratory have led to the conclusion that one is not justified in using the classical Marston theory indiscriminately for loads on underground pipe. To allow for pressure redistribution across the top of a buried flat-roofed structure, a different differential element must be assumed. The one chosen was the shape of a circular arch. After selecting the differential element, the problem of determining the location of the soil arch support in the soil mass for the differential element arises. There is no physical justification for assuming that the arch extends only across the prism of soil directly above the buried structure. The location of the soil arch support was assumed to be at the location of the maximum shear stress within the soil mass as determined by the theory of elasticity. If any movement or strain in the soil should occur, the major part of it should take place in the region of maximum shear stress. The theory of elasticity is not used for determining the stress in the differential soil arch; it is used only to locate the region of maximum shear stress before any slippage of the soil grains occurs. It is proposed that a movement or strain within the soil mass will cause the differential arch to form. A differential equation was written using the circular arch. When all of the necessary parameters, including nonlinear modulus of passive resistance for soil, were included, the resulting differential equation was not readily integrable; therefore, a numerical integration procedure was used to obtain solutions. Results were compared with model studies and with several field installations where adequate information was available.

•THE inadequacies of the methods of analysis of underground structures are apparent when the actual deflection and ultimate load carrying capacity of these structures are compared with values predicted by existing theories. With the advent of the Interstate Highway System and the interest of Civil Defense in underground blast shelters, buried structures have become very important. Several theories to determine loads on buried structures have been presented, but they only partially explain the observed phenomena. One of the first studies made on the analysis of loads on underground conduits was undertaken by Marston (6). Figure 1 shows a free body diagram of loading which Marston assumed in deriving the equation for loads on underground pipe.

Laboratory observations of flexible membranes over flat topped model structures have yielded results that the Marston theory cannot explain. Figure 2 shows a model used in the test. By placing a parapet wall above the top of the structure, pressures transmitted to the flexible membrane are greatly reduced (3). The Marston theory cannot explain pressure redistribution across the top of the membrane. Measured results show the pressure at the edge of the membrane to be much greater than the pressure at the center. Because the Marston theory does not allow for pressure redistribution across the top of flat top structures, nor for pressure reduction on the membrane

Paper sponsored by Committee on Buried Structures and Committee on Culverts and Culvert Pipe and presented at the 46th Annual Meeting.

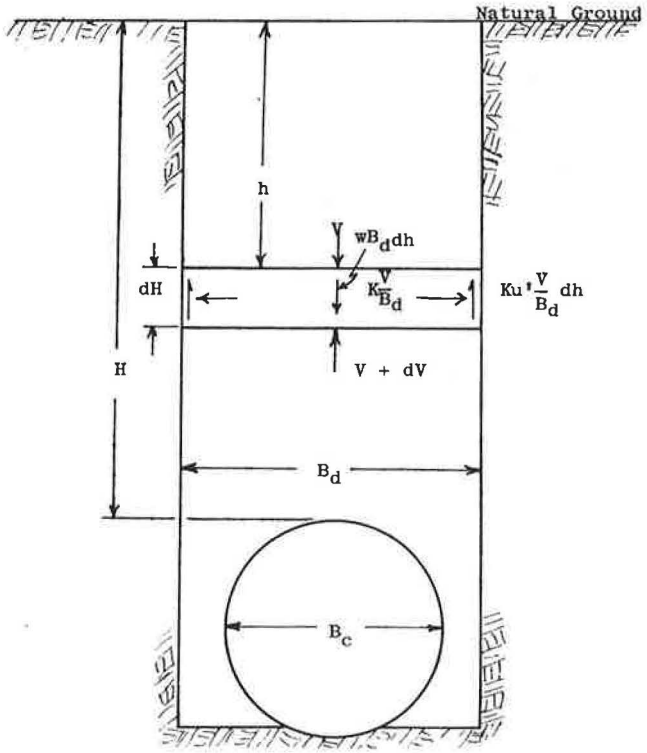

Figure 1. Classical free body diagram of loading assumed on buried conduits.

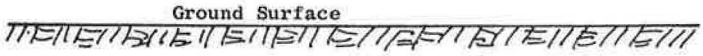

Backfill Material

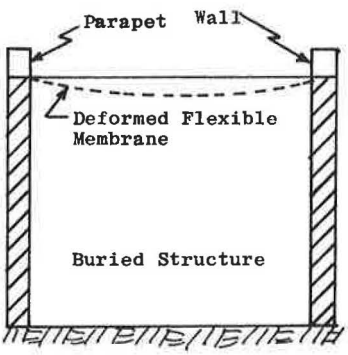

Figure 2. Buried flexible membrane.

caused by placing a parapet wall above the structures, a different shape of differential element has been selected for this study. Another disadvantage in the use of the Marston theory is the selection of a proper settlement ratio for installations other than the ditch conduit. Spangler's tables (9) indicate that the load transmitted to the buried structure depends greatly on the settlement ratio. At the present time the selection of a settlement ratio is based on experience with field installations.

There have been many other theories (1, 2, 7, 12), but each is either an adaptation in some form of Marston's original concept or of the theory of elasticity.

ANALYSIS OF THE PROBLEM

To allow for pressure redistribution across the top of the structure and pressure reduction caused by the parapet wall, a different differential element must be accepted. Several types of elements could be used, but the arch seems to be the most convenient and logical one. Using a differential element the shape of an arch, redistribution across the top of the structure and pressure reduction caused by placing the parapet wall above the flexible membrane can be explained. One arch is assumed to act on top of another. The pressure transmitted away from the buried structure is the pressure which acts as the differential arch support.

As the support for the differential element gets closer to the structure, the stresses increase. These stresses are normally slightly greater than the active pressure. On reaching the parapet wall, the stresses approach the at-rest pressure condition. This causes the arch to transmit the greater part of the pressure to the parapet wall rather than to the roof of a membrane structure. As the radius of the arch grows smaller, the assumed arch support acts on the roof of the structure. The arch support stresses are higher at the edge than at the center of the roof. The pressure on each succeeding differential element becomes lower than the one directly above it. This causes the pressure at the arch support to decrease as it moves towards the center of the structure. The pressure acting on the roof is the arch support pressure.

If the loading on the differential element is uniformly vertical, an arch must be selected that has no tensile stresses within its assumed shape. Such an arch is parabolic. If the loading is the uniform radial loading, the shape of the arch must be circular in order that no tensile stresses or bending stresses occur in the section. The vertical components of each one of these loadings are the same. Therefore, a radial loading can be assumed and still give the same vertical pressure distribution as the parabolic arch.

Once the shape of the arch is selected, the problem of locating the arch supports arises. Unless the conduit is in a trench with relatively rigid sides, there is no physical basis for assuming that the arch extends only through a prism of soil directly above the pipe. If the vertical prism cannot be assumed, other means must be used for locating the soil arch supports.

LOCATION OF SOIL ARCH SUPPORTS IN AN EARTH FILL

If the conduit is placed in an earth fill with no well-defined shear planes for the arch to form against, other means must be used for determining the location of soil arch supports. If it is assumed that most of the strain or movement within the soil above the conduit occurs between regions of maximum shear stress and that the movement of soil between the regions of maximum shear stress is downward, an approximate solution can be found. According to the theory of elasticity, two regions of maximum shear stress form, one on each side of a hole, at approximately 45 deg. The exact location is shown later. The maximum shear stress in a soil conduit system is assumed to act in the same location.

The pressure of a flexible conduit causes it to deflect downward. The soil directly above the conduit follows, causing the soil arch to form. The ends of the arch or arch supports are assumed to be at the region where the shear stress was maximum before any movement occurred. As the soil moves downward it acts as a wedge, and the more the movement the higher the stresses in the soil arch. Consequently, more force is transmitted away from the pipe into the surrounding fill, and the total load the pipe is required to carry is reduced.

The region of maximum shearing stress can be determined from the theory of elasticity. However, when the shear stress in the soil causes the grains to move, there is a redistribution of stress, and the theory of elasticity no longer applies. But, as soon as the grains move, the soil arch forms; therefore, the theory of elasticity can be used to locate supports resulting from an incipient motion of the soil arch. Timoshenko and Goodier (15) have given the equations for stress at a point in an infinite plate with a circular hole. Watkins and Nielson (13) have taken the equations and determined the region of maximum shearing stress. The equation is

$$\cos 2\theta = \frac{3a^4 - 2a^2r^2 - r^4}{4(-3a^2r^2 + 2r^4)} \tag{1}$$

where

θ = angle from vertical to plane of maximum shear,
a = radius of hole, and
r = distance to point (r, θ) on maximum shear plane.

This equation can be approximated fairly accurately with a hyperbola as follows:

$$\cos 2\theta = a^2/r^2 \tag{2}$$

Figure 3 shows a comparison between Eqs. 1 and 2.

The validity of this analysis as applied to soils can be evaluated by a critical analysis of studies made to determine the movement of soils around a buried pipe. One such study was made by Watkins (14) who placed lead shot in a grid pattern in the soil mass around a model pipe. As the model was loaded, the movement of the lead shot was followed by taking a series of X-ray pictures (Figs. 4 and 5).

To determine the stress patterns induced by the addition of a pipe in the soil, the displacements of the soil without the pipe (Fig. 5) were subtracted from the displacement of the soil with the pipe in place (Fig. 4). Figure 6 shows the relative magnitude of difference in displacement by arrows which represent the direction and magnitude movement of the soil due only to the influence of the pipe. The direction of the arrows indicates the direction of the major principal stress in a soil medium. The minor principal stress is at an angle of 90 deg to the major principal stress.

If a line is drawn through the soil mass perpendicular to the major principal stress at all points (Fig. 6), it will trace out the line of action of the differential soil arch that

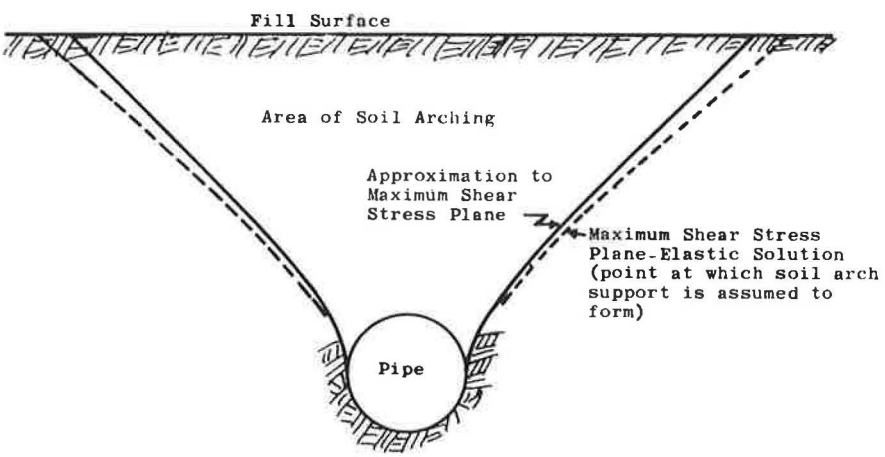

Figure 3. Comparison of elastic solution and assumed approximation for location of region of maximum shear stress which is assumed as location of soil arch support.

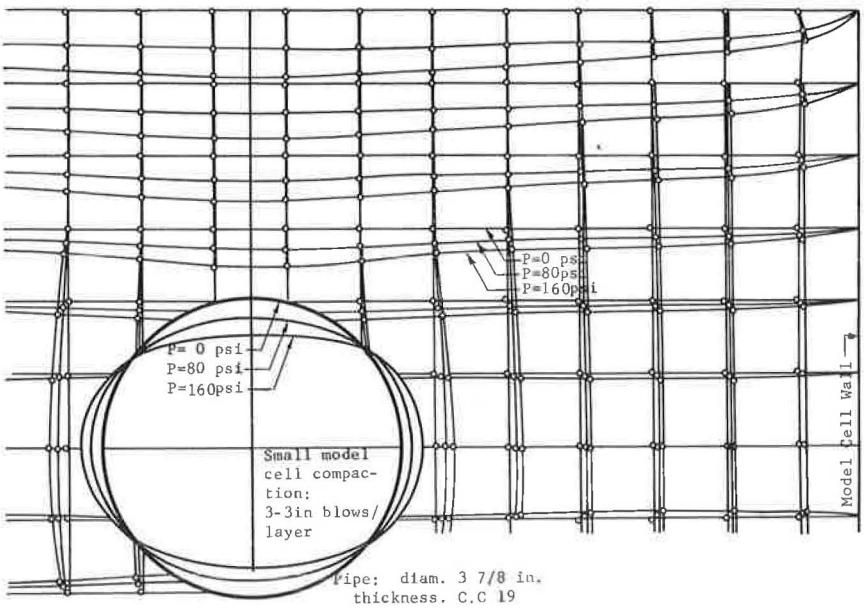

Figure 4. Superimposed position of lead shot in loess from X-ray photographs at various pressures (after Watkins).

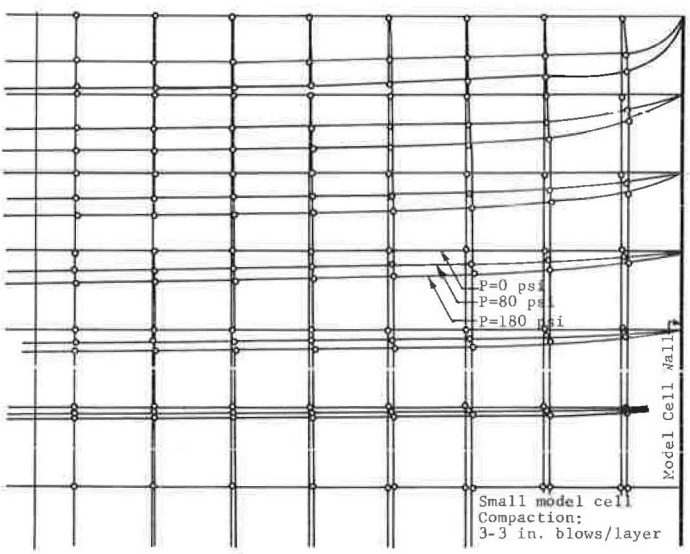

Figure 5. Superimposed positions of lead shot from X-ray photographs for loess with no model pipe at various pressures (after Watkins).

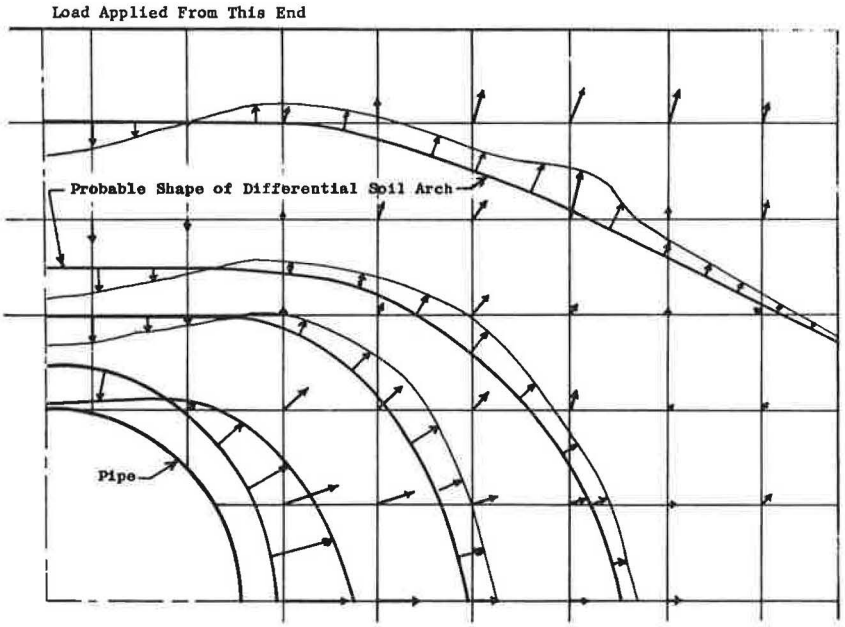

Figure 6. Movement of lead shot due only to influence of pipe as determined from X-ray study (determined by subtracting movement in Fig. 5 from movement in Fig. 4).

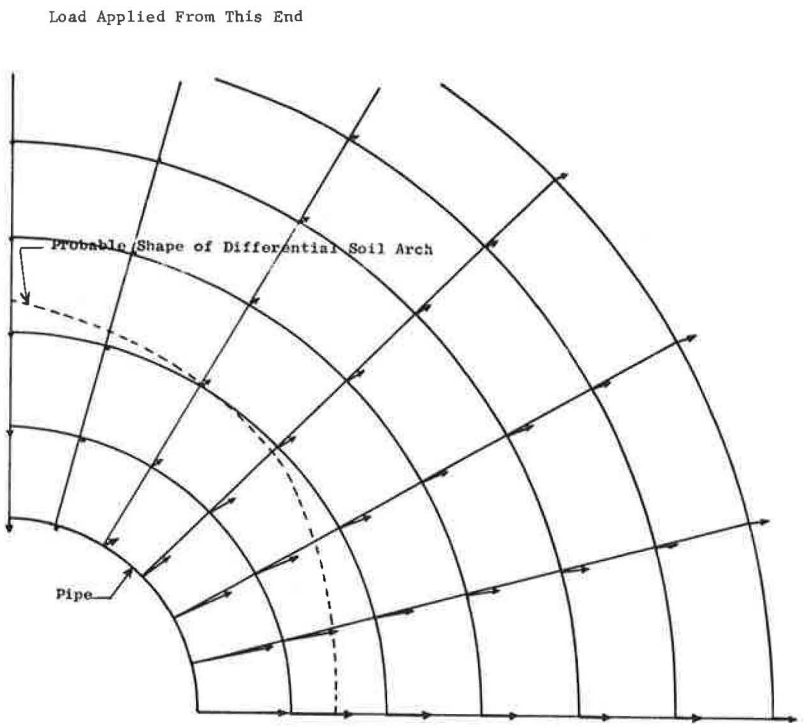

Figure 7. Displacements in elastic plate as determined from theory of elasticity; obtained by subtracting displacements in plate with no hole from displacements in plate with pipe.

has no shear or bending stress within its section. The differential element traced out is somewhat flatter than the circular arch. It is not known what effect the boundaries of the cell had on the displacement pattern obtained. To get some idea of the magnitude of the influence of the cell wall, an analysis of the same problem was made using the theory of elasticity with the equations presented by Burns and Richard (1). The displacement of an infinite elastic plate with a stiffening ring was calculated, and the displacement of an infinite elastic plate without the ring was calculated and subtracted, as before with the X-ray study. The results should show the displacement pattern of the median due only to the influence of the ring (Fig. 7). The displacement pattern was approximately the same as those obtained from the X-ray analysis, except that the line following the direction of the minor principal stress is somewhat higher than a circle. The differential element which would be obtained from this analysis would be more the shape of a parabola.

There is one difference between the displacement obtained in the soil by the X-ray analysis and those obtained from the theory of elasticity. The movement of the soil directly above the pipe is greater in the soil than in the elastic media. As a result of movement in the soil mass, the arch in the soil would be somewhat flatter or would approach a configuration of a true circle. It seems justifiable to assume the shape of the differential arch in a soil mass as a circle without adding an appreciable error to the solution.

The results of another study by Watkins and Nielson (13) are shown in Figure 8. It shows only the difference in vertical displacement between soil mass with the pipe in place and the same soil mass under the same loading conditions without the model pipe or hole. There is one major difference between this study and the X-ray study: the pipe in this study was bored into place. The soil was compacted without the pipe; then a hole was bored slightly larger than the diameter of the pipe, and the pipe was placed in the hole. As the pipe was loaded it could exert only limited, if any, horizontal pressure because the hole was larger than the pipe. Therefore, the horizontal component of pressure exerted by the pipe on the soil mass was missing. Eq. 2 essentially bound the observed displacements.

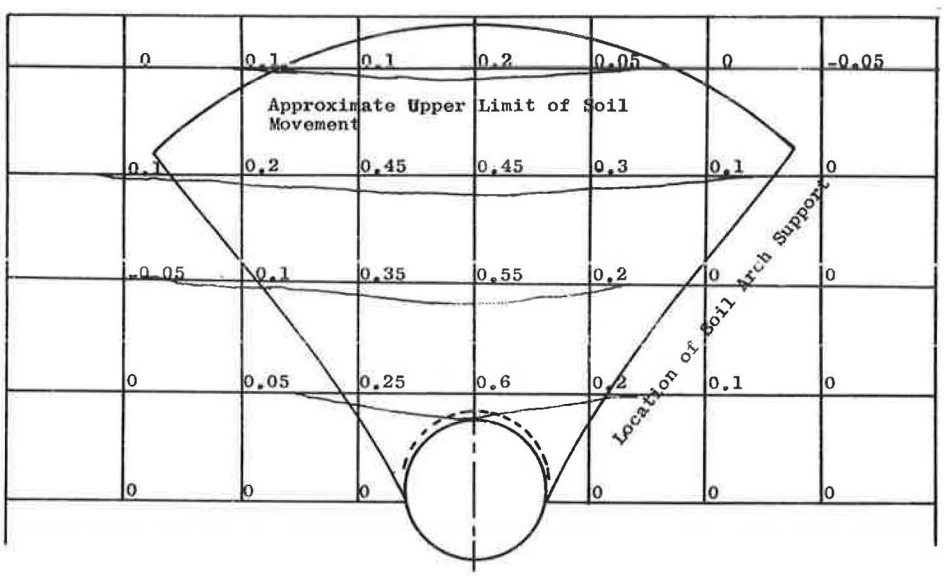

Figure 8. Vertical soil deformation at various elevations above a model conduit (each number is the difference in soil movement with and without the conduit in place).

Loads on Underground Conduits

The loads transmitted through the soil to underground conduits can be determined using the concept of the soil arch. Figure 9 shows a free-body diagram of the assumed loading. The differential equation can be obtained by summing [Fy = 0], the vertical component of forces on the differential element. The circular arch is assumed because of its simplicity and because the X-ray study indicates that the displacement pattern is approximately circular. The vertical component of forces acting down on top of the differential arch is

$$2 \int_0^{\theta} (P + dP) \cos\theta \, d\theta = 2(P + dP) \, r \, \sin\theta \qquad (3)$$

For notation see Figure 9.
Likewise, the vertical component of force acting on the bottom of the differential arch is

$$2 \int_0^{\theta} P \cos\theta \, d\theta = 2 \, P \, r \, \sin\theta \qquad (4)$$

Equations 3 and 4, which were obtained from radial pressure distribution, show that the vertical components of the force are the same as those obtained for a uniform vertical loading on a differential element. The distance between the arch supports is $2 r \sin\theta$. The right hand side of the Eq. 4 can be obtained by multiplying $2 r \sin\theta$ by the appropriate uniform vertical pressure.

The total weight of the soil for a differential circular arch is

$$2 \gamma \, dr \int_0^{\theta} r \, d\theta \, (1) = 2 \, r \, \gamma \, \theta \, dr \qquad (5)$$

If the circular arch is used, an equivalent radial pressure, P', should be applied to the arch to include the influence of the weight of soil. The equivalent pressure would

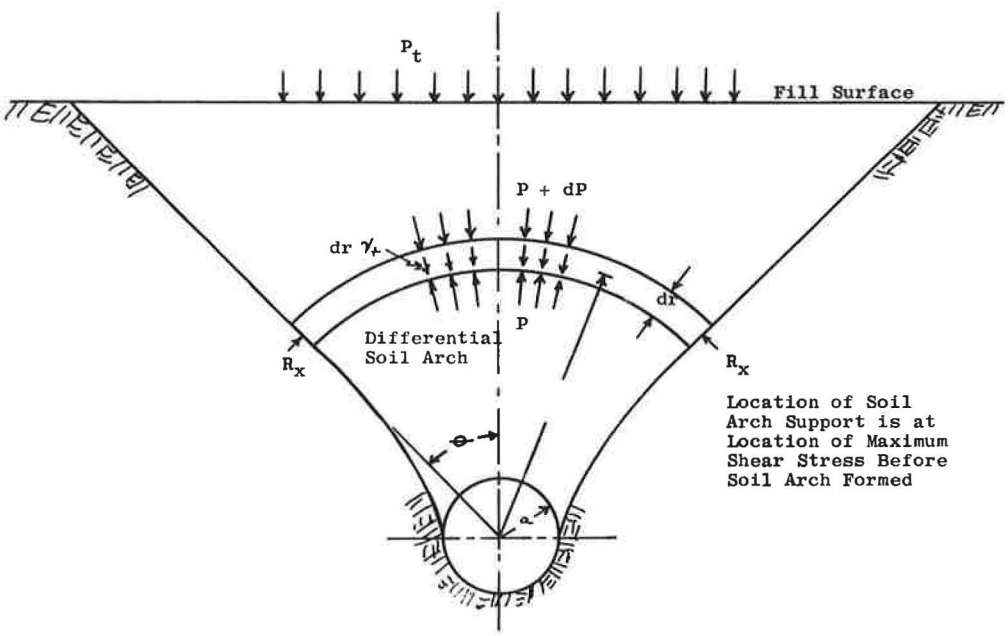

Figure 9. Free-body diagram for determining loads on buried conduits by an arching analysis.

be equal to weight of soil in the element divided by the distance between supports or

$$P' = \frac{2\ r\ \gamma\ \theta_{max}\gamma\ dr}{2\ r\ \sin\ \theta_{max}} = \frac{\gamma\ \theta_{max} dr}{\sin\ \theta_{max}} \tag{6}$$

where θ_{max} = the value of θ at the soil arch support.

The sum of the vertical components on the equivalent load would be equal to the weight of the soil in the differential element.

The vertical component of force acting on the support of differential element is

$$R_x dr\ (1)\ \sin\theta \tag{7}$$

where R_x = stress in the line of action of the arch at the soil arch support.

By taking the summation of the forces on the elements equal to zero, the differential equation can be derived as follows.

$$2(P + dP)r\ \sin\theta - 2P\ r\ \sin\theta + 2\ r\ \theta\ \gamma\ dr - 2\ R_x\ dr\ \sin\theta = 0$$

or

$$dp = \frac{R_x \sin\theta\ dr - r\ \theta\ \gamma\ dr}{r\ \sin\theta} \tag{8}$$

where

P = pressure acting on differential arch,
R_x = stress in line of action of arch at arch support,
r = radius of circular arch,
θ = angle at center of pipe from horizontal to arch support, and
γ = unit weight of soil.

Equation 8 cannot be integrated unless the values of R_x and θ are determined in terms of the radius r. The relationship between θ and r is given by Eq. 2.

Equilibrium conditions are satisfied by Eq. 8. Compatibility of the soil deformation and pipe deformation is discussed in the following section.

Stresses at the Differential Soil Arch Support

The value of the support pressure R_x at the differential soil arch is difficult to determine. The first approach assumed that the stress was simply the radial pressure in the soil at this point multiplied by the active pressure coefficient (K_a). In this approach, when the friction angle of the soil is reduced, the theory predicts more attenuation of pressure. Laboratory measurements (11) indicate that it should be just the opposite; therefore, it was necessary to use some other means of determining the pressure at the soil arch support. If the radial pressure in the soil multiplied by the passive pressure coefficient (K_p) is used to evaluate the support pressure, the attenuation increases with an increase in friction angle. This, however, is obviously inconsistent with the physical characteristics of the system in which active soil conditions exist.

To obtain some type of relationship for R_x, it is assumed that the soil surrounding the pipe acts like an arch with no wall stiffness.

The deflection in an element similar in shape to the arch shown in Figure 9 can be shown to be

$$y = \int_0^r \frac{R_x}{E}\ dy = \frac{R_x}{E}\ r \tag{9}$$

The deflection at the top of the arch is assumed to equal the value of the deflection of the top of the pipe. It is assumed that the deflection of the vertical diameter is equal to the deflection of the horizontal diameter which can be determined by the Spangler (10) deflection equation, which follows.

$$\Delta X = \frac{KW_c r^3}{E\ I + 0.061\ E' r^3} \tag{10}$$

where

K = coefficient,
W_c = load on conduit,
r = radius of conduit,
E I = pipe wall stiffness, and
E' = modulus of soil reaction.

Because the soil has no flexural stiffness, the value of E I can be neglected and

$$\frac{R_X}{E}\ r = \frac{K\ W_c}{0.061\ E'} \tag{11}$$

Substituting $\frac{R_X}{\Delta X / D}$ for E' and $2\sigma r$ for W_c and reducing yields:

$$R_X = \frac{2\ K(\Delta X)E}{0.061\ r} \tag{12}$$

Spangler (9) gives values of K ranging from 0.083 to 0.110; if K = 0.110

$$R_X = 3.62\ \frac{E\ \Delta X}{r} \tag{13}$$

where

R_X = compressive pressure on soil arch support,
ΔX = deflection of pipe at horizontal diameter, and
r = distance from center of pipe to arch (Fig 9).

Equation 13 assumes a hyperbolic distribution of stress in the soil mass. When r becomes large, the value of R_X approaches zero indicating that the arching takes place immediately in the vicinity of the pipe. If the pipe is infinitely rigid, the value of ΔX will be zero, and R_X will also be zero allowing no arching in action to occur.

For Poisson's ratio = ¼, E' can be shown to be 1.8 E (8). Substituting the value of E' yields

$$R_X = \frac{2\ E'\ \Delta X}{r} \tag{14}$$

Because of the assumptions involved in the derivation of Eq. 14 dimensional analysis was also used to obtain some type of a relationship for R_X. If the following tabulated variables are considered important in determination of R_X, then through principles of similitude a functional relationship can be obtained. The variables considered are as follows:

Variable	Symbol	Dimensions
Stress at soil arch support	R_X	psi-FL^{-2}
Soil modulus	E'	psi-FL^{-2}
Pipe deflection		in. -L
One-half length of soil arch	L	in. -L
Radius of pipe	a	in. -L

The modulus of elasticity of the soil is not included in the above list of variables because it is not independent of the soil modulus, E'. The radius of the pipe is assumed to influence only the deflection and is therefore not independent.

There are four variables or primary quantities and only two dimensions. Therefore, according to the Buckingham pi theorem, there must be two pi terms. These pi terms may be formulated into a functional equation as follows:

$$\frac{R_x}{E'} = f\left(\frac{}{L}\right) \tag{15}$$

The length of the arc, L can be expressed in terms of the radius of the soil arch and the angle φ. Because the angle φ is approximately 45 deg throughout the soil mass, L is assumed to equal 0. 785 x r.

It can be shown by other analysis that the correct order of the second pi term should be /1.

The functional relationship in Eq. 15 was determined by assuming a relationship and substituting it into Eq. 15 which was in turn substituted into Eq. 8 and comparing with model data. If the computed data did not compare with the model data another functional relationship was assumed. The process was repeated until the functional relationship was found. This analysis showed the functional relationship to be 2.

The value of R_X used in the analysis was then

$$R_X = \frac{2E'}{0.785r} \tag{16}$$

where

R_X = compressive pressure on soil arch support perpendicular to line of action in arch,
= deflection of soil arch support at pipe boundary,
r = distance from center of pipe to arch, and
E' = modulus of passive resistance of soil.

The value of the stress at the soil arch support depends on the soil modulus, E', and the deflection of the soil arch support. But the soil modulus also depends on the applied stress and the deflection of the soil arch support which in turn depends on the stress level and on the soil modulus. To make some allowance for the interaction of the foregoing variables, Eq. 16 was used to determine the stress at the soil arch support. To compare with field data, the value of R_X used in the analysis was

$$R_X = \frac{2\ E'\ \Delta X}{0.785\ r} \tag{17}$$

where

R_X = compressive pressure of soil arch support perpendicular to line of action in arch,
ΔX = deflection of pipe,
r = distance from center of pipe (Fig. 9), and
E' = modulus of soil reaction.

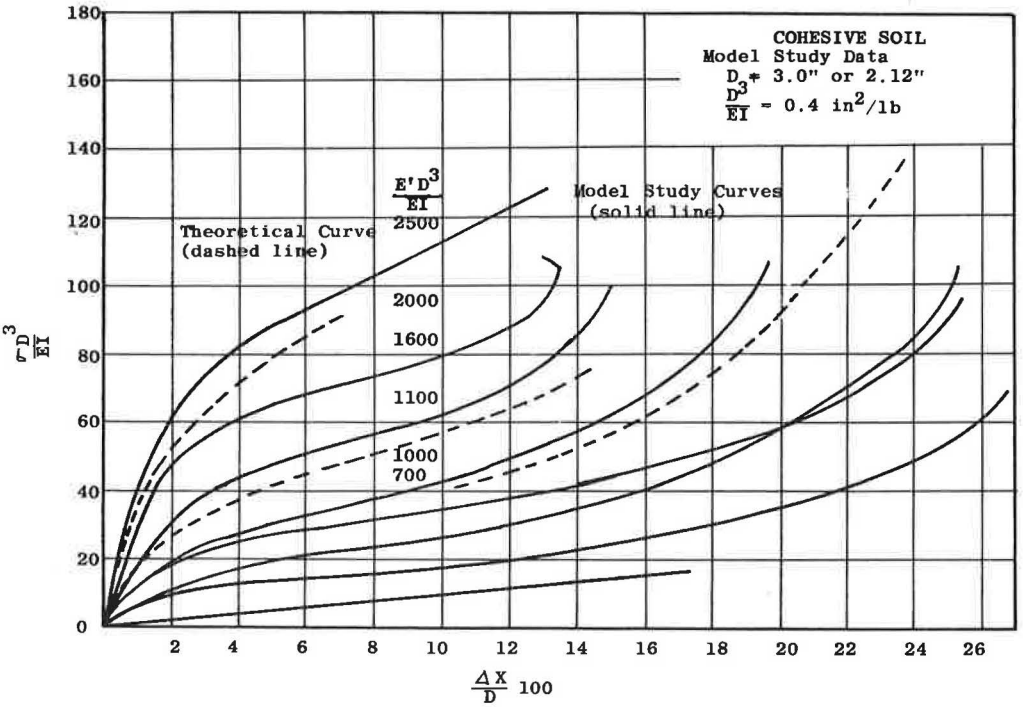

Figure 10. Model study curves vs theoretical curves.

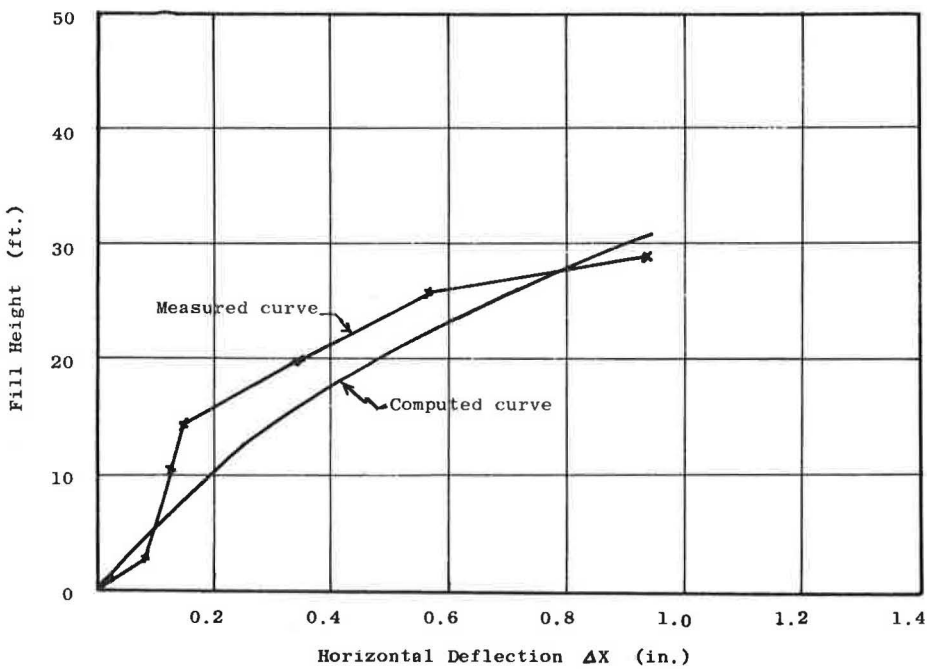

Figure 11. Deflection of 78-in. pipe measured by Kaiser Aluminum Corp. vs values computed by arching theory.

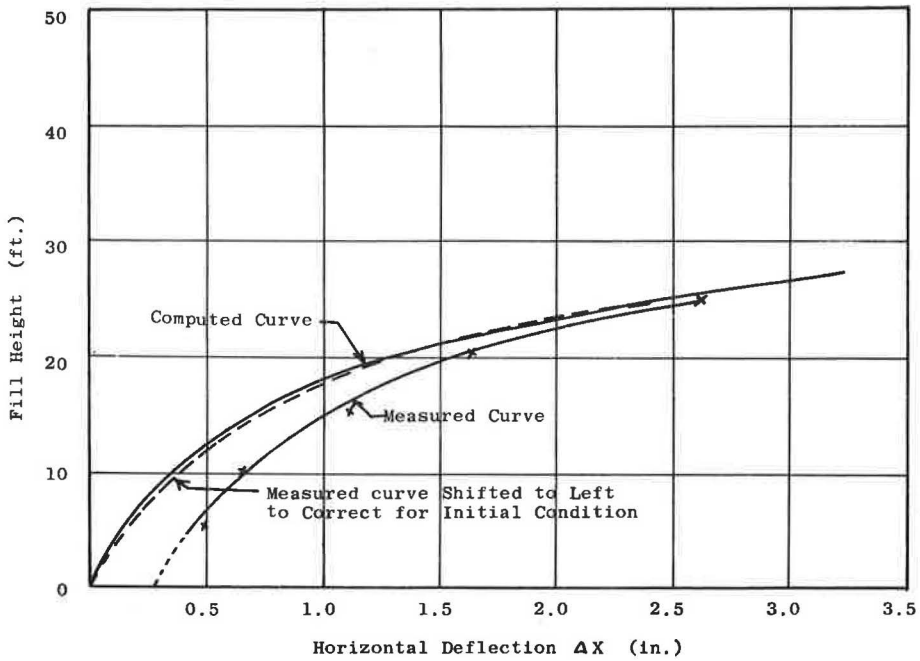

Figure 12. Deflection of 48-in. pipe measured by Koepf vs values computed by arching theory.

Equation 17 can be substituted into Eq. 8 for the value of R_X and Eq. 2 can be substituted for the value of theta. The resulting equation becomes difficult to integrate. At this point the computer and numerical integration procedures were used.

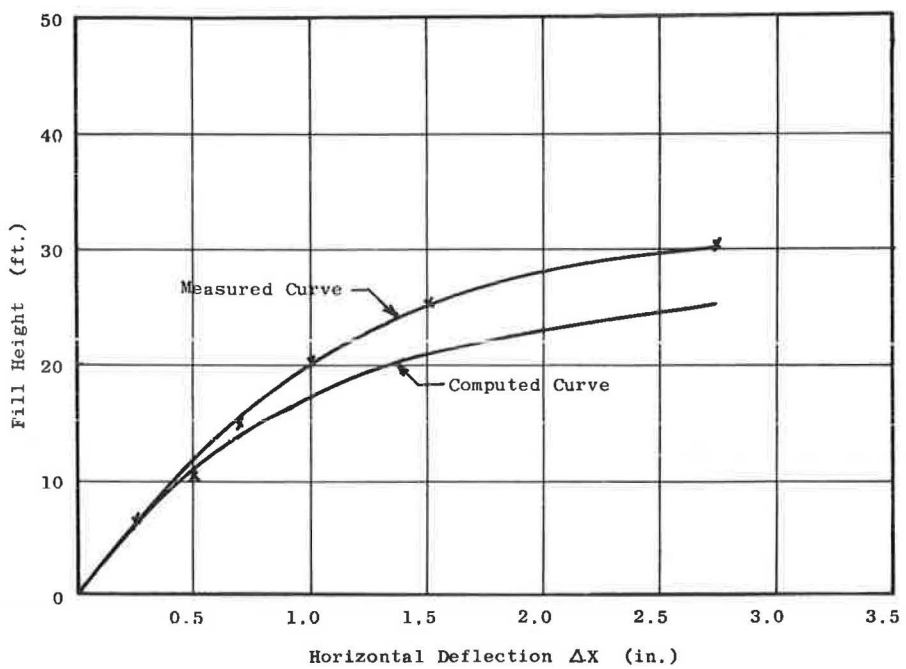

Figure 13. Deflection of 60-in. pipe measured by Koepf vs values computed by arching theory.

The value of ΔX in Eq. 17 is unknown, therefore it is impossible to solve Eq. 8 because there are two unknowns in one equation. Another equation must be obtained to meet compatibility requirements. Equation 10 with modifications for the nonlinear soil modulus is used. With relationship for delta, it is possible to solve the Eq. 8 for the pressure at the top and the deflection of the conduit. It is still a trial and error procedure because of the nonlinear soil modulus.

Verification of Load Theory

To verify any theory, it is necessary to resort to laboratory or field studies. Model analysis in the laboratory is one of the most rewarding methods because many data can be collected. Figure 10 shows a comparison between the computer selection and model tests obtained by Watkins and Nielson (13) for a clay soil. There are several field studies reported in the literature. One study was made by Kaiser Aluminum Corporation (4). Figure 11 shows the comparison between this company's measured values and the values obtained from the computer solution. The values for the soil modulus in this particular soil were measured by Watkins in the modpares device. Kaiser Aluminum supplied Watkins with the soil to measure modulus of soil reaction. Koepf (5) also reported results of a field study in which two aluminum pipes, 48 in. and 60 in. in diameter, were used. The data for determination of the soil modulus were determined by measuring the pressure at the side of a conduit during the loading tests. Figures 12 and 13 show a comparison of the measured and computed deflection for each pipe. The agree-

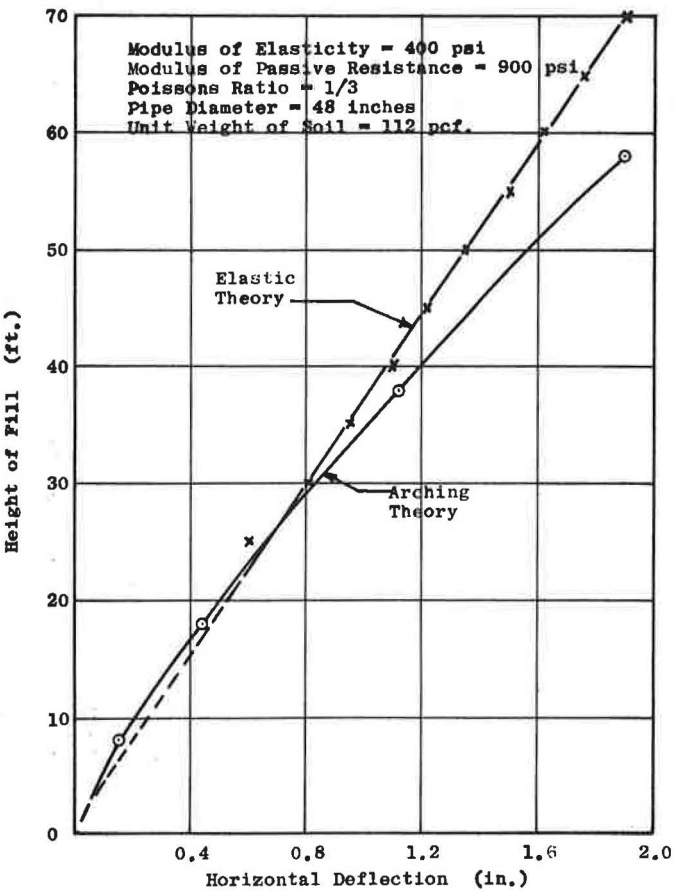

Figure 14. Deflections calculated from elastic theory vs arching theory.

ment between these curves and the predicted curves is sufficiently close to justify the approach and the assumptions made.

In addition to comparing the arching theory with field tests and model studies, it was compared with the theory of elasticity. Figure 14 shows a comparison of the deflection calculated from the two theories. A linear elastic medium was assumed for this comparison. The agreement is reasonably good for a fill height below approximately 60 ft. The deflections predicted by the arching theory are on the conservative side if the deflections computed by the theory of elasticity are assumed to be correct.

SUMMARY AND CONCLUSIONS

The concept of a differential soil arch has been used as a differential element in determining the load transmitted to underground structures. A differential equation was developed, but because of difficulties in integration it was necessary to resort to numerical procedures. The concept of the soil arch can be used to calulate loads and pressures transmitted to underground structures and explains pressure redistribution across the top of flat top structures as well as pressure reduction on membranes caused by placing parapet walls for the soil to arch on. More field studies are needed to correlate with laboratory findings. The procedure seems adequate for design including both deflections and pressures transmitted to the buried pipe.

REFERENCES

1. Burns, J. Q., and Richard, R. M. Attenuation of Stresses for Buried Cylinders. Proc. of Symposium on Soil Structure Interaction, Univ. of Arizona, Tucson, Ariz., 1964.
2. Chelapati, C. V. Arching in Soil Due to the Deflection on a Rigid Horizontal Strip. Proc. of Symposium on Soil Structure Interaction, Univ. of Arizona, Tucson, Ariz., 1964.
3. A Study of Counterforce Defense System Methodology Applied to Tucson, Arizona and Evirons. Eng. Res. Lab., Univ. of Arizona, ERL, Tucson, Ariz.
4. Kaiser Aluminum Corp. Fill Height Test on Circular and Pipe Arches. Kaiser Aluminum and Chemical Sales, Inc., Oakland, Calif., 1963.
5. Koepf, A. H. Structural Consideration and Development of Aluminum Alloy Culverts. HRB Bull. 361, 1962, pp. 25-70.
6. Marston, A., and Anderson. The Theory of Loads on Pipe in Ditches and Tests on Cement and Clay Drain Tile and Sewer Pipe. Bull. 31, Iowa Eng. Exper. Sta., Ames, Iowa, 1913.
7. Newmark, N. M., and Haltswanger, J. D. Air Force Design Manual. Air Force Special Weapons Center, Kirtland Air Force Base, N. M., 1962.
8. Nielson, F. D. Modulus of Soil Reaction as Determined by the Tiaxial Shear Test. Presented at the 46th Annual Meeting and published in this RECORD.
9. Spangler, M. G. Soil Engineering. International Textbook Co., Scranton, Pa., 1960.
10. Spangler, M. G. The Structural Design of Flexible Pipe Culverts. Bull. 153, Iowa Eng. Exper. Sta., Ames, Iowa, 1942.
11. Terzaghi, K. Theoretical Soil Mechanics. John Wiley & Sons, New York, 1943.
12. Truesdale, W. B., and Vey, E. An Investigation on Panel Arching Effects in Noncohesive Soil. Proc. of Symposium on Soil Structure Interaction. Univ. of Arizona, 1964.
13. Watkins, R. K., and Nielson, F. D. Development and Use of the Modpares Device in Predicting the Deflection of Flexible Conduits Embedded in Soil. Eng. Exper. Sta. Utah State Univ., Logan, Utah. In ASCE Pipeline Journal, (ASCE Pipeline Crossing Committee), Jan. 1964.
14. Watkins, R. K. Characteristics of the Modulus of Passive Resistance of Soil. Unpubl. Ph.D. dissert., Iowa State Univ., 1957.
15. Timoshenko and Goodier. Theory of Elasticity. 2nd Ed., McGraw-Hill Book Co., New York, 1951.

An Analytical-Experimental Method for Determining Interface Tractions for Buried Structures Subjected to Static Loads

LESTER H. GABRIEL, Associate Professor and Head, Department of Civil Engineering, and
LEO DABAGHIAN, Assistant Professor, Department of Mechanical Engineering, Sacramento State College, California

The outer boundary tractions of normal pressure and shear may be determined for a rigid circular culvert by studying the displacement field of the inner boundary. Given the inner boundary displacements, the elastic response of the structure will yield, on analysis, that unique loading responsible for the displacements. This paper develops the equations of the elastic analysis of the culvert and plots charts for ease in application of the parameters.

•THE DESIGN engineer responsible for the structural design of culverts is faced with the unenviable task of having to design the structure without any clear knowledge of the loadings on it. This deficiency inhibits his direct determination, in a design sense, of the state of stress throughout the structure.

This paper shows that the displacement response of the inner boundary of a buried rigid circular culvert furnishes sufficient information to determine that unique soil loading causing this response. Knowledge of this soil loading (surface tractions on the buried structure) would permit a quantitative estimate of the phenomenon of soil arching. Knowledge of these soil-structure interface tractions would also permit a critical evaluation of the effectiveness of some current design assumptions of loads, bedding conditions, and backfill techniques. This paper is only concerned with the demonstration of the fact that inner boundary displacements are sufficient to determine the soil loadings. In short, the buried structure is used as a transducer.

ASSUMPTIONS

1. Symmetry of loading about a vertical axis exists and variations from this assumption are small, normally distributed (in a statistical sense), and self-compensating.
2. The culvert responds in a linear elastic manner. Any variations from this idealization are assumed to be small enough to be neglected at the usual levels of working stress for concrete.
3. No assumption is made concerning the response of the soil to self-induced loading. No claim is made that the measured displacements are historically independent of the character and placement of the backfill. Only the response of the structure is of interest.
4. Deflections of the culvert are small enough so that the principle of superposition may be invoked for the stresses and displacements of the culvert.
5. In the central interior portion of the buried culvert, far from its ends, conditions are such that the problem may reasonably be studied in the domain of plane strain.

Paper sponsored by Committee on Buried Structures and presented at the 46th Annual Meeting.

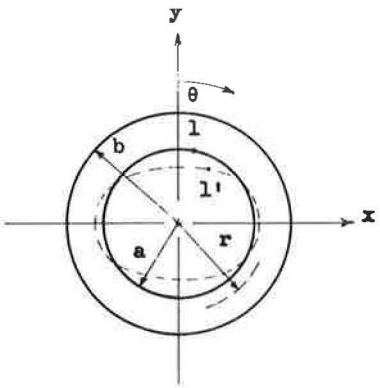

Figure 1. Inner boundary displacements.

DESCRIPTION OF INNER BOUNDARY DISPLACEMENTS

In Figure 1, point 1 on the original circular boundary moves to point 1′ on the distorted boundary. The displacement in the radial direction is denoted by u, and the displacement in the tangential direction by v. When it is radially outward, u is considered positive; v is positive when in the direction of increasing θ.

With the displacements of sufficiently many points (such as point 1 in Fig. 1) measured experimentally, it is possible to deduce, in a statistical sense, a contour which best describes the movement of all points of the inner boundary due to the movement of the measured points. It can be shown mathematically that of all trigonometric polynomials, those of the Fourier series type provide the best approximation (in the sense of least squares) to a contour described by discrete points (1).

Figure 1 also shows that initial polar symmetry of the geometry coupled with symmetry of displacements about the y-axis ($\theta = 0$) implies that the shape of the inner boundary to the left of the vertical axis is the mirror image of that to the right of the vertical axis. The radial displacements on the left are equal to the corresponding radial displacements on the right. Likewise, the tangential displacements on the left are the negatives of the tangential displacements on the right. As a consequence, the radial displacement, u, may be described only by even functions, and the tangential displacement, v, may be described only by odd functions.

Therefore, the displacement field of the structure has been described in general as:

$u = u(r, \theta) \equiv$ radial displacement = even function of θ, and
$v = v(r, \theta) \equiv$ tangential displacement = odd function of θ.

In particular on the inner boundary, where $r = a$, we have

$$u(a, \theta) = A_0 + \sum_{n=1}^{\infty} A_n \cos n\theta$$

$$v(a, \theta) = \sum_{n=1}^{\infty} B_n \sin n\theta$$

where the coefficients A_0, A_n, and B_n are readily calculated from the experimentally determined inner boundary displacements by means of a regression analysis using trigonometric functions of sines and cosines. Computer programs are available for these computations.

DESCRIPTION OF OUTER BOUNDARY TRACTIONS

Let the stresses in the plane of the culvert cross section be designated by the following:

$\tau_{rr} = \tau_{rr}(r, \theta) \equiv$ normal radial stress,
$\tau_{\theta\theta} = \tau_{\theta\theta}(r, \theta) \equiv$ normal tangential stress, and
$\tau_{r\theta} = \tau_{r\theta}(r, \theta) \equiv$ shear stress.

The traction on the boundary of the soil-structure interface can be arbitrarily described by the two following components:

$p(\theta) = \tau_{rr}(b, \theta) \equiv$ normal component of surface traction (pressure), and
$q(\theta) = \tau_{r\theta}(b, \theta) \equiv$ shear component of surface traction.

Using the same argument of symmetry as was used in the case of the inner boundary displacements, the pressure, p, may be described by even functions only and the shear at the interface by odd functions only (Fig. 2).

If it is the case that the true form of p and q can be described by a function that is at least piecewise continuous, then these functions can always be represented by a Fourier series; consequently,

$$p(\theta) = \tau_{rr}(b, \theta) = a_o + \sum_{n=1}^{\infty} a_n \cos n\theta$$

$$q(\theta) = \tau_{r\theta}(b, \theta) = \sum_{n=1}^{\infty} b_n \sin n\theta$$

where a_o, a_n, and b_n are the as yet undetermined coefficients which will be found in the elastic analysis that follows.

The sign convention adopted is as follows: (a) p is positive when its effect is to produce tension, and p is negative when its effect is to produce compression; and (b) q is positive when its effect is to produce clockwise shear, and q is negative when its effect is to produce counterclockwise shear.

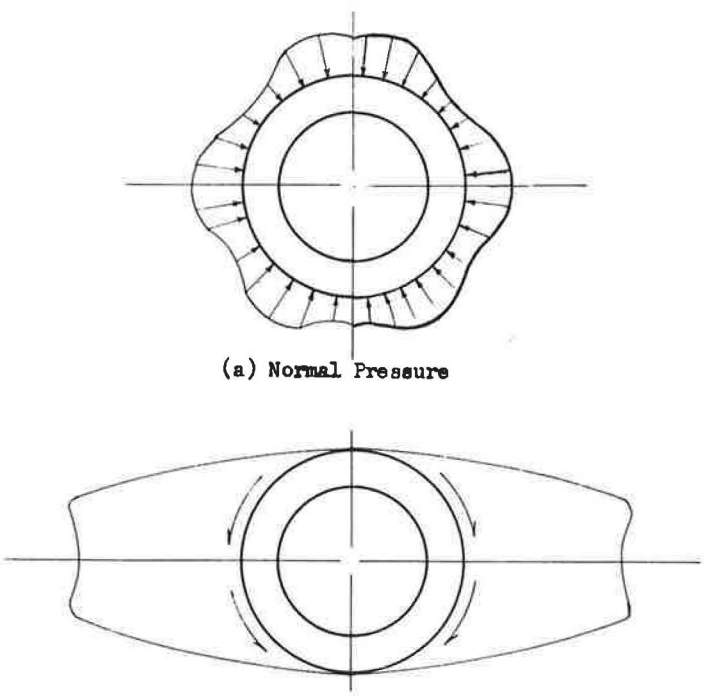

(a) Normal Pressure

(b) Shear

Figure 2. Normal pressure and shear.

ELASTIC ANALYSIS OF THE RIGID CIRCULAR CULVERT

The elastic analysis begins with the displacements of the inner boundary which are considered known; i. e., obtainable by experiment.

$$u(a, \theta) = A_0 + \sum_{n=1}^{\infty} A_n \cos n\theta \qquad (1a)$$

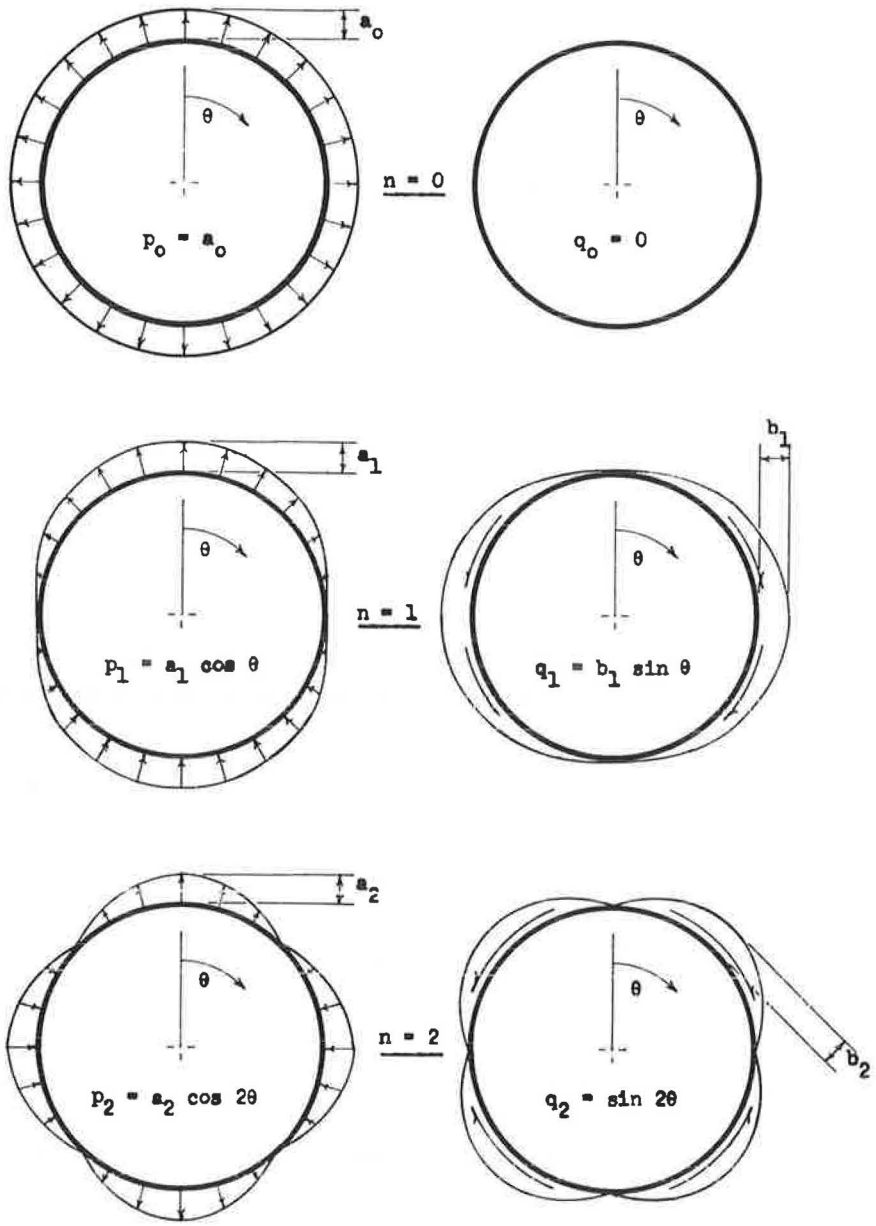

Figure 3. Soil structure interface loading components, Fourier harmonics, n = 0, 1, 2, 3, 4, 5.

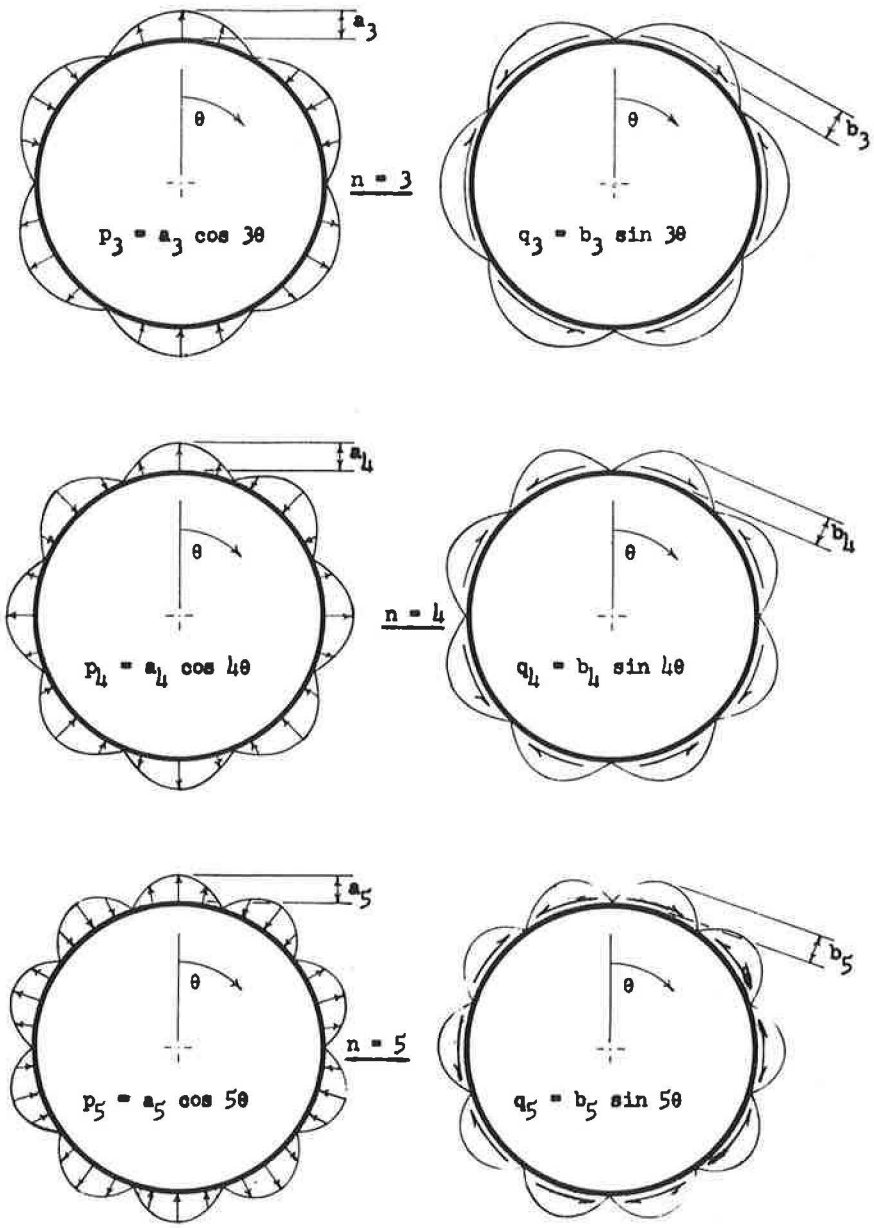

Figure 3. (Continued)

$$v(a, \theta) = \sum_{n=1}^{\infty} B_n \sin n\theta \qquad (1b)$$

Eqs. 1a and 1b are a consequence of the experimentally determined inner boundary displacements. (Of course, for numerical work the series shown will be truncated at some finite number of terms which will, however, be large enough to assure accuracy as well as consistency with the experimental data.)

The tractions on the outer boundary are unknown, but as previously stated, if they can be described by functions that are at least piecewise continuous, then they may be described by a Fourier series as follows:

$$\tau_{rr}(b,\theta) = p(\theta) = \sum_{n=0}^{\infty} p_n = a_0 + \sum_{n=1}^{\infty} a_n \cos n\theta \qquad (2a)$$

$$\tau_{r\theta}(b,\theta) = q(\theta) = \sum_{n=0}^{\infty} q_n = \sum_{n=1}^{\infty} b_n \sin n\theta \qquad (2b)$$

Invoking the principle of superposition (previously discussed), we will now calculate the response displacement of the structure to each harmonic of loading.

Zeroth Harmonic

Considering only the n = 0 term of the summations in Eqs. 2a and 2b, we obtain the following (Fig. 3):

$p_0 = a_0$
$q_0 = 0$

In Appendix A the relations between stresses and displacements are derived, and the following is obtained for the zeroth harmonic of inner boundary displacement:

$u(a,\theta) = A_0$
$v(a,\theta) = 0$

The corresponding outer boundary tractions are

$$p_0 = \frac{A_0}{2a}\left(1 - \frac{a^2}{b^2}\right) E_1 = \frac{E}{2a(1-\nu^2)}\left(1 - \frac{a^2}{b^2}\right) A_0$$

$$q_0 = 0$$

Here E_1 denotes the "plane strain" modulus of elasticity.

$$E_1 = \frac{E}{(1-\nu^2)}$$

First Harmonic

For the n = 1 terms in Eqs. 2a and 2b, we obtain the tractions of the first harmonic loading (Fig. 3):

$p_1 = a_1 \cos\theta$
$q_1 = b_1 \sin\theta$

Reference is again made to Appendix A where the derivation of the relations between stresses and displacements is shown.

For the first harmonic of inner boundary displacement,

$u(a,\theta) = A_1 \cos\theta$
$v(a,\theta) = B_1 \sin\theta$

the corresponding outer boundary tractions are

$$p_1 = \frac{b}{a^2}\left(1 - \frac{a^4}{b^4}\right)\left(\frac{E_1}{1-\nu_1}\right) A_1 \cos\theta = \frac{b}{a^2}\left(1 - \frac{a^4}{b^4}\right)\frac{E}{(1+\nu)(1-2\nu)} A_1 \cos\theta$$

$$q_1 = \frac{b}{a^2}\left(1 - \frac{a^4}{b^4}\right)\left(\frac{E_1}{3+2\nu_1}\right) B_1 \sin\theta = \frac{b}{a^2}\left(1 - \frac{a^4}{b^4}\right)\frac{E}{(1+\nu)(3-\nu)} B_1 \sin\theta$$

Here again, E_1 denotes the "plane strain" modulus of elasticity and $\nu_1 = \nu/(1 - \nu)$ denotes the "plane strain" Poisson's ratio.

nth Harmonic, $n \geq 2$

In Eqs. 2a and 2b the tractions of the nth harmonic of loading are described as follows (Fig. 3):

$$p_n = a_n \cos n\theta$$
$$q_n = b_n \sin n\theta$$

Again, the analysis of Appendix A results in the following: for the nth harmonic of inner boundary displacement,

$$u(a, \theta) = A_n \cos n\theta$$
$$v(a, \theta) = B_n \sin n\theta$$

The corresponding outer boundary tractions are

$$p_n = \frac{E}{2a(1 - \nu^2)} \left[\frac{(C_{1n})^3 A_n + (C_{2n})^3 B_n}{(C_{3n})^3 A_n + (C_{4n})^3 B_n}\right] A_n \cos n\theta$$

$$q_n = \frac{E}{2a(1 - \nu^2)} \left[\frac{(C_{5n})^3 A_n + (C_{6n})^3 B_n}{(C_{7n})^3 A_n + (C_{8n})^3 B_n}\right] B_n \sin n\theta$$

In the foregoing equations the coefficients C_{1n}, C_{2n}, ..., C_{8n} are quantities functionally dependent on α, the ratio of inner boundary diameter to outer boundary diameter. For ease in future computations and applications, these coefficients were precalculated by digital computer for a range of values of α and are charted in Appendix B.

CONCLUSION

It is possible to use a round circular culvert under fill directly as a transducer for the determination of the unique outer boundary loading causing the experimentally determined displacements. The displacements of the inner boundary are represented in the form of a Fourier series:

$$\text{radial displacement} = u(a, \theta) = A_o + \sum_{n=1}^{\infty} A_n \cos n\theta$$

$$\text{tangential displacement} = v(a, \theta) = \sum_{n=1}^{\infty} B_n \sin n\theta$$

The A_o, A_n, and B_n which are determined by a regression analysis of the experimental data are now used as inputs in the solutions for the outer boundary tractions as follows:

$$p(b, \theta) = \frac{E}{2a(1 - \nu^2)} \left[1 - \left(\frac{a}{b}\right)^2\right] A_0 + \frac{E}{(1 - \nu)(1 - 2\nu)} \frac{b}{a^2} \left[1 - \left(\frac{a}{b}\right)^4\right] A_1 \cos\theta$$

$$+ \sum_{n=2}^{\infty} \frac{E}{2a(1 - \nu^2)} \left[\frac{(C_{1n})^3 A_n + (C_{2n})^3 B_n}{(C_{3n})^3 A_n + (C_{4n})^3 B_n}\right] A_n \cos n\theta$$

$$q(b, \theta) = \frac{E}{(1 + \nu)(3 - \nu)} \frac{b}{a^2} \left[1 - \left(\frac{a}{b}\right)^4\right] B_1 \sin \theta$$

$$+ \sum_{n=2}^{\infty} \frac{E}{2a(1 - \nu)^2} \left[\frac{(C_{5n})^3 A_n + (C_{6n})^3 B_n}{(C_{7n})^3 A_n + (C_{8n})^3 B_n}\right] B_n \sin n\theta$$

The n may be chosen so as to give any predetermined degree of precision to these converging series. With the A_0, A_1, ..., A_n and B_1, ..., B_n known, and with the $C1n$, $C2n$, ..., $C8n$ calculated or taken from the charts in Appendix B, the normal traction, p, and the tangential traction, q, may be calculated.

REFERENCE

1. Gaskell, Robert E. Engineering Mathematics. Dryden Press, p. 220, 1958.

Appendix A

DERIVATION OF RELATIONS BETWEEN STRESSES AND DISPLACEMENTS

Given:

1. Displacements of inner boundary (r = a)

$$u(a, \theta) = A_0 + \sum_{n=1}^{\infty} (A_n \cos n\theta) \tag{3a}$$

$$v(a, \theta) = \sum_{n=1}^{\infty} (B_n \sin n\theta) \tag{3b}$$

2. Tractions on outer boundary (r = b)

$$p = \tau_{rr}(b, \theta) = a_0 + \sum_{m=1}^{\infty} (a_m \cos m\theta)$$

$$q = \tau_{r\theta}(b, \theta) = \sum_{m=1}^{\infty} (b_m \sin m\theta)$$

denote the radial tension and the tangential traction, respectively. To show:

1. $a_0 = f_1(A_0)$
   $a_0 = 0$ when $n \geq 1$
2. $a_m = f_2(A_n, B_n)$ when $m = n \geq 1$
   $a_m = 0$ when $m \neq n \geq 1$
3. $b_m = f_3(A_n, B_n)$ when $m = n \geq 1$
   $b_m = 0$ when $m \neq n \geq 1$

In addition, the tractions on the outer boundary will be evaluated as functions of the displacements of the inner boundary.

Zeroth Harmonic

Tractions of the zeroth harmonic of loading are described as:

$$p_0 = a_0 \tag{4a}$$

$$q_0 = 0 \tag{4b}$$

The general solution (2, pp. 58-59) of the problem of a stress distribution symmetrical about a longitudinal axis (the Lamé problem) is obtained as follows:

Stress function $\varphi = A \log r + Br^2 \log r + Cr^2 + D$

The stresses are given by:

$$\tau_{rr} = \frac{1}{r}\frac{\partial \varphi_0}{\partial r} = \frac{A}{r^2} + B(1 + 2 \log r) + 2C$$

$$\tau_{\theta\theta} = \frac{\partial^2 \varphi_0}{\partial r^2} = -\frac{A}{r^2} + B(3 + 2 \log r) + 2C$$

$$\tau_{r\theta} = -\frac{\partial}{\partial r}\left(\frac{1}{r}\frac{\partial \varphi_0}{\partial \theta}\right) = 0$$

Single valued displacements require B = 0 (2, p. 68). Therefore,

$$\tau_{rr} = \frac{A}{r^2} + 2C \tag{5a}$$

$$\tau_{\theta\theta} = -\frac{A}{r^2} + 2C \tag{5b}$$

$$\tau_{r\theta} = 0 \tag{5c}$$

Substituting the boundary conditions:

$$p_0 = \tau_{rr}(b, \theta) = a_0 = \frac{A}{b^2} + 2C$$

$$q_0 = \tau_{rr}(a, \theta) = 0 = \frac{A}{a^2} + 2C$$

Solving for A and C and substituting in Eqs. 5a, 5b, and 5c, we obtain the following:

$$\tau_{rr} = \frac{a_0 b^2}{(b^2 - a^2)}\left(1 - \frac{a^2}{r^2}\right) = K_0\left(1 - \frac{a^2}{r^2}\right) \tag{6a}$$

$$\tau_{\theta\theta} = \frac{a_0 b^2}{(b^2 - a^2)}\left(1 + \frac{a^2}{r^2}\right) = K_0\left(1 + \frac{a^2}{r^2}\right) \tag{6b}$$

$$\tau_{r\theta} = 0 \tag{6c}$$

where

$$K_0 = \frac{a_0 b^2}{(b^2 - a^2)}$$

For the two-dimensional system of polar coordinates employed, the strain-displacement relations are (2, pp. 65-66):

$$\epsilon_{rr} = \frac{\partial u}{\partial r} \tag{7a}$$

$$\epsilon_{\theta\theta} = \frac{u}{r} + \frac{1}{r}\frac{\partial v}{\partial \theta} \tag{7b}$$

$$\gamma_{r\theta} = 2\epsilon_{r\theta} = \frac{1}{r}\frac{\partial u}{\partial \theta} + \frac{\partial v}{\partial r} - \frac{v}{r} \tag{7c}$$

The stress-strain relations for an elastic body in a two-dimensional polar coordinate system are (2, pp. 65-66).

$$\epsilon_{rr} = \frac{1}{E_1}(\tau_{rr} - \nu_1 \tau_{\theta\theta}) \tag{8a}$$

$$\epsilon_{\theta\theta} = \frac{1}{E_1}(\tau_{\theta\theta} - \nu_1 \tau_{\theta\theta}) \tag{8b}$$

$$\gamma_{r\theta} = \frac{1}{G_1}\tau_{r\theta} \tag{8c}$$

Here E_1 and ν_1 are the "plane strain" elastic constants where

$$E_1 = \frac{E}{1 - \nu^2}, \quad \nu_1 = \frac{\nu}{1 - \nu}, \quad G_1 = G = \frac{E_1}{2(1 + \nu_1)}$$

Eliminating the strains between the strain-displacement relations and the stress-strain relations (Eqs. 7a, 7b, 7c and 8a, 8b and 8c) we obtain:

$$\frac{\partial u}{\partial r} = \frac{1}{E_1}(\tau_{rr} - \nu_1 \tau_{\theta\theta}) \tag{9a}$$

$$\frac{\partial v}{\partial \theta} = \frac{1}{E_1}(\tau_{\theta\theta} - \nu_1 \tau_{rr}) - u \tag{9b}$$

$$\frac{1}{r}\frac{\partial u}{\partial \theta} + \frac{\partial v}{\partial r} - \frac{v}{r} = \frac{1}{G_1}\tau_{r\theta} \tag{9c}$$

Substituting the equation for stress (Eq. 6a) in Eq. 9a:

$$\frac{\partial u}{\partial r} = \frac{K_0}{E_1}\left[\left(1 - \frac{a^2}{r^2}\right) - \nu_1\left(1 + \frac{a^2}{r^2}\right)\right] \tag{10}$$

Integrating with respect to r:

$$u(r, \theta) = \frac{K_0 r}{E_1}\left[\left(1 + \frac{a^2}{r^2}\right) - \nu_1\left(1 - \frac{a^2}{r^2}\right)\right] + g_1(\theta) \tag{11}$$

Substituting the equation for stress (Eq. 6b) and the equation for displacement $u(r, \theta)$, Eq. 11, into the stress-displacement relation Eq. 9b:

$$\frac{\partial v}{\partial \theta} = -g_1(\theta)$$

Integrating with respect to θ:

$$v(r, \theta) = - \int g_1 (\theta)\, d\theta + g_2 (r) \tag{12}$$

To evaluate the functions $g_1 (\theta)$ and $g_2 (r)$, Eqs. 11, 12 and 6c are substituted in Eq. 9c. There results

$$\left[\frac{\partial g_1 (\theta)}{\partial \theta} + \int g_1 (\theta)\, d\theta\right] + \left[r \frac{\partial g_2 (r)}{\partial r} - g_2 (r)\right] = 0 \tag{12a}$$

Inasmuch as the foregoing must be true for all r and θ,

$$\frac{\partial g_1 (\theta)}{\partial \theta} + \int g_1 (\theta)\, d\theta = C_1$$

$$\frac{r \partial g_2 (r)}{\partial r} - g_2 (r) + - C_1$$

where C_1 is the arbitrary constant of integration.

Let:

$$g_1 (\theta) = H \sin \theta + L \cos \theta \tag{13a}$$

$$g_2 (r) = Fr \tag{13b}$$

where F, H, L are arbitrary constant. These satisfy Eq. 12a identically for all values of r and θ.

Substituting Eqs. 13a and 13b in Eqs. 11 and 12:

$$u(r, \theta) = \frac{K_0 r}{E_1} \left[\left(1 + \frac{a^2}{r^2}\right) - \nu_1 \left(1 - \frac{a^2}{r^2}\right)\right] + H \sin \theta + L \cos \theta \tag{14a}$$

$$v(r, \theta) = H \cos \theta + L \sin \theta + Fr \tag{14b}$$

To evaluate H, L, and F, the following conditions are employed:

1. By symmetry of tangential displacements $v(r, 0) = v(r, \pi) = 0$; substitution in Eq. 14b leads to $F = 0$.

2. On the inner boundary $v(a, \theta) = \sum_{n=1}^{\infty} (B_n \sin n\theta)$ from Eq. 3b. Comparing coefficients with Eq. 14b and setting $F = 0$ as a consequence of item 1 above, it follows that $L = 0$.

3. On the inner boundary $u(a, \theta) = A_0 + \sum_{n=1}^{\infty} (A_n \cos n\theta)$ from Eq. 3a. Comparing coefficients with Eq. 14a and setting $L = 0$ as a consequence of item 2 above, it follows that $H = 0$.

The following displacement field now results:

$$u(r, \theta) = \frac{K_0 r}{E_1} \left[\left(1 + \frac{a^2}{r^2}\right) - \nu_1 \left(1 - \frac{a^2}{r^2}\right)\right]$$

$$v(r, \theta) = 0$$

On the inner boundary:

$$u(a, \theta) = \frac{2K_0 a}{E_1} = \frac{2a_0 ab^2}{(b^2 - a^2) E_1} \tag{15a}$$

$$v(r, \theta) = 0 \tag{15b}$$

Comparing Eqs. 3a and 3b with Eqs. 15a and 15b, respectively, it follows

$$\frac{2a_0\, ab^2}{(b^2 - a^2)\, E_1} = A_0,\ A_n = 0,\ B_n = 0 \text{ for } n \geq 1$$

Therefore

$$a_0 = A_0 \frac{(b^2 - a^2)}{2ab^2} E_1 \tag{16}$$

From Eqs. 4a and 4b, it now follows

$$p_0 = A_0 \frac{(b^2 - a^2)}{2ab^2} E_1 = \frac{A_0}{2a}\left(1 - \frac{a^2}{b^2}\right) E_1 \tag{17a}$$

$$q_0 = 0 \tag{17b}$$

It has now been established that for the zeroth harmonic of inner boundary displacement, the tractions of the outer boundary are described by their zeroth harmonic only. This is precisely the objective as indicated earlier. Knowing A_0, the amplitude of the zeroth harmonic of inner boundary displacement, the normal and shearing tractions of the outer boundary may be evaluated with the aid of Eqs. 17a and 17b.

Substituting Eq. 16 in Eqs. 6a, 6b, and 6c, the description of the entire state of stress throughout the culvert (due to the zeroth harmonic loading) is obtained as:

$$\tau_{rr} = \frac{A_0}{2a}\left(1 - \frac{a^2}{r^2}\right) E_1 \tag{17c}$$

$$\tau_{\theta\theta} = \frac{A_0}{2a}\left(1 + \frac{a^2}{r^2}\right) E_1 \tag{17d}$$

$$\tau_{r\theta} = 0 \tag{17e}$$

Summary—Zeroth Harmonic

The displacements to be experimentally determined are

$$u(a, \theta) = A_0$$
$$v(a, \theta) = 0$$

The corresponding outer boundary tractions are

$$p_0 = \tau_{rr}(b, \theta) = \frac{A_0}{2a}\left(1 - \frac{a^2}{b^2}\right) E_1$$

$$q_0 = \tau_{r\theta}(b, \theta) = 0$$

First Harmonic (Fig. 3)

Tractions of the first harmonic loading are described as:

$$p_1 = a_1 \cos\theta \tag{18a}$$

$$q_1 = b_1 \sin\theta \tag{18b}$$

The most general form of stress function, φ_1, satisfying the requirement that its form be that of the first harmonic was given by Michell (2, p. 116) as:

$$\varphi_1 = \overset{1}{\varphi}_1 + \overset{2}{\varphi}_1 + \overset{3}{\varphi}_1 + \overset{4}{\varphi}_1$$

where

$$\overset{1}{\varphi}_1 = \frac{C_1}{2} r\theta \sin\theta$$

$$\overset{2}{\varphi}_1 = (C_2 r^3 + C_3 r^{-1} + C_4 r \log r) \cos\theta$$

$$\overset{3}{\varphi}_1 = \frac{-C_5}{2} r\theta \cos\theta$$

$$\overset{4}{\varphi}_1 = (C_6 r^3 + C_7 r^{-1} + C_8 r \log r) \sin\theta$$

Timoshenko (2, p. 119) argues that when the resultant of all forces on each boundary is zero, then $C_1 = C_4 = C_5 = C_8 = 0$. As this is certainly the case for an empty culvert in equilibrium with the tractions applied to its outer boundary, the stress function for this case becomes:

$$\varphi_1 = \overset{2}{\varphi}_2 + \overset{4}{\varphi}_1$$

where

$$\overset{2}{\varphi}_1 = (C_2 r^3 + C_3 r^{-1}) \cos\theta$$

$$\overset{4}{\varphi}_1 = (C_6 r^3 + C_7 r^{-1}) \sin\theta$$

The stresses are given by

$$\tau_{rr} = \frac{1}{r}\frac{\partial\varphi_1}{\partial r} + \frac{1}{r^2}\frac{\partial^2\varphi_1}{\partial\theta^2} = 2(C_2 r - C_3 r^{-3}) \cos\theta + 2(C_6 r - C_7 r^{-3}) \sin\theta \quad (19a)$$

$$\tau_{\theta\theta} = \frac{\partial^2\varphi_1}{\partial r^2} = 2(3C_2 r + C_3 r^{-3}) \cos\theta + 2(3C_6 r + C_7 r^{-3}) \sin\theta \quad (19b)$$

$$\tau_{r\theta} = -\frac{\partial}{\partial r}\left(\frac{1}{r}\frac{\partial\varphi_1}{\partial\theta}\right) = 2(C_2 r - C_3 r^{-3}) \sin\theta - 2(C_6 r - C_7 r^{-3}) \cos\theta \quad (19c)$$

The following conditions exist on the boundaries:

$$\tau_{rr}(a, \theta) = 0 \quad (20a)$$

$$\tau_{r\theta}(a, \theta) = 0 \quad (20b)$$

$$\tau_{rr}(b, \theta) = p_1 = a_1 \cos\theta \quad (20c)$$

$$\tau_{r\theta}(b, \theta) = q_1 = b_1 \sin\theta \quad (20d)$$

Matching coefficients of Eq. 19a when r = b with Eq. 20c it follows:

$$\tfrac{1}{2} a_1 = C_2 b - C_3 b^{-3} \quad (21a)$$

$$0 = C_6 b - C_7 b^{-3} \quad (21b)$$

Matching coefficients of Eq. 19c when r = b with Eq. 20d it follows:

$$\tfrac{1}{2} b_1 = C_2 b - C_3 b^{-3} \quad (21c)$$

$$0 = C_6 b - C_7 b^{-3}$$

For both Eqs. 21a and 21c to agree, it follows that

$$a_1 = b_1$$

This result is also a necessary condition for the tractions, Eqs. 18a and 18b, to be in equilibrium.

Boundary conditions (Eq. 20a and Eq. 20b) supply the additional information necessary for the evaluation of the constants C_2, C_3, C_6, and C_7. Substituting the value $r = a$ in Eqs. 19a and 19c and matching coefficients with Eqs. 20a and 20b, it follows:

$$C_2 a - C_3 a^{-3} = 0 \tag{22a}$$

$$C_6 a - C_7 a^{-3} = 0 \tag{22b}$$

The four equations, Eqs. 21a, 21b, 22a, and 22b are solved simultaneously and yield the following values for the four constants.

$$C_2 = \frac{a_1}{2b\left[1 - \left(\frac{a}{b}\right)^4\right]}$$

$$C_3 = \frac{a_1 a^4}{2b\left[1 - \left(\frac{a}{b}\right)^4\right]} = a^4 C_2$$

$$C_6 = 0$$

$$C_7 = 0$$

These expressions for constants C_2, C_3, C_6, C_7 are now substituted into the expressions for stress Eqs. 19a, 19b and 19c. Therefore,

$$\tau_{rr}(r,\theta) = \frac{r}{b}\frac{\left(1 - \frac{a^4}{r^4}\right)}{\left(1 - \frac{a^4}{b^4}\right)} a_1 \cos\theta = k_1 r \left(1 - \frac{a^4}{r^4}\right) a_1 \cos\theta \tag{23a}$$

$$\tau_{\theta\theta}(r,\theta) = \frac{r}{b}\frac{\left(3 + \frac{a^4}{r^4}\right)}{\left(1 - \frac{a^4}{b^4}\right)} a_1 \cos\theta = k_1 r \left(3 + \frac{a^4}{r^4}\right) a_1 \cos\theta \tag{23b}$$

$$\tau_{r\theta}(r,\theta) = \frac{r}{b}\frac{\left(1 - \frac{a^4}{r^4}\right)}{\left(1 - \frac{a^4}{b^4}\right)} a_1 \sin\theta = k_1 r \left(1 - \frac{a^4}{r^4}\right) a_1 \sin\theta \tag{23c}$$

when

$$k_1 = \frac{1}{b\left(1 - \frac{a^4}{b^4}\right)}$$

These values of stress are now substituted into the stress-displacement relations, Eqs. 9a, 9b, and 9c. For Eq. 9a:

$$\frac{\partial u}{\partial r} = \frac{k_1}{E_1} r \left[\left(1 - \frac{a^4}{r^4}\right) - \nu_1 \left(3 + \frac{a^4}{r^4}\right)\right] a_1 \cos\theta$$

Integrating:

$$u(r,\theta) = \frac{k_1}{2E_1} r^2 \left[\left(1 + \frac{a^4}{r^4}\right) - \nu_1 \left(3 - \frac{a^4}{r^4}\right)\right] a_1 \cos\theta + g_3(\theta) \tag{24}$$

Putting this result and the stresses (Eqs. 23a, 23b, and 23c) into Eq. 9b:

$$\frac{\partial v}{\partial \theta} = \frac{k_1 r^2}{2E_1} \left[\left(5 + \frac{a^4}{r^4}\right) + \nu_1 \left(1 + \frac{a^4}{r^4}\right)\right] a_1 \cos\theta - g_3(\theta)$$

Integrating:

$$v(r,\theta) = \frac{k_1 r^2}{2E_1} \left[\left(5 + \frac{a^4}{r^4}\right) + \nu_1 \left(1 + \frac{a^4}{r^4}\right)\right] a_1 \sin\theta - \int g_3(\theta)\, d\theta + g_4(r) \tag{25}$$

Substituting Eqs. 24, 25, and 23c, in Eq. 9c:

$$\left[\frac{\partial g_3(\theta)}{\partial \theta} + \int g_3(\theta)\, d\theta\right] + \left[r \frac{\partial g_4(r)}{\partial r} - g_4(r)\right] = 0$$

Symmetry conditions are now introduced to evaluate $g_3(\theta)$ and $g_4(r)$.

Symmetry Condition No. 1

$v(r,0) = 0$ for $b \geq r \geq a$ - $\int g_3(\theta)\, d\theta + g_4(r) = 0$ for $\theta = 0$ and $b \geq r \geq a$

As this must be true for all r ($b \geq r \geq a$), then $g_4(r) \equiv 0$. Consequently

$$\int g_3(\theta)\, d\theta = 0 \text{ when } \theta = 0 \tag{26}$$

Symmetry Condition No. 2

$u(r,\theta) = u(r,-\theta)$

Substituting in Eq. 24:

$$g_3(\theta) = g_3(-\theta), \text{ for all } \theta \tag{27}$$

which implies $g_3(\theta)$ is an even function. We now search for a function $g_3(\theta)$ which will satisfy Eq. 26 and Eq. 27. Let

$$G_3(\theta) = \int g_3(\theta)\, d\theta = C_1\theta \sin\theta + C_2\theta \cos\theta + C_3\theta\, C_4 + C_5 \sin\theta \cos\theta + C_6 \sin\theta \cos\theta + C_7 \sin\theta + C_8 \cos\theta \tag{28}$$

Applying Eq. 26:

$$C_4 + C_8 = 0 \tag{29}$$

Solving now for $g_3(\theta) = \frac{d}{d\theta} \int g_3(\theta)\, d\theta$ and applying Eqs. 27 and 29:

$C_1 = C_4 = C_6 = C_8 = 0$

Eq. 28 then becomes

$$G_3(\theta) = C_2\theta\cos\theta + C_3\theta + C_5\sin\theta\cos\theta + C_7\sin\theta = 0$$

Single-Valuedness of Displacements Condition No. 3

$$v(r,\theta) = v(r,\theta + 2\pi n) \tag{30}$$

With Eq. 30 and $g_4(r) = 0$, Eq. 25 yields

$$C_2\theta\cos\theta + C_3\theta = 0, \text{ for all } \theta$$

This is true only if $C_2 = C_3 = 0$ so that Eq. 28 becomes

$$G_3(\theta) = C_5\sin\theta\cos\theta + C_7\sin\theta$$

and thus

$$g_3(\theta) = C_5(1 - 2\sin^2\theta) + C_7\cos\theta$$

Eqs. 24 and 25 now become

$$u(r,\theta) = \frac{k_1}{2E_1}r^2\left[\left(1 + \frac{a^4}{r^4}\right) - \nu_1\left(3 - \frac{a^4}{r^4}\right)\right]a_1\cos\theta + C_5(1 - 2\sin^2\theta) + C_7\cos\theta \tag{31}$$

$$v(r,\theta) = \frac{k_1 r^2}{2E_1}\left[\left(5 + \frac{a^4}{r^4}\right) + \nu_1\left(1 + \frac{a^4}{r^4}\right)\right]a_1\sin\theta - C_5\sin\theta\cos\theta - C_7\sin\theta$$

Symmetry Condition No. 4

$$u(a,0) = -u(a,\pi)$$

This condition will serve to keep the origin of the coordinates at the midpoint of the vertical diameter.

Substituting in Eq. 31:

$$C_5 + C_7 = -(C_5 - C_7)$$

This implies $C_5 = 0$. The following displacement field now results:

$$u(r,\theta) = \frac{k_1 r^2}{2E_1}\left[\left(1 + \frac{a^4}{r^4}\right) - \nu_1\left(3 - \frac{a^4}{r^4}\right)\right]a_1\cos\theta$$

$$v(r,\theta) = \frac{k_1 r^2}{2E_1}\left[\left(5 + \frac{a^4}{r^4}\right) + \nu_1\left(1 + \frac{a^4}{r^4}\right)\right]a_1\sin\theta$$

On the inner boundary: (recalling $a_1 = b_1$)

$$u(a,\theta) = \frac{a^2}{b}\cdot\frac{b^4}{(b^4 - a^4)}\left(\frac{1 - \nu_1}{E_1}\right)a_1\cos\theta \tag{32a}$$

$$v(a,\theta) = \frac{a^2}{b}\cdot\frac{b^4}{(b^4 - a^4)}\left(\frac{3 + 2\nu_1}{E_1}\right)b_1\sin\theta \tag{32b}$$

Comparing Eqs. 3a and 3b with Eqs. 32a and 32b, respectively, it follows

$$A_0 = 0$$

$$A_1 = \frac{a^2}{b} \cdot \frac{b^4}{(b^4 - a^4)} \left(\frac{1 - \nu_1}{E_1}\right) a_1$$

$$B_1 = \frac{a^2}{b} \cdot \frac{b^4}{(b^4 - a^4)} \left(\frac{3 + 2\nu_1}{E_1}\right) b_1$$

$$A_n = B_n = 0 \text{ for } n \geq 2$$

Therefore,

$$a_1 = A_1 \frac{b}{a^2} \cdot \frac{(b^4 - a^4)}{b^4} \left(\frac{E_1}{1 - \nu_1}\right) \tag{33a}$$

$$b_1 = B_1 \frac{b}{a^2} \cdot \frac{(b^4 - a^4)}{b^4} \left(\frac{E_1}{3 + 2\nu_1}\right) \tag{33b}$$

From Eqs. 18a and 18b it now follows

$$p_1 = A_1 \frac{b}{a^2} \left(1 - \frac{a^4}{b^4}\right) \left(\frac{E_1}{1 - \nu_1}\right) \cos\theta \tag{34a}$$

$$q_1 = B_1 \frac{b}{a^2} \left(1 - \frac{a^4}{b^4}\right) \left(\frac{E_1}{3 + 2\nu_1}\right) \sin\theta \tag{34b}$$

It has now been established that for the first harmonics of inner boundary displacements, the tractions of the outer boundary are described by the first harmonics only. Knowing A_1 and B_1, the amplitudes of the first harmonics of the inner boundary displacements, the normal and shearing tractions on the boundary may be evaluated with the aid of Eqs. 34a and 34b.

Substituting Eqs. 33a and 33b in Eqs. 23a, 23b, and 23c; we have

$$\tau_{rr}(r, \theta) = A_1 \frac{r}{a^2} \left(1 - \frac{a^4}{r^4}\right) \left(\frac{E_1}{1 - \nu_1}\right) \cos\theta \tag{34c}$$

$$\tau_{\theta\theta}(r, \theta) = A_1 \frac{r}{a^2} \left(3 + \frac{a^4}{r^4}\right) \left(\frac{E_1}{1 - \nu_1}\right) \cos\theta \tag{34d}$$

$$\tau_{r\theta}(r, \theta) = B_1 \frac{r}{a^2} \left(1 - \frac{a^4}{r^4}\right) \left(\frac{E_1}{3 + 2\nu_1}\right) \sin\theta \tag{34e}$$

Summary—First Harmonic

The displacements to be determined experimentally are

$$u(a, \theta) = A_1 \cos\theta$$

$$v(a, \theta) = B_1 \sin\theta$$

The corresponding outer boundary tractions are

$$p_1 = \tau_{rr}(b, \theta) = \frac{b}{a^2} \left(1 - \frac{a^4}{b^4}\right) \left(\frac{E_1}{1 - \nu_1}\right) A_1 \cos\theta$$

$$q_1 = \tau_{r\theta}(b, \theta) = \frac{b}{a^2} \left(1 - \frac{a^4}{b^4}\right) \left(\frac{E_1}{3 + 2\nu_1}\right) B_1 \sin\theta$$

nth Harmonic, $n \geq 2$

The tractions of the nth harmonic of loading are:

$$p_n = a_n \cos n\theta$$
$$q_n = b_n \sin n\theta$$

The most general form of stress function, φ_n, satisfying the requirement that its form be that of the nth harmonic was given by Michell (2, p. 116) as:

$$\varphi_n = \overset{1}{\phi}_n + \overset{2}{\phi}_n$$

where

$$\overset{1}{\phi}_n = (A_n r^n + B_n r^{n+2} + A'_n r^{-n} + B'_n r^{-n+2}) \cos n\theta \tag{35a}$$

$$\overset{2}{\phi}_n = (C_n r^n + D_n r^{n+2} + C'_n r^{-n} + D'_n r^{-n+2}) \sin n\theta \tag{35b}$$

The stresses are given by:

$$\tau_{rr} = \frac{1}{r}\frac{\partial \varphi_n}{\partial r} + \frac{1}{r^2}\frac{\partial^2 \varphi_n}{\partial \theta^2} \tag{36a}$$

$$\tau_{\theta\theta} = \frac{\partial^2 \varphi_n}{\partial r^2} \tag{36b}$$

$$\tau_{r\theta} = -\frac{\partial}{\partial r}\left(\frac{1}{r}\frac{\partial \varphi_n}{\partial \theta}\right) \tag{36c}$$

Substituting Eqs. 35a and 35b in 36a, we obtain:

$$\tau_{rr} = h_1(r) \cos n\theta + h_2(r) \sin n\theta \tag{37a}$$

where

$$h_1(r) = -n(n-1) A_n r^{n-2} \quad (n \quad 2)(n \; 1) B_n r^n \quad n(n \; 1) A'_n r^{-n-2}$$
$$(n+2)(n-1) B'_n r^{-n}$$

$$h_2(r) = -n(n-1) C_n r^{n-2} - (n-2)(n+1) D_n r^n - n(n+1) C'_n r^{-n-2} -$$
$$(n+2)(n-1) D'_n r^{-n}$$

Substituting Eqs. 35a and 35b into Eq. 36c, we obtain:

$$\tau_{r\theta} = h_3(r) \cos n\theta + h_4(r) \sin n\theta \tag{37b}$$

where

$$h_3(r) = -n(n-1) C_n r^{n-2} - n(n+1) D_n r^n + n(n+1) C'_n r^{-n-2} +$$
$$n(n-1) D'_n r^{-n}$$

$$h_4(r) = n(n-1) A_n r^{n-2} + n(n+1) B_n r^n - n(n+1) A'_n r^{-n-2} -$$
$$n(n-1) B'_n r^{-n}$$

$$\tau_{\theta\theta} = h_5(r)\cos n\theta + h_6(r)\sin n\theta \tag{37c}$$

where

$$h_5(r) = n(n-1)A_n r^{n-2} + (n+2)(n+1)B_n r^n + n(n+1)A_n' r^{-n-2} + (n-2)(n-1)B_n' r^{-n}$$

$$h_6(r) = n(n-1)C_n r^{n-2} + (n+2)(n+1)D_n r^n + n(n+1)C_n' r^{-n-2} + (n-2)(n-1)D_n' r^{-n}$$

Study the boundary conditions:

(i) $\tau_{rr}(a,\theta) = h_1(a)\cos n\theta + h_2(a)\sin n\theta = 0$

(ii) $\tau_{r\theta}(a,\theta) = h_3(a)\cos n\theta + h_4(a)\sin n\theta = 0$

(iii) $\tau_{rr}(b,\theta) = h_1(b)\cos n\theta + h_2(b)\sin n\theta = a_n\cos n\theta$

(iv) $\tau_{r\theta}(b,\theta) = h_3(b)\cos n\theta + h_4(b)\sin n\theta = b_n\sin n\theta$

The following relationships must be satisfied for these conditions to hold true for all θ.

$h_1(a) = 0$
$h_4(a) = 0$
$h_1(b) = a_n$
$h_4(b) = b_n$
$h_2(a) = 0$
$h_3(a) = 0$
$h_2(b) = 0$
$h_3(b) = 0$

The foregoing system of eight equations and eight unknowns yields the following results.

$$C_n = D_n = C_n' = D_n' = 0 \tag{38}$$

$$A_n = \frac{-a_n}{2n(n-1)b^{n-2}} \left\{ \frac{(n-1)\left[n-(n+2)\beta_n\right] + \left[n+(n-2)\beta_n\right]\alpha^{-2n} - n^2(1-\beta_n)\alpha^2}{\alpha^{-2n} + \alpha^{2n} - n^2(\alpha^{-2}+\alpha^2) + 2(n^2-1)} \right\} \tag{39a}$$

$$B_n = \frac{-a_n}{2(n+1)b^n} \left\{ \frac{\alpha^{-2}\left[(n+2)\beta_n - n\right] - \alpha^{-2n}(1+\beta_n) + (1-\beta_n)(n+1)}{\alpha^{-2n} + \alpha^{2n} - n^2(\alpha^{-2}+\alpha^2) + 2(n^2-1)} \right\} \tag{39b}$$

$$A_n' = \frac{a_n b^{n+2}}{2n(n+1)} \left\{ \frac{\alpha^{2n}\left[n-(n+2)\beta_n\right] - n^2\left[1-\alpha^2(1+\beta_n)\right] - n - (n+1)(n-2)\beta_n}{\alpha^{-2n} + \alpha^{2n} - n^2(\alpha^{-2}+\alpha^2) + 2(n^2-1)} \right\} \tag{39c}$$

$$B_n' = \frac{a_n b^n}{2(n-1)} \left\{ \frac{\alpha^{-2}\left[n+(n-2)\beta_n + \alpha^{2n+2}(-1+\beta_n)\right] - (n-1)(n+\beta_n)}{\alpha^{-2n} + \alpha^{2n} - n^2(\alpha^{-2}+\alpha^2) + 2(n^2-1)} \right\} \tag{39d}$$

where

$$\alpha \equiv \text{ratio of pipe diameters} = \frac{a}{b} \tag{40a}$$

and

$$\beta_n \equiv \text{ratio of tangential to normal amplitudes of the n th harmonic} = \frac{b_n}{a_n} \tag{40b}$$

Returning to Eqs. 37a, 37b, and 37c and introducing Eqs. 38, and 39a through 39d, we obtain:

$$\tau_{rr} = \frac{a_n}{2D}\left[\left(\frac{r}{b}\right)^{n-2} N_1 + \left(\frac{r}{b}\right)^{n} (n-2)\, N_2 - \left(\frac{r}{b}\right)^{-n-2} N_3 - \left(\frac{r}{b}\right)^{-n} (n+2)\, N_4\right] \cos n\theta \tag{41a}$$

$$\tau_{\theta\theta} = -\frac{a_n}{2D}\left[\left(\frac{r}{b}\right)^{n-2} N_1 + \left(\frac{r}{b}\right)^{n} (n+2)\, N_2 - \left(\frac{r}{b}\right)^{-n-2} N_3 - \left(\frac{r}{b}\right)^{-n} (n-2)\, N_4\right] \cos n\theta \tag{41b}$$

$$\tau_{r\theta} = -\frac{a_n}{2D}\left[\left(\frac{r}{b}\right)^{n-2} N_1 + \left(\frac{r}{b}\right)^{n} (n)\, N_2 + \left(\frac{r}{b}\right)^{-n-2} N_3 + \left(\frac{r}{b}\right)^{-n} (n)\, N_4\right] \sin n\theta \tag{41c}$$

where

$$D = \alpha^{-2n} + \alpha^{2n} - n^2 (\alpha^{-2} + \alpha^2) + 2 (n^2 - 1) \tag{41d}$$

$$N_1 = (n-1)\left[n - (n+2)\beta_n\right] + \left[n + (n-2)\beta_n\right] \alpha^{-2n} - n^2 (1 - \beta_n) \alpha^2 \tag{41e}$$

$$N_2 = \alpha^{-2}\left[(n+2)\beta_n - n\right] - \alpha^{-2n} (1 + \beta_n) + (1 - \beta_n)(n+1) \tag{41f}$$

$$N_3 = \alpha^{2n}\left[n - (n+2)\beta_n\right] - n^2\left[1 - \alpha^2 (1 + \beta_n)\right] - n - (n+1)(n-2)\beta_n \tag{41g}$$

$$N_4 = \alpha^{-2}\left[n + (n-2)\beta_n + \alpha^{2n+2}(-1 + \beta_n)\right] - (n-1)(1 + \beta_n) \tag{41h}$$

and where α and β_n are as defined in Eqs. 40a and 40b.

Substituting Eqs. 41a through 41h in the stress displacement relations (Eqs. 9a, 9b and 9c) and integrating, we obtain the following:

$$u(r,\theta) = \frac{r}{2DE_1}\left\{(1+\nu_1)\left(\frac{r}{b}\right)^{n-2} \frac{N_1}{(n-1)} + \left[(n-2) + \nu_1 (n+2)\right]\left(\frac{r}{b}\right)^{n} \frac{N_1}{(n+1)} + (1+\nu_1)\left(\frac{r}{b}\right)^{-n-2} \frac{N_3}{(n+1)} + \left[(n+2) + \nu_1 (n-2)\right]\left(\frac{r}{b}\right)^{-n} \frac{N_4}{(n-1)}\right\} a_n \cos n\theta + h_7(\theta) \tag{42}$$

$$v(r,\theta) = \frac{r}{2DE_1\beta_n}\left\{-(1+\nu_1)\left(\frac{r}{b}\right)^{n-2}\frac{N1}{(n-1)} - \left[n(1+\nu_1)+4\right]\left(\frac{r}{b}\right)^{n}\right.$$
$$\frac{N_2}{(n+1)} + (1+\nu_1)\left(\frac{r}{b}\right)^{-n-2}\frac{N_3}{(n+1)} + \left[n(1+\nu_1)-4\right]$$
$$\left.\left(\frac{r}{b}\right)^{-n}\frac{N1}{(n-1)}\right\} b_n \sin n\theta - \int h_7(\theta)\,d\theta + h_8(r) \quad (43)$$

and

$$\left[\frac{\partial h_7(\theta)}{\partial\theta} + \int h_7(\theta)\,d\theta\right] + \left[r\frac{\partial h_8(r)}{\partial r} - h_8(r)\right] = 0$$

and where D, N_1, N_2, N_3, and N_4 are described by Eqs. 41a through 41h.

As in the case when n = 1, introduction of the following conditions leads to the conclusion that

$$h_7(\theta) = h_8(r) \equiv 0 \quad (44)$$

Symmetry condition No. 1: $v(r,0) = 0$ for $b \geq r \geq a$
Symmetry condition No. 2: $u(r,\theta) = u(r,-\theta)$
Single-valuedness of displacements condition No. 3: $v(r,\theta) = v(r,\theta+2\pi n)$
Symmetry condition No. 4: $u(a,0) = -u(a,\pi)$

Substituting Eq. 44 into Eq. 42 and comparing with Eqs. 3a and 3b, it follows that:

$A_0 = A_1 = B_1 = 0$

$$A_n = \frac{a}{2DE_1}\overset{u}{\gamma}_n a_n$$

$$B_n = \frac{a}{2DE_1\beta_n}\overset{v}{\gamma}_n b_n \qquad \text{for } n \geq 2.$$

Therefore

$$a_n\overset{u}{\gamma}_n = \frac{2DE_1}{a}A_n \quad (45a)$$

$$\frac{b_n\overset{v}{\gamma}_n}{\beta_n} = \frac{2DE_1}{a}B_n \quad (45b)$$

where

$$\frac{\overset{u}{\gamma}_n}{4} = \left[\frac{n}{(n+1)}\alpha^{n-2} + \frac{n}{(n-1)}\alpha^{-n-2} - \frac{n}{(n-1)}\alpha^{n} - \frac{n}{(n+1)}\alpha^{-n}\right]$$
$$+\left[-\frac{(n+2)}{(n+1)}\alpha^{n-2} + \frac{(n-2)}{(n-1)}\alpha^{-n-2} + \frac{n}{(n-1)}\alpha^{n} - \frac{n}{(n+1)}\alpha^{-n}\right]\beta_n$$

$$\frac{\overset{v}{\gamma}_n}{4} = \left[\frac{n}{(n+1)}\alpha^{n-2} - \frac{n}{(n-1)}\alpha^{-n-2} - \frac{(n-2)}{(n-1)}\alpha^{n} + \frac{(n+2)}{(n+1)}\alpha^{-n}\right]$$
$$+\left[-\frac{(n+2)}{(n+1)}\alpha^{n-2} - \frac{(n-2)}{(n-1)}\alpha^{-n-2} + \frac{(n-2)}{(n-1)}\alpha^{n} + \frac{(n+2)}{(n+1)}\alpha^{-n}\right]\beta_n$$

It should be noted that γ_n^u, γ_n^v, and β_n are functions of a_n and b_n. Simultaneous solution of Eqs. 45a and 45b yield the values for a_n and b_n indicated in the summary that follows. Refer to Appendix B for the substantiating calculations.

Summary—n th Harmonic, $n \geq 2$

Given the experimental displacements

$$u(a, \theta) = A_n \cos n\theta$$
$$v(a, \theta) = B_n \sin n\theta$$

$$a_n = \frac{E}{2a\,(1 - \nu^2)} \left[\frac{(C_{1n})^3 A_n + (C_{2n})^3 B_n}{(C_{3n})^3 A_n + (C_{4n})^3 B_n} \right] A_n$$

$$b_n = \frac{E}{2a\,(1 - \nu^2)} \left[\frac{(C_{5n})^3 A_n + (C_{6n})^3 B_n}{(C_{7n})^3 A_n + (C_{8n})^3 B_n} \right] B_n$$

These values are then substituted in the equations below

$$p_n = a_n \cos n\theta$$
$$q_n = b_n \sin n\theta$$

For definition and evaluation of the coefficients $C_{1n}, \ldots, C_{8n}$ see Appendix B.

Reference

2. Timoshenko and Goodier. Theory of Elasticity. McGraw-Hill, 2nd Ed., 1951.

Appendix B

COMPUTER CALCULATIONS OF COEFFICIENTS $C_{1n}, C_{2n}, \ldots, C_{8n}$

Recall from Appendix A

$$a_n = \frac{2DE_1}{a\,\gamma_n^u} A_n \tag{46a}$$

$$b_n = \frac{2DE_1}{a\,\gamma_n^v} \beta_{11}\,\beta_{11} \tag{46b}$$

where

$$E_1 = \frac{E}{(1 - \nu^2)}$$

$$D = \alpha^{-2n} + \alpha^{2n} - n^2\,(\alpha^{-2} + \alpha^2) + 2\,(n^2 - 1)$$

$$\beta_n = \frac{M_1 A_n + M_2 B_n}{M_3 A_n + M_4 B_n}$$

$$\overset{u}{\gamma}_n = M_5 + M_6 \beta_n$$

$$\overset{v}{\gamma}_n = M_7 + M_8 \beta_n$$

and where

$$M_1 = \left[-n(n-1)\alpha^{n-2} + n(n+1)\alpha^{-n-2} + (n+1)(n-2)\alpha^n - (n-1)(n+2)\alpha^{-n}\right]$$

$$M_2 = \left[n(n-1)\alpha^{n-2} + n(n+1)\alpha^{-n-2} - n(n+1)\alpha^n - n(n-1)\alpha^{-n}\right]$$

$$M_3 = \left[-(n-1)(n+2)\alpha^{n-2} - (n-2)(n+1)\alpha^{-n-2} + (n+1)(n-2)\alpha^n + (n-1)(n+2)\alpha^{-n}\right]$$

$$M_4 = \left[(n-1)(n+2)\alpha^{n-2} - (n-2)(n+1)\alpha^{-n-2} - n(n+1)\alpha^n + n(n-1)\alpha^{-n}\right]$$

$$M_5 = \left[\frac{n}{(n+1)}\alpha^{n-2} + \frac{n}{(n-1)}\alpha^{-n-2} - \frac{n}{(n-1)}\alpha^n - \frac{n}{(n+1)}\alpha^{-n}\right]$$

$$M_6 = \left[-\frac{(n+2)}{(n+1)}\alpha^{n-2} + \frac{(n-2)}{(n-1)}\alpha^{-n-2} + \frac{n}{(n-1)}\alpha^n - \frac{n}{(n+1)}\alpha^{-n}\right]$$

$$M_7 = \left[\frac{n}{(n+1)}\alpha^{n-2} - \frac{n}{(n-1)}\alpha^{-n-2} - \frac{(n-2)}{(n-1)}\alpha^n + \frac{(n+2)}{(n+1)}\alpha^{-n}\right]$$

$$M_8 = \left[-\frac{(n+2)}{(n+1)}\alpha^{n-2} - \frac{(n-2)}{(n-1)}\alpha^{-n-2} + \frac{(n-2)}{(n-1)}\alpha^n + \frac{(n+2)}{(n+1)}\alpha^{-n}\right]$$

Eqs. 46a and 46b now become

$$a_n = \frac{E}{2a(1-\nu^2)}\left[\frac{(C_{1n})^3 A_n + (C_{2n})^3 B_n}{(C_{3n})^3 A_n + (C_{4n})^3 B_n}\right] A_n \qquad (47a)$$

$$b_n = \frac{E}{2a(1-\nu^2)}\left[\frac{(C_{5n})^3 A_n + (C_{6n})^3 B_n}{(C_{7n})^3 A_n + (C_{8n})^3 B_n}\right] B_n \qquad (47b)$$

where the $C_{1n}, \ldots, C_{8n}$ are as given below and are displayed in the charts which follow.

$$C_{1n} = (DM_3)^{1/3} \qquad (48a)$$

$$C_{2n} = (DM_4)^{1/3} \qquad (48b)$$

$$C_{3n} = (M_3 M_5 + M_1 M_6)^{1/3} \qquad (48c)$$

$$C_{4n} = (M_4 M_5 + M_2 M_6)^{1/3} \qquad (48d)$$

$$C_{5n} = (DM_1)^{1/3} \tag{48e}$$

$$C_{6n} = (DM_4)^{1/3} \tag{48f}$$

$$C_{7n} = (M_1 M_8 + M_3 M_8)^{1/3} \tag{48g}$$

$$C_{8n} = (M_2 M_8 + M_4 M_7)^{1/3} \tag{48h}$$

```
C           CALCULATION OF CONSTANTS  C1 THRU C8

      PUNCH 100
  100 FORMAT(1X,1HN,1X,5HALPHA,5X,2HC1,6X,2HC2,6X,2HC3,6X,2HC4,6X,2HC5
     16X,2HC6,6X,2HC7,6X,2HC8)
      DIMENSION A(20)
      G=1./3.
      READ 1, (A(I), I=1,20)
    1 FORMAT (20F4.2)
      DO 2 N=2,9
      DO 2 I=1,20
      X=N
      V=X-2.
      W=X-1.
      Y=X+1.
      Z=X+2.
      DON=A(I)**(-2.*X)+A(I)**(2.*X)-(X**2.)*((A(I)**(-2.))+(A(I)**2.))+
     12.*((X**2.)-1.)
      B=A(I)**V
      C=A(I)**(-Z)
      D=A(I)**X
      E=A(I)**(-X)
      XN1N=-X*W*B    +X*Y*C    +Y*V*D    -W*Z*E
      XN2N=X*W*B    +X*Y*C    -X*Y*D    -X*W*E
      XN3N=-W*Z*B    -V*Y*C    +Y*V*D    +W*Z*E
      XN4N=W*Z*B    -V*Y*C    -X*Y*D    +X*W*E
      XN5N = ((X*B)/Y)+((X*C)/W)-((X*D)/W)-((X*E)/Y)
      XN6N = -((Z*B)/Y)+((V*C)/W)+((X*D)/W)-((X*E)/Y)
      XN7N = ((X*B)/Y)-((X*C)/W)-((V*D)/W)+((Z*E)/Y)
      XN8N = -((Z*B)/Y)-((V*C)/W)+((V*D)/W)+((Z*E)/Y)
      CAU=DON*XN3N
      IF(CAU)11,12,13
11    CAU=CAU*(-1.)
      C1=CAU**G
      C1=C1*(-1.)
      GO TO 4
12    C1=0
      GO TO 4
13    C1=CAU**G
4     CBU=DON*XN4N
      IF(CBU)15,16,17
15    CBU=CBU*(-1.)
      C2=CBU**G
      C2=C2*(-1.)
      GO TO 5
16    C2=0
      GO TO 5
17    C2=CBU**G
5     CAL=XN5N*XN3N+XN6N*XN1N
      IF(CAL)18,19,20
18    CAL=CAL*(-1.)
      C3=CAL**G
      C3=C3*(-1.)
```

```
      GO TO 6
19    C3=0
      GO TO 6
20    C3=CAL**G
6     CBL =(XN5N*XN4N+XN6N*XN2N)
      IF(CBL)21,22,23
21    CBL=CBL*(-1.)
      C4=CBL**G
      C4=C4*(-1.)
      GO TO 7
22    C4=0
      GO TO 7
23    C4=CBL**G
    7 CA2U = DON * XN1N
      IF(CA2U)24,25,26
24    CA2U=CA2U*(-1.)
      C5=CA2U**G
      C5=C5*(-1.)
      GO TO 8
25    C5=0
      GO TO 8
26    C5=CA2U**G
    8 CB2U = DON * XN2N
      IF(CB2U) 27, 28, 29
   27 CB2U = CB2U * (-1.)
      C6 = CB2U ** G
      C6 = C6 * (-1.)
      GO TO 9
   28 C6 = 0
      GO TO 9
   29 C6 = CB2U ** G
    9 CA2L=XN1N*XN8N+XN3N*XN7N
      IF (CA2L) 30, 31, 32
   30 CA2L = CA2L * (-1.)
      C7 = CA2L ** G
      C7 = C7 * (-1.)
      GO TO 10
   31 C7 = 0
      GO TO 10
   32 C7 = CA2L ** G
   10 CB2L = XN2N * XN8N + XN4N* XN7N
      IF (CB2L) 33, 34, 35
   33 CB2L=CB2L*(-1.)
      C8 = CB2L ** G
      C8 = C8 * (-1.)
      GO TO 2
   34 C8 = 0
      GO TO 2
   35 C8 = CB2L ** G
    3 FORMAT (I2, F6.4, 8F8.3)
    2 PUNCH 3,N,A(I),C1,C2,C3,C4,C5,C6,C7,C8
      CALL EXIT
      END
+.75+.76+.77+.78+.79+.80+.81+.82+.83+.84+.85+.86+.87+.88+.89+
 .90+.91+.92+.93+.'
```

PROGRAM OUTPUT

N	ALPHA	C1	C2	C3	C4	C5	C6	C7	C8
2	.7500	.711	.785	.937	.010	1.044	1.175	.010	.937
2	.7600	.653	.725	.871	.010	.952	1.076	-.006	.871
2	.7700	.598	.668	.807	.012	.866	.982	-.008	.807
2	.7800	.546	.613	.747	.010	.785	.894	.004	.747
2	.7900	.497	.561	.690	.010	.710	.812	-.005	.690
2	.8000	.451	.512	.635	0.000	.640	.735	.007	.635
2	.8100	.408	.465	.582	-.006	.574	.662	.004	.582
2	.8200	.367	.421	.533	0.000	.513	.594	0.000	.533
2	.8300	.329	.379	.485	0.000	.457	.531	0.000	.485
2	.8400	.293	.339	.440	.008	.404	.472	-.007	.440
2	.8500	.259	.302	.397	.008	.355	.417	-.006	.397
2	.8600	.227	.267	.356	.007	.310	.365	-.006	.356
2	.8700	.198	.233	.318	0.000	.268	.318	0.000	.318
2	.8800	.171	.202	.281	.008	.230	.274	-.007	.281
2	.8900	.146	.174	.246	.004	.195	.233	-.006	.246
2	.9000	.123	.147	.214	.007	.163	.196	.002	.214
2	.9100	.101	.122	.183	.007	.134	.162	-.005	.183
2	.9200	.082	.099	.154	.005	.108	.131	.002	.154
2	.9300	.065	.079	.127	.005	.085	.103	0.000	.127
2	.9400	.049	.060	.102	.002	.064	.079	.002	.102
3	.7500	.912	-.524	1.734	-.016	2.603	2.972	-.014	1.734
3	.7600	.887	.513	1.609	-.012	2.356	2.707	-.008	1.609
3	.7700	.850	.660	1.490	.008	2.127	2.459	-.014	1.490
3	.7800	.805	.708	1.377	.015	1.916	2.229	-.014	1.377
3	.7900	.756	.716	1.269	.012	1.720	2.015	-.011	1.269
3	.8000	.704	.703	1.167	.012	1.539	1.816	-.010	1.167
3	.8100	.650	.676	1.069	-.007	1.372	1.631	-.007	1.069
3	.8200	.596	.640	.977	-.007	1.218	1.458	-.008	.977
3	.8300	.543	.599	.889	.007	1.076	1.299	-.006	.889
3	.8400	.490	.554	.806	0.000	.945	1.150	-.009	.806
3	.8500	.439	.507	.726	.006	.825	1.013	-.007	.726
3	.8600	.390	.459	.651	.005	.716	.886	-.005	.651
3	.8700	.343	.411	.580	.005	.615	.769	-.010	.580
3	.8800	.299	.364	.513	.010	.524	.661	-.008	.513
3	.8900	.257	.318	.449	0.000	.441	.562	-.005	.449
3	.9000	.217	.273	.389	-.008	.367	.471	-.005	.389
3	.9100	.181	.231	.333	-.007	.300	.389	.004	.333
3	.9200	.147	.191	.280	-.006	.240	.315	-.005	.280
3	.9300	.117	.153	.231	.005	.187	.248	-.007	.231
3	.9400	.089	.119	.185	-.005	.141	.189	-.005	.185

N	ALPHA	C1	C2	C3	C4	C5	C6	C7	C8
4	.7500	-2.548	-3.369	2.659	-.025	5.158	5.828	.026	2.659
4	.7600	-2.208	-2.972	2.461	.018	4.634	5.272	.012	2.461
4	.7700	-1.899	-2.610	2.274	.014	4.155	4.761	-.012	2.274
4	.7800	-1.619	-2.278	2.097	.015	3.716	4.290	-.008	2.097
4	.7900	-1.363	-1.976	1.929	.015	3.313	3.856	.012	1.929
4	.8000	-1.130	-1.699	1.770	-.010	2.945	3.456	-.008	1.770
4	.8100	-.914	-1.445	1.620	-.014	2.608	3.088	-.004	1.620
4	.8200	-.711	-1.213	1.477	-.010	2.300	2.748	-.008	1.477
4	.8300	-.507	-.999	1.343	-.008	2.019	2.436	-.011	1.343
4	.8400	-.220	-.800	1.215	-.014	1.762	2.149	-.010	1.215
4	.8500	.351	-.610	1.094	-.009	1.529	1.885	-.013	1.094
4	.8600	.392	-.414	.980	.009	1.317	1.642	.007	.980
4	.8700	.387	.185	.872	-.011	1.125	1.420	-.007	.872
4	.8800	.363	.334	.770	0.000	.952	1.217	-.010	.770
4	.8900	.328	.351	.674	-.010	.797	1.032	.008	.674
4	.9000	.289	.335	.584	-.010	.657	.863	.006	.584
4	.9100	.248	.303	.499	.007	.533	.711	.007	.499
4	.9200	.206	.263	.420	-.010	.424	.574	.004	.420
4	.9300	.167	.220	.346	-.011	.328	.452	-.005	.346
4	.9400	.129	.176	.277	-.008	.245	.344	-.002	.277
5	.7500	-5.628	-6.946	3.731	0.000	9.084	10.118	.027	3.731
5	.7600	-4.920	-6.144	3.443	.021	8.102	9.084	.023	3.443
5	.7700	-4.285	-5.418	3.172	-.027	7.211	8.142	-.018	3.172
5	.7800	-3.716	-4.761	2.917	.021	6.404	7.285	-.030	2.917
5	.7900	-3.206	-4.167	2.677	.021	5.671	6.504	.029	2.677
5	.8000	-2.749	-3.630	2.451	-.022	5.007	5.792	.020	2.451
5	.8100	-2.342	-3.145	2.238	.012	4.406	5.143	-.015	2.238
5	.8200	-1.978	-2.707	2.037	.010	3.861	4.552	.016	2.037
5	.8300	-1.655	-2.312	1.848	.023	3.368	4.012	-.015	1.848
5	.8400	-1.367	-1.957	1.669	-.018	2.922	3.521	.013	1.669
5	.8500	-1.112	-1.638	1.501	.020	2.520	3.073	0.000	1.501
5	.8600	-.886	-1.352	1.343	.014	2.158	2.666	-.009	1.343
5	.8700	-.685	-1.096	1.193	-.008	1.833	2.296	-.011	1.193
5	.8800	-.504	-.868	1.053	.010	1.542	1.960	-.010	1.053
5	.8900	-.333	-.663	.920	.007	1.282	1.655	-.009	.920
5	.9000	.054	-.478	.796	.005	1.051	1.381	-.009	.796
5	.9100	.222	-.297	.680	.010	.848	1.134	-.009	.680
5	.9200	.222	.162	.572	.010	.669	.913	.003	.572
5	.9300	.195	.222	.471	-.010	.515	.717	-.005	.471
5	.9400	.160	.205	.377	.006	.382	.544	.005	.377

N	ALPHA	C1	C2	C3	C4	C5	C6	C7	C8
6	.7500	-10.279	-12.249	4.978	.043	14.890	16.373	.039	4.978
6	.7600	-8.959	-10.786	4.577	.041	13.174	14.574	-.027	4.577
6	.7700	-7.785	-9.475	4.202	-.039	11.636	12.956	0.000	4.202
6	.7800	-6.741	-8.301	3.852	-.031	10.257	11.501	.031	3.852
6	.7900	-5.815	-7.249	3.524	.027	9.019	10.190	.021	3.524
6	.8000	-4.992	-6.307	3.217	.034	7.908	9.009	.029	3.217
6	.8100	-4.264	-5.464	2.930	-.027	6.912	7.944	-.021	2.930
6	.8200	-3.619	-4.709	2.660	.021	6.018	6.984	.026	2.660
6	.8300	-3.050	-4.034	2.407	-.012	5.216	6.117	-.024	2.407
6	.8400	-2.548	-3.431	2.170	.027	4.499	5.336	.018	2.170
6	.8500	-2.108	-2.895	1.948	.019	3.857	4.631	.021	1.948
6	.8600	-1.723	-2.418	1.739	.020	3.284	3.996	-.012	1.739
6	.8700	-1.387	-1.995	1.543	0.000	2.773	3.424	-.013	1.543
6	.8800	-1.096	-1.622	1.359	.012	2.319	2.910	-.013	1.359
6	.8900	-.845	-1.293	1.187	.010	1.918	2.447	.012	1.187
6	.9000	-.629	-1.007	1.025	.020	1.564	2.034	.007	1.025
6	.9100	-.444	-.757	.875	.013	1.254	1.664	-.011	.875
6	.9200	-.282	-.541	.735	.010	.984	1.336	-.010	.735
6	.9300	-.096	-.353	.604	.013	.752	1.046	.007	.604
6	.9400	.149	-.168	.484	.011	.555	.792	-.008	.484
7	.7500	-17.193	-19.975	6.434	.079	23.277	25.328	.027	6.434
7	.7600	-14.894	-17.467	5.890	.046	20.418	22.337	.021	5.890
7	.7700	-12.871	-15.246	5.385	-.046	17.885	19.680	0.000	5.385
7	.7800	-11.091	-13.278	4.917	.050	15.640	17.319	-.021	4.917
7	.7900	-9.526	-11.535	4.483	.041	13.647	15.218	0.000	4.483
7	.8000	-8.149	-9.989	4.079	0.000	11.878	13.347	.031	4.079
7	.8100	-6.939	-8.619	3.702	0.000	10.308	11.679	.021	3.702
7	.8200	-5.877	-7.404	3.352	.034	8.914	10.192	.026	3.352
7	.8300	-4.947	-6.327	3.025	-.021	7.677	8.866	.024	3.025
7	.8400	-4.134	-5.375	2.720	0.000	6.579	7.682	-.022	2.720
7	.8500	-3.425	-4.532	2.435	.028	5.606	6.626	-.018	2.435
7	.8600	-2.808	-3.789	2.170	.020	4.745	5.683	-.022	2.170
7	.8700	-2.275	-3.135	1.921	.028	3.985	4.843	-.012	1.921
7	.8800	-1.815	-2.562	1.689	-.015	3.314	4.093	.020	1.689
7	.8900	-1.422	-2.061	1.473	.024	2.726	3.427	.011	1.473
7	.9000	-1.088	-1.626	1.271	.022	2.211	2.835	.013	1.271
7	.9100	-.807	-1.251	1.083	.017	1.763	2.310	-.016	1.083
7	.9200	-.574	-.930	.908	-.008	1.376	1.848	-.012	.908
7	.9300	-.381	-.659	.746	-.008	1.046	1.442	-.010	.746
7	.9400	-.220	-.433	.597	-.014	.767	1.090	-.012	.597

N	ALPHA	C1	C2	C3	C4	C5	C6	C7	C8
8	.7500	-27.268	-31.061	8.145	-.084	35.219	38.000	.088	8.145
8	.7600	-23.443	-26.933	7.418	-.084	30.606	33.181	-.058	7.418
8	.7700	-20.116	-23.323	6.751	.073	26.570	28.956	0.000	6.751
8	.7800	-17.221	-20.163	6.137	0.000	23.034	25.247	.069	6.137
8	.7900	-14.700	-17.395	5.571	0.000	19.934	21.987	0.000	5.571
8	.8000	-12.506	-14.968	5.049	.031	17.214	19.119	.039	5.049
8	.8100	-10.596	-12.840	4.566	-.027	14.826	16.593	.027	4.566
8	.8200	-8.935	-10.972	4.120	0.000	12.729	14.366	-.027	4.120
8	.8300	-7.492	-9.334	3.706	-.027	10.886	12.402	.027	3.706
8	.8400	-6.241	-7.898	3.323	-.021	9.268	10.669	.029	3.323
8	.8500	-5.158	-6.639	2.967	-.027	7.848	9.139	-.018	2.967
8	.8600	-4.224	-5.537	2.637	-.027	6.603	7.788	.021	2.637
8	.8700	-3.420	-4.575	2.330	-.023	5.512	6.595	-.015	2.330
8	.8800	-2.733	-3.738	2.044	.015	4.560	5.543	.017	2.044
8	.8900	-2.148	-3.011	1.779	.010	3.729	4.615	.014	1.779
8	.9000	-1.654	-2.383	1.533	.021	3.009	3.799	.019	1.533
8	.9100	-1.242	-1.846	1.304	-.023	2.387	3.082	-.011	1.304
8	.9200	-.900	-1.388	1.092	.019	1.854	2.455	.016	1.092
8	.9300	-.623	-1.004	.897	.013	1.402	1.909	.013	.897
8	.9400	-.401	-.687	.717	.010	1.022	1.438	-.003	.717
9	.7500	-41.737	-46.801	10.167	-.100	52.060	55.792	-.058	10.167
9	.7600	-35.574	-40.199	9.208	-.079	44.791	48.208	-.092	9.208
9	.7700	-30.277	-34.501	8.334	.084	38.511	41.645	.046	8.334
9	.7800	-25.720	-29.575	7.538	-.066	33.080	35.956	.046	7.538
9	.7900	-21.797	-25.311	6.810	.109	28.376	31.019	.046	6.810
9	.8000	-18.419	-21.617	6.144	-.066	24.297	26.728	.043	6.145
9	.8100	-15.509	-18.413	5.534	0.000	20.758	22.994	-.031	5.534
9	.8200	-13.004	-15.634	4.974	-.021	17.684	19.741	.039	4.974
9	.8300	-10.848	-13.221	4.459	-.034	15.014	16.905	.027	4.459
9	.8400	-8.994	-11.126	3.984	.021	12.693	14.431	0.000	3.984
9	.8500	-7.404	-9.309	3.547	0.000	10.677	12.270	.024	3.547
9	.8600	-6.042	-7.733	3.143	.031	8.926	10.383	.021	3.143
9	.8700	-4.880	-6.368	2.770	.031	7.407	8.735	-.017	2.770
9	.8800	-3.892	-5.189	2.424	-.022	6.092	7.295	.017	2.424
9	.8900	-3.058	-4.174	2.105	-.012	4.955	6.039	-.012	2.105
9	.9000	-2.357	-3.304	1.810	-.025	3.977	4.944	-.009	1.810
9	.9100	-1.774	-2.562	1.538	-.025	3.139	3.991	-.013	1.538
9	.9200	-1.295	-1.934	1.286	-.010	2.426	3.165	-.004	1.286
9	.9300	-.907	-1.410	1.054	.010	1.825	2.452	.011	1.054
9	.9400	-.600	-.979	.842	-.021	1.324	1.840	.007	.842

Modulus of Soil Reaction as Determined from Triaxial Shear Test

F. DWAYNE NIELSON, Assistant Professor of Civil Engineering, New Mexico State University

In 1942 Spangler published his classical theory for the deflection of underground conduits. This theory has received only limited use, partially because of the inability to determine the proper numerical value of the modulus of soil reaction. Several different attempts have been made to determine this modulus in the laboratory, but each has met with only limited success. Burns and Richard (1964) solved the problem of the buried conduit, using the theory of elasticity by assuming ideal elastic conditions. Their equations have been used to calculate the modulus of soil reaction. The ensuing equation became very difficult to evaluate; therefore, the computer was used to determine an approximate relationship for the necessary variables and the modulus of soil reaction. The modulus has also been shown to be determinable from the triaxial shear test. The modulus is dependent on Poisson's ratio and the modulus of elasticity. Both values can be determined from a single triaxial shear test. Data obtained from a triaxial shear test are used to calculate the modulus of soil reaction which is then compared with the value measured in the device constructed by Watkins and Nielson called the modpares device.

•IN 1942, Spangler (3) published his classical theory for the prediction of deflection of circular underground pipe. He postulated the following equation:

$$\Delta X = \frac{KW_c r^3}{EI + 0.061E'r^3} \tag{1}$$

where

ΔX = change in horizontal diameter of pipe under load W_c,
K = bedding constant (0.083 for 180-deg bedding),
r = mean radius of pipe,
EI = pipe wall stiffness,
E' = modulus of passive resistance which equals er, and
e = modulus of passive resistance.

In the derivation of Eq. 1 the value er was used instead of E'. The value of e is analogous to the modulus of subgrade reaction obtained from the plate bearing test. The value of e was assumed to be a constant for the soil under given conditions. Later Watkins and Spangler (5) showed that e was not constant, but the proper constant was $er = E'$.

Paper sponsored by Committee on Buried Structures and Committee on Culverts and Culvert Pipe and presented at the 46th Annual Meeting.

Eq. 1 has received only limited use because of the inability to determine a numerical value for the modulus of soil reaction, E′. Spangler (3) presented values which were determined by calculating E′ from measured deflections of actual field installations.

To measure the modulus of soil reaction, Watkins and Nielson (6) constructed a device which simulated the side of a pipe being forced into the side fill. Satisfactory results were obtained, but the complexity of the test and the requirement of special equipment limit the device's use. It would be desirable to devise a method of measuring the modulus of soil reaction by some equipment which is common to most soil mechanics laboratories.

THEORY

Watkins and Nielson (6) have shown the modulus of soil reaction to be

$$E' = \frac{h}{\frac{\Delta X}{D}} \tag{2}$$

where

E' = modulus of soil reaction,
h = pressure at side of pipe caused by forcing side of pipe into side fill,
ΔX = change in horizontal diameter of pipe under loading, and
D = original diameter of pipe.

Eq. 2 has the same form as the equation for the modulus of elasticity for a metal, i.e.,

$$E = \frac{P}{\frac{\Delta L}{L}} \tag{3}$$

where

E = modulus of elasticity,
P = applied pressure,
ΔL = deflection, and
L = length.

Because the equations are similar and each relates pressure and deflection, there should exist a relationship between the modulus of soil reaction, E', and the modulus of elasticity of the soil, E.

Figure 1 shows a buried pipe. An infinitesimal cube, A, is shown on the right side of the pipe at the horizontal diameter. Burns and Richard (2) derived the following equations for the pressure σ_1 and σ_3 and the deflection $\Delta X/2$ as shown on the pipe, using the theory of elasticity:

$$\sigma_1 = P\{B[1 - a_0^*(R/r)^2] - C[1 - 3a_2^*(R/r)^4 - 4b_2^*(R/r)^2]\} \tag{4}$$

$$\sigma_3 = P\{B[1 + a_0^*(R/r)^2] + C[1 - 3a_2^*(R/r)^4]\} \tag{5}$$

$$\frac{\Delta X}{2} = \frac{PR}{M^*}\,\tfrac{1}{2}\{[1 - (B/C)a_0^*(R/r)^2] - [1 + a_2^*(R/r)^4 + (2/B)b_2^*(R/r)^2]\} \tag{6}$$

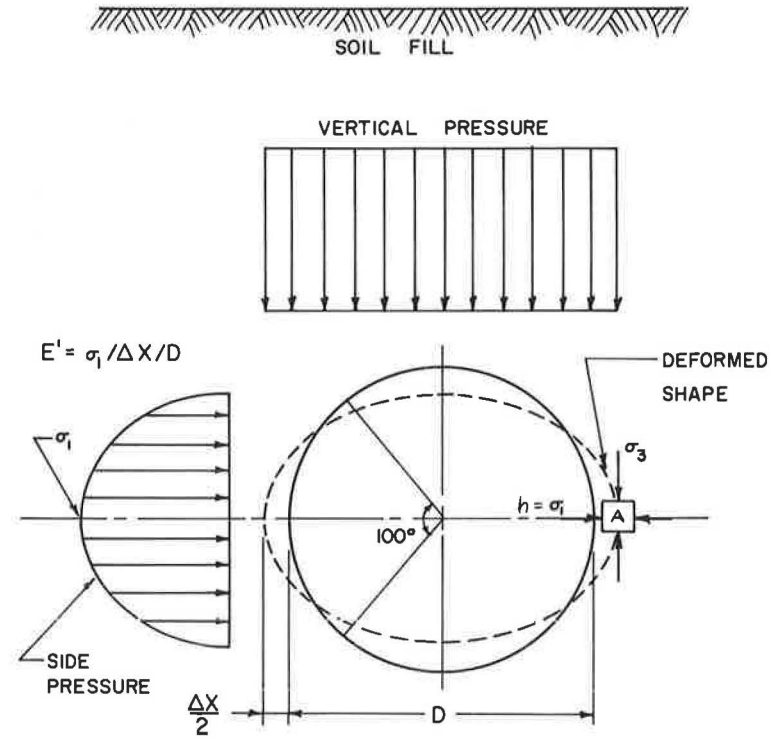

Figure 1. Buried pipe.

where

$M^* = \frac{E^*(1-u)}{(1+u)(1-2u)}$ which represents constrained modulus of elasticity of soil,
r = radius from center of pipe to point in fill,
E^* = modulus of elasticity of soil,
u = Poisson's ratio,
R = radius of pipe,

$C = \frac{1}{2}\left(\frac{1-2u}{1-u}\right)$,

$B = \frac{1}{2}\left(\frac{1}{1-u}\right)$,

$UF = \frac{2B\,M^*R}{EA}$,

E = modulus of elasticity of pipe wall materials,
A = area per unit length of pipe wall material,
I = moment of inertia of pipe wall per unit length,

$VF = 2C\frac{M^*R^3}{EI}$,

$a_0^* = \frac{UF-1}{UF+B/C}$,

$a_2^* = \frac{C(1-UF)\,VF-(C/B)\,UF+2B}{(1+B)\,VF+C(VF+1/B)\,UF+2(1+C)}$, and

$b_2^* = \frac{[B+C(UF)]\,VF-2B}{(1+B)\,VF+C(VF+1/B)\,UF+2(1+C)}$.

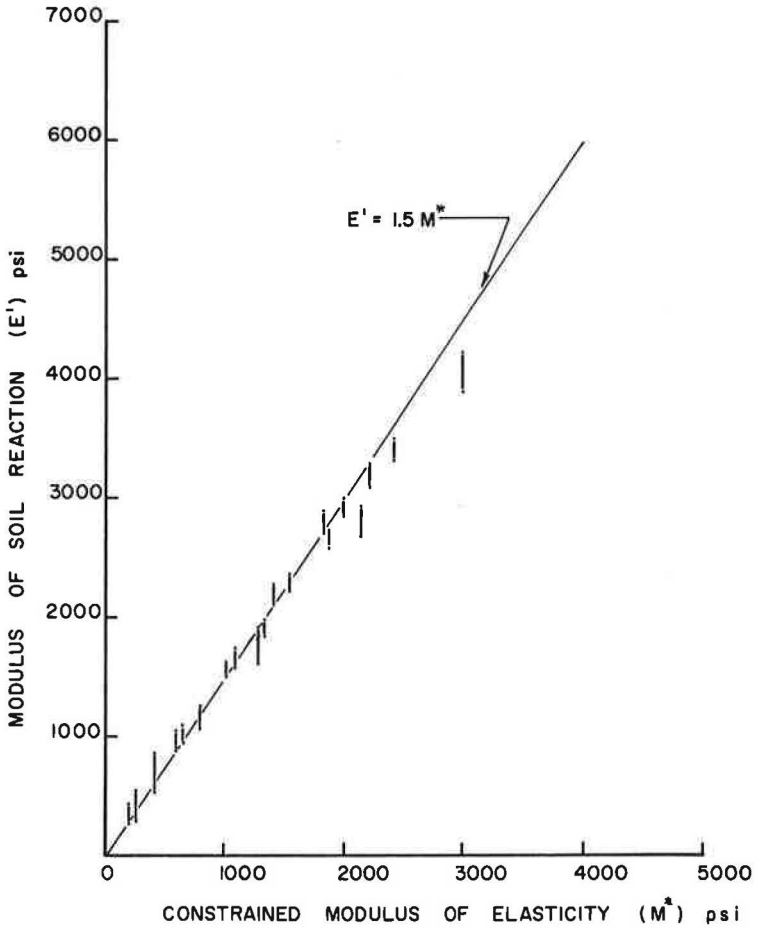

Figure 2. Comparison of modulus of soil reaction and constrained modulus of elasticity as determined from theory of elasticity.

Substituting Eqs. 4 and 6 into Eq. 2 and letting r = R, the resulting equation relates the modulus of soil reaction, E', and the modulus of elasticity, E, as follows:

$$E' = \frac{2M^*[B(1 - a_0^*) - C(1 - 3a_2^* - 4b_2^*)]}{[1 + (B/C)a_0^*] - [1 - a_2^* + (2/B)b_2^*]} \tag{7}$$

Eq. 7 is rather difficult to solve; therefore, the computer was used to establish the relationship between E' and M^*. A wide range of values for each variable was read into the computer program. Figure 2 shows a curve of the results obtained. The vertical lines represent limits for the modulus of soil reaction obtained by varying pipe radius, Poisson's ratio, pipe wall stiffness, etc. The modulus of soil reaction E' can now be approximated by:

$$E' = 1.5M^* = 1.5\frac{E(1 - u)}{(1 + u)(1 - 2u)} \tag{8}$$

where

E' = modulus of soil reaction,
E = modulus of elasticity,
u = Poisson's ratio, and
M^* = constrained modulus of elasticity.

TRIAXIAL SHEAR TEST

An approximation of the modulus of elasticity E and Poisson's ratio u can be determined from the triaxial shear test. Most textbooks in strength of materials give the stress-strain relationship for three-dimensional stress as:

$$\epsilon_1 = \frac{1}{E}(\sigma_1 - u\sigma_2 - u\sigma_3) \tag{9}$$

where

ϵ_1 = maximum principal strain,
σ_1 = maximum principal stress,
u = Poisson's ratio,
σ_2 = intermediate principal stress,
σ_3 = minor principal stress, and
E = modulus of elasticity.

In the normal triaxial shear test the intermediate principal stress σ_2 and the minor principal stress σ_3 are equal and constant. For the triaxial shear test, Eq. 9 can be rewritten as:

$$\epsilon_1 = \frac{\sigma_1}{E} - C \tag{10}$$

where

$$C = \frac{(+ u\sigma_2 + u\sigma_3)}{E} = \frac{+2\ u\sigma_3}{E} = \epsilon_0$$

This substitution assumed Poisson's ratio and the modulus of elasticity to be constant, which is probably not valid for soils.

However, by making the assumption that Poisson's ratio is constant, a value for the modulus of elasticity and Poisson's ratio can be approximated. Figure 3 shows a typical stress-strain curve obtained from a triaxial shear with constant lateral pressure. Eq. 9 shows that the axial strain occurring in a triaxial specimen during the application of the chamber pressure σ_3, at which time $\sigma_1 = \sigma_2 = \sigma_3$, is

$$\epsilon_1 = \frac{\sigma_3}{E} - u\frac{\sigma_3}{E} - u\frac{\sigma_3}{E} \tag{11}$$

$$\epsilon_1 = \frac{\sigma_3}{E}(1 - 2u) \tag{12}$$

or

$$u = \frac{\sigma_3 - \epsilon_1 E}{2\sigma_3} \tag{13}$$

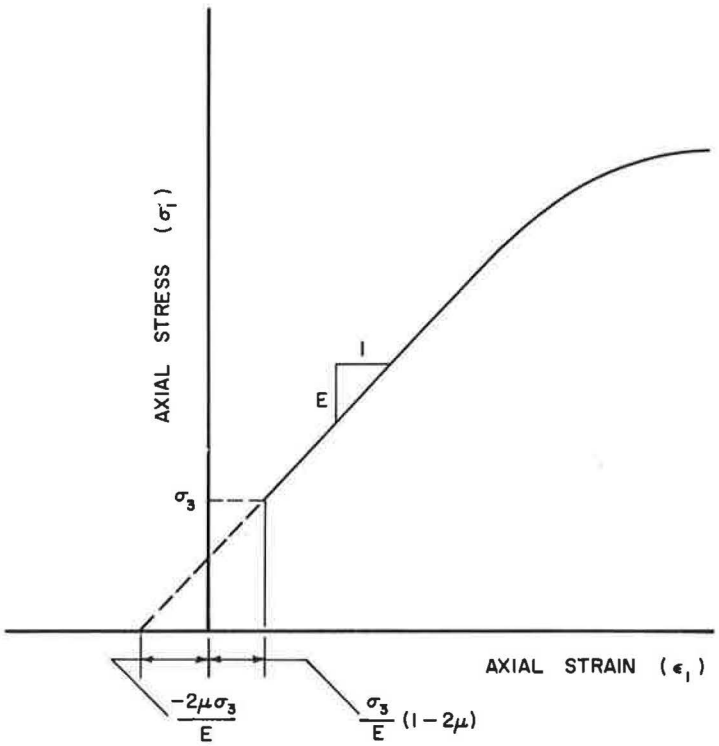

Figure 3. Triaxial shear test with constant lateral pressures.

Eq. 13 shows that an approximation of Poisson's ratio can be determined by measuring the axial strains ϵ_1 or the decrease in length that occurs in the sample during the application of the chamber pressure, σ_3. E is assumed to be the slope of the stress-strain curve above the value of $\sigma_1 = \sigma_3$. Typical values of u for soils with σ_3 ranging from 15 to 45 psi show E varying from 1000 to 7000 psi and u ranging from 0.25 to 0.35. Values of Poisson's ratio obtained by Barkan (1) indicate that it ranges between 0.3 and 0.35 for sands. Tsytouich (4) recommends the value of Poisson's ratio for sands as u = 0.15 to 0.25, for clays with sand and silt 0.30 to 0.35, for clays, 0.35 to 0.40.

If the value change occurring in the triaxial shear sample is measured, Poisson's ratio can be determined by another method. The volume change ΔV that occurs during testing divided by the original volume is the cubical dilatation and is approximately given by:

$$\frac{\Delta V}{V} = \epsilon_1 + \epsilon_2 + \epsilon_3 \qquad (14)$$

where

ΔV = volume change of specimen,
V = original volume of specimen, and
$\epsilon_1, \epsilon_2, \epsilon_3$ = strains.

The original volume of the specimen is known and ΔV and ϵ_1 can be measured. By the nature of the triaxial shear test $\epsilon_2 = \epsilon_3$, therefore, the only unknown is ϵ_3. If the principal stresses and strains are known, Poisson's ratio can be solved by using Eq. 9 and the similar equation for ϵ_2.

Indications are that Poisson's ratio can be assumed to be approximately 0.25 for most design work. This does not increase the error significantly more than error

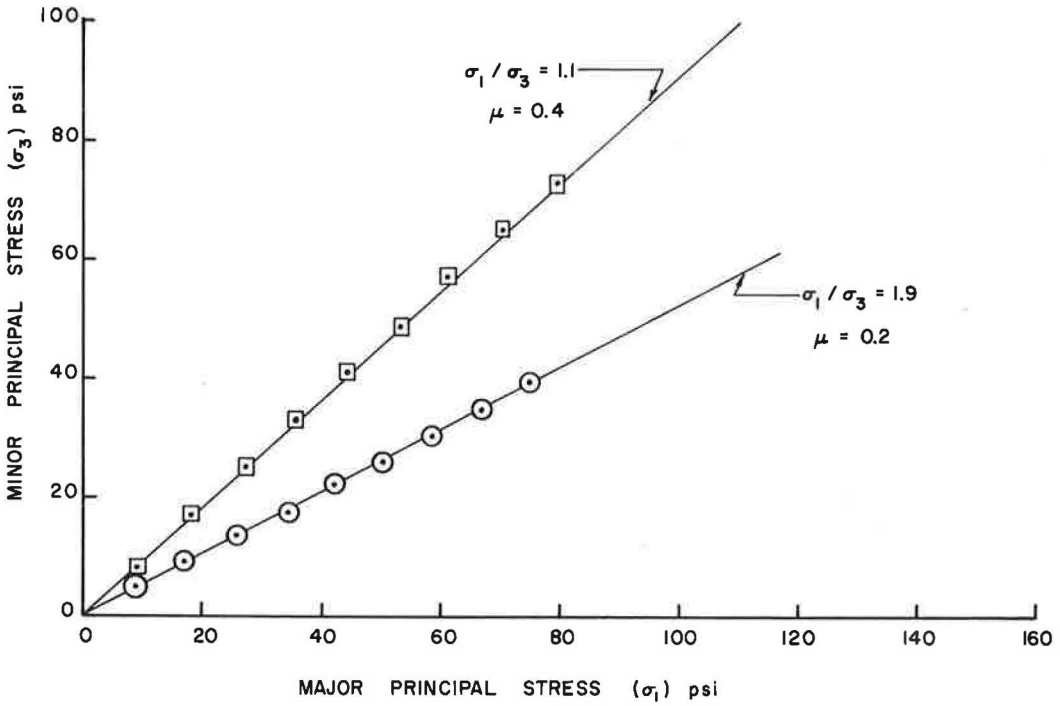

Figure 4. Relationship between major and minor principal stresses for various Poisson's ratio as determined from the theory of elasticity.

already present in the measuring procedures because of the nonlinear stress-strain diagram.

The proper lateral pressure σ_3 in the triaxial chamber has to be determined so that correct stress-strain curve can be obtained. The value of σ_3 should change with the value of σ_1 to simulate the stress conditions shown in Figure 1. The effects of the intermediate principal stress are assumed negligible. Evaluation of Eqs. 4 and 5 shows that the ratio of σ_1/σ_3 is approximately 1.1 for Poisson's ratio = 0.4 and 1.9 for Poisson's ratio = 0.2. Figure 4 shows the relationship of σ_1/σ_3 as calculated from Eqs. 4 and 5 for two of the different values of Poisson's ratio.

The ratio of 1.1 is not realistic for soils. Load-deflection curves observed in the field are not possible unless the ratio of σ_1/σ_3 approaches $\tan^2 [45- (\Phi/2)]$ for a cohesionless soil.

For the sake of simplicity, with the understanding that results are only approximate, it is recommended that the lateral pressure used in making the triaxial shear test be set at $^3/_8$ of the actual weight of the completed fill above the mid-height of the pipe. Evaluation of Eq. 5 shows that the lateral pressure should be approximately $^3/_4$ of the vertical load, P. A value of lateral pressure σ_3 equal to $^3/_8$ of the weight of soil is the average value of the σ_3 during the construction of the fill.

When a pipe is strutted before the fill is placed over it, the lateral pressure σ_3 must be increased to approximately $^3/_4$ the weight of the vertical column of fill. No deflection (or negligible deflection) is allowed to take place before the struts are removed. Therefore, the maximum lateral pressure of approximately $^3/_4$ the weight of the fill would be exerted before any deflection was allowed.

DEFLECTION-STRAIN RELATIONSHIP

It is necessary to get a relationship between the deflection of the pipe and the strain in the soil. The strain in the soil can be obtained by differentiating Eq. 6 with respect to r and then letting r = R. A wide range of values was again substituted into the

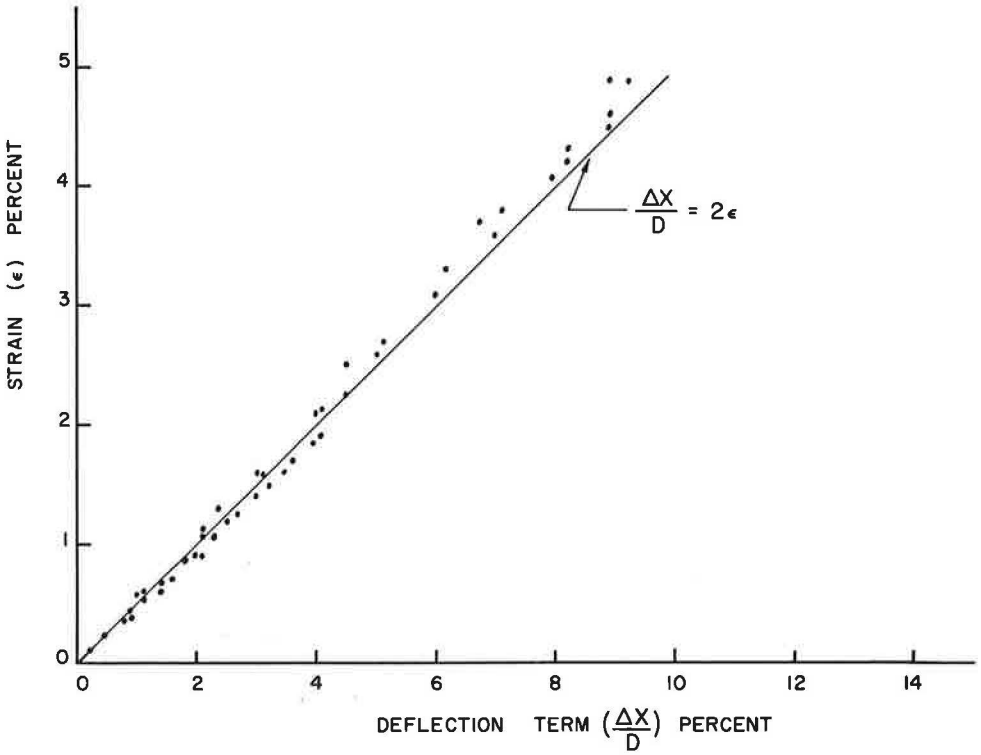

Figure 5. Comparison between soil strain and percent deflection of pipe.

computer. Figure 5 shows the results obtained for typical soil values for each variable. Figure 5 shows that

$$\frac{\Delta X}{D} = 2\epsilon \tag{15}$$

OBTAINING THE MODULUS OF SOIL REACTION

Equations 2 and 8 give the value for h as

$$h = 1.5\, M^* \frac{\Delta X}{D} \tag{16}$$

Because

$$\Delta X/D = 2\epsilon$$

$$h = 1.5M^* 2\epsilon = 3\frac{(1-u)\, E\, \epsilon}{(1+u)\,(1-2u)} \tag{17}$$

If Poisson's ratio equals 0.4

$$h = 4.29\, E\, \epsilon$$

For Poisson's ratio equals 0.3

$$h = 3.1\, E\, \epsilon \tag{18}$$

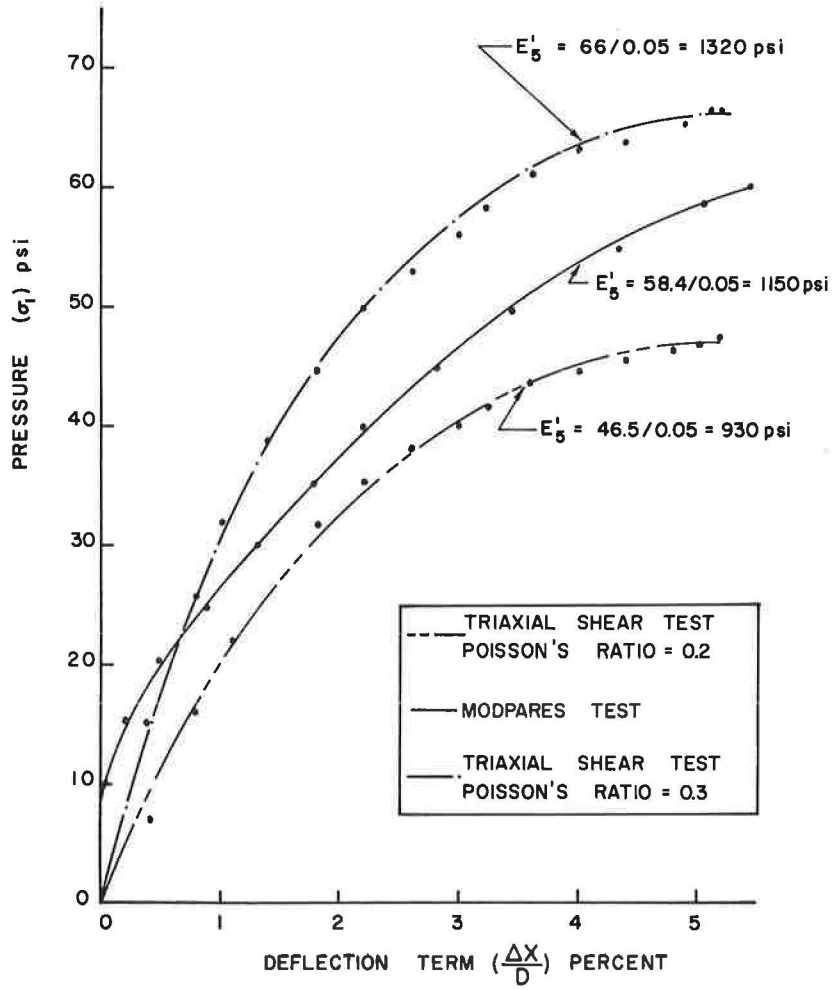

Figure 6. Modpares curve for determining modulus of soil reaction vs curves calculated from triaxial shear test for fine sand.

or if Poisson's ratio equals 0.2

$$h = 2.2\,E\,\epsilon \tag{19}$$

The value of h can be reduced to

$$h = 4.29\,\sigma \quad \text{for } u = 0.4$$

$$h = 3.1\,\sigma \quad \text{for } u = 0.3$$

or

$$h = 2.2\,\sigma \quad \text{for } u = 0.2 \tag{20}$$

where σ equals vertical pressure on the triaxial specimen which equals P/A.

The modulus of soil reaction E' can be solved by substituting one of the values from Eq. 20 and Eq. 15 into Eq. 2. Figure 6 shows a comparison of the curves for the modulus soil reaction calculated from a triaxial shear test and one measured in the device

constructed by Watkins and Nielson (6). The soil in each case has a density of approximately 87 percent AASHO T-180 density. The soil to be tested in the triaxial shear test must have the same density and moisture content as the sample compacted around the pipe. Data for Figure 6 are given in the Appendix.

CONCLUSIONS

The modulus of soil reaction can be determined by the triaxial shear test with sufficient accuracy for use in design work. The modulus is sensitive to the value of Poisson's ratio. For design work, a value of 0.25 is recommended.

ACKNOWLEDGMENTS

The author wishes to express his appreciation to the New Mexico State University Computer Center for its help and to the personnel in the Soil Mechanics Laboratory for making the required soil test. The author also wishes to express thanks to Dr. Ti Huang, Professor of Civil Engineering, for his help with the theory of elasticity.

REFERENCES

1. Barken, D. D. Dynamics of Bases and Foundations. McGraw-Hill, New York, 1962.
2. Burns, J. Q., and Richard, R. M. Attenuation of Stresses for Buried Cylinders. Proc. of the Symposium on Soil Structure Interaction, Univ. of Arizona, 1964.
3. Spangler, M. G. The Structural Design of Flexible Pipe Culverts. Bull. 153, Iowa Eng. Exper. Sta., Ames, Iowa, 1942.
4. Tystouich, N. A. Mekhanika Gruntov, Gosstroyizdat, Moscow (summarized in Ref. 1), 1937.
5. Watkins, R. K., and Spangler, M. G. Some Characteristics of the Modulus of Passive Resistance of Soil: A Study in Similitude. HRB Proc., Vol. 37, pp. 576-583, 1958.
6. Watkins, R. K., and Nielson, F. D. Development and Use of the Modpares Device in Predicting the Deflection of Flexible Conduits Embedded in Soil. Eng. Exper. Sta., Utah State Univ., 1962. Publ. by ASCE Pipeline Crossing Committee in ASCE Pipe Line Journal, Jan. 1964.

Appendix

TABLE 1

MODPARES TEST[a]

Membrane Pressure (psi)	Deflection (in. × 10^{-3})	Membrane Pressure (psi)	Deflection (in. × 10^{-3})
0.0	0.0	35.1	35.5
5.0	0.0	40.0	43.8
10.2	1.3	45.2	56.0
15.0	3.6	50.0	68.3
20.0	9.5	55.2	87.3
25.2	17.0	60.0	108.6
30.1	27.3		

[a]Soil sample: fine sand
Compactive effort: 3440 ft-lb/ft^3
Wet wt: 112.1 pcf
Dry wt: 99.2 pcf
Date: Jan. 10, 1966
Vertical pressure: 25 psi
Moisture content: 13.1%

TABLE 2

TRIAXIAL SHEAR TEST[a]

Length Change (in.)	Proving Ring Dial (in. × 10^4)	Strain	Area (sq in.)	Axial (lb)	P/A (psi)	σ_1 (psi)
0	0	0	6.158	0	0	10.000
0.010	17	0.002	6.169	21.658	3.511	13.511
0.020	36	0.004	6.180	45.864	7.421	17.421
0.030	50	0.005	6.191	63.700	10.288	20.288
0.040	62	0.007	6.203	78.988	12.734	22.734
0.050	71	0.009	6.214	90.454	14.556	24.556
0.060	79	0.011	6.226	100.646	16.166	26.166
0.070	84	0.013	6.237	107.016	17.157	27.157
0.080	89	0.015	6.249	113.386	18.145	28.145
0.090	93	0.016	6.261	118.482	18.925	28.925
0.100	97	0.018	6.272	123.578	19.702	29.702
0.110	100	0.020	6.284	127.400	20.274	30.274
0.120	102	0.022	6.296	129.948	20.641	30.641
0.130	105	0.024	6.307	133.770	21.208	31.208
0.140	107	0.026	6.319	136.318	21.572	31.572
0.150	108	0.027	6.331	137.592	21.732	31.732
0.200	113	0.037	6.391	143.962	22.525	32.525
0.250	116	0.046	6.452	147.784	22.903	32.903

[a]Sample: fine sand
Location: Lohman interchange
Specific gravity: 2.64

Test No.: special
Date: June 22, 1966
Tested by: Don Bell

Specimen Dimensions

Diameter = 2.80 in.
Length = 5.47 in.

Proving ring no. = 1535
Calibration factor = 1.274 lb/div
Chamber pressure = 10.0 psi
Deformation rate = 0.0600 in./min
Void ratio = 0.59
Dry unit weight = 103.4 lb/CF
Max. stress = 32.90 at 4.571 percent strain

Specimen Weights

Wt tare + soil = 1420.000 gm
Wt tare = 387.60 gm
Wt soil = 1420.00 gm

Moisture Content

Wt tare and wet soil = 926 gm
Wt tare and dry soil = 200 gm
Wt tare = 0 gm
Moisture content = 13 percent